

Energieforschungsprogramm

Publizierbarer Endbericht

Programmsteuerung:

Klima- und Energiefonds

Programmabwicklung:

Österreichische Forschungsförderungsgesellschaft mbH (FFG)

Endbericht

erstellt am

11/01/2020

Projekttitel:

Tes4seT - Thermal Energy Storages for
Sustainable Energy Technologies

Projektnummer: 845020

Energieforschungsprogramm – 4. Ausschreibung

Klima- und Energiefonds des Bundes – Abwicklung durch die Österreichische Forschungsförderungsgesellschaft FFG

Ausschreibung	4. Ausschreibung Energieforschungsprogramm
Projektstart	01/04/2014
Projektende	31/03/2018
Gesamtprojektdauer (in Monaten)	48 Monate
ProjektnehmerIn (Institution)	AEE INTEC
AnsprechpartnerIn	Dr. Wim van Helden
Postadresse	Feldgasse 19, A-8200 Gleisdorf
Telefon	0043-3112-5886-228
Fax	0043-3112-5886-18
E-mail	w.vanhelden@aee.at
Website	www.aee-intec.at

Tes4seT

Thermal Energy Storages for Sustainable Energy Technologies

AutorInnen:

TU Graz – Hermann Schranzhofer

Fachhochschule Oberösterreich – Bernhard Zettl, Gerald Steinmaurer

Technische Universität Wien – Andreas Werner

Technische Universität Wien – Michael Schnürch

AIT – Christoph Zauner

1 Table of contents

1	Table of contents	4
2	Introduction	6
2.1	Goals and results	8
2.1.1	Development Line A	8
2.1.2	Development Line B	8
2.1.3	Development Line C	9
2.1.4	Development Line D	10
2.1.5	Development Line E	11
3	Line A: Novel seasonal solar sorption storage for buildings	12
3.1	Experimental results on the sorption collector	12
3.1.1	System setup	15
3.2	Control Strategy	18
3.2.1	Simulation results	19
4	Line B: Heat storage for car battery temperature conditioning	22
4.1	Boundary conditions and system design	22
4.1.1	Battery- Definition	22
4.1.2	Requirements of the Components	22
4.2	Materials selection and development	23
4.3	Component Development	27
4.3.1	Component Design	27
4.3.2	Dedicated Component Experiments	28
4.4	Storage system development	30
4.4.1	Storage system design	30
4.4.2	Storage system experiments	32
4.4.3	Storage system simulations	34
4.4.4	Operation state of the storage in the simulation cases	35
4.5	Control development	36
4.5.1	Subsystem battery	37
4.5.2	Subsystem thermal storage	38
4.5.3	Objective and system simulation design	38
5	Line C: Storage for efficient energy systems in railway vehicles	40
5.1	Boundary conditions and system design	40
5.2	Materials selection and development	43
5.3	Component Development	49
5.4	Storage system development and numerical simulation	54
5.5	System Integration and Control	60
5.5.1	Study 1: Integration Concept and Demonstration of a PCM Storage in a Rail HVAC Application	60

5.5.2	Study 2: Integration of the Storage Evaporator Model into the Refrigeration System	
	Simulation Environment	66
5.5.3	Simulation of required Energy Rates of the Storage System for a defined Use Case	67
5.5.4	Results and Discussion	69
5.5.5	ACS HVAC Simulation Results – Batch Dehumidification.....	72
5.5.6	ACS HVAC Simulation Results – Sorption Rotor Dehumidification.....	75
6	Line D: Industrial waste heat recovery with novel thermochemical heat storage	81
6.1	Boundary conditions and system design:	81
6.2	Materials selection and development.....	81
6.2.1	Sorptive Materials:.....	81
6.2.2	Attritions tests.....	95
6.3	Line D, WP3: Component Development.....	97
6.4	Line D, WP4: Storage system development	100
7	Line E: Novel medium temperature PCMs for industrial applications.....	102
7.1	Boundary conditions and system design	102
7.2	Materials selection and development.....	103
7.2.1	Conclusions.....	116
7.3	Component Development.....	117
8	Results and conclusions	127
8.1.1	Development Line A	127
8.1.2	Development Line B	127
8.1.3	Development Line C	128
8.1.4	Development Line D.....	129
8.1.5	Development Line E	130
9	Literature.....	131
10	Contact information.....	132

2 Introduction

Efficient short and long term thermal energy storage technologies are crucial in enhancing energy security and in improving energy efficiency in energy conversion, distribution and end use. This is underlined by (inter)national technology visions and roadmaps.

The Tes4seT had as aim to make a decisive contribution towards a new generation of efficient and compact thermal energy storage systems in three sectors of energy use: buildings, industry, and mobility. The new generation of storage technology will help to achieve the objective of Austria's policy for energy efficiency and renewable energy technologies. The results and progress achieved by the Tes4seT project will further strengthen and expand the leading role of Austria in the above mentioned sectors.

In the three application areas buildings, industry and mobility, the development targets and economic effects of the Tes4seT project are:

- Buildings - Development of compact and efficient seasonal solar thermal storage based on sorption technology, with a dedicated novel sorption solar collector and higher efficiency of the sorption storage through vapour transport. This will strengthen the leading role of Austrian solar thermal manufacturers by increasing their portfolio with very high solar fraction systems, and increase the leading role of Austrian device and system designers through the novel tools and methods.
- Industry - For application in industry, both novel thermochemical storage technologies and new phase change materials on medium temperature will be developed, giving the engineering companies new tools and technologies to provide industry with energy saving and renewable energy measures. Besides, industry can produce the novel PCM and sorption materials for the growing international market.
- Mobility - Development of a sorption thermal storage for car battery temperature conditioning and the development of a thermal storage system to make high-efficient energy systems for railway vehicles. Through these innovative technologies, important for the rapidly expanding market of hybrid and electric vehicles and for the very large market of (underground) railway vehicles, the Austrian mobility technology manufacturing and supply industry will expand its strong role in Europe.

Hence, the Tes4seT project fully addresses the key intelligent storage flagship objectives of the call: improved thermochemical energy storage (5.1) and improved heat stores for industrial energy systems (5.4).


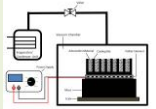
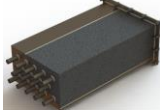


The project consortium consists of key scientific institutions active in the field of heat storage technologies and top-leading industry partners which will provide the basis for further industrial development.

The Tes4seT project is an Austrian Flagship project, funded by the National Climate and Energy Fund and administered by the FFG, with project number 845020.

In the project, 5 R&D organisations collaborated with 12 partners from industry to work in 5 parallel Development Lines (A to E) on thermal energy storage technologies for the three different application areas. Each development line was led by one of the 5 R&D organisations, as shown in the figure below.

Energieforschungsprogramm – 4. Ausschreibung

Klima- und Energiefonds des Bundes – Abwicklung durch die Österreichische Forschungsförderungsgesellschaft FFG

A	Sorption seasonal storage for buildings	AEE INTEC	
B	Heat storage for car battery temperature conditioning	AEE INTEC	
C	Storage for efficient energy systems in railway vehicles	ASiC	
D	Industrial waste heat recovery with novel thermochemical heat storage	TU Wien	
E	Novel medium temperature PCMs for industrial applications	AIT	

This report gives an overview of the main research and development activities and of the results achieved in the Tes4seT project. In the first chapter, a summary of the work and findings is given and in the following chapters each Development Line is presented in a more detailed way.

2.1 Goals and results

2.1.1 Development Line A

The goal of Line A is to develop and demonstrate a seasonal closed sorption storage system to cover the domestic hot water and space heating demand of a single family house. The aim is to use the surplus of heat produced by solar thermal collectors in summer to store it for covering the heat demand in winter. Since the storing period is over several months a technology with low losses is required. In addition, the system should have a high compactness because of limited available space in a residential building. A technology, which can meet these requirements, is the sorption technology. The aim of Line A is to improve the performance of a sorption storage system by optimizing the so-called charge boost process and evaluate to which extent the performance can be improved.

For the investigations, a realistic scale storage system was designed and built up in the laboratory of AEE INTEC, which comprises several sorption storage vessels (two main storages and a room storage) and a new solar collector with integrated sorption material. The system was equipped with extensive measurement equipment in order to enable a detailed analysis of all components and of different operational modes. A system simulation model was set up, in order to represent the storage system with all its main components. The model was built in TRNSYS using about 60 single component models. Measurements from the laboratory test rig were used to parameterize and validate the model. Annual simulations were performed in order to test the developed control strategy and to assess the system efficiency for different configurations of the system.

2.1.2 Development Line B

The general goal of Line B is to develop a thermal management for batteries in electric or hybrid vehicles based on sorption thermal energy storage technology. The range of possible scenarios in this respect is too broad for a single project, thus we focused on hybrid vehicles only. In that case there is the additional benefit that waste heat of the combustion engine can be re-used to charge the thermal storage, which can then later be discharged to supply either heat or cold. The thermochemical material (TCM) (Sapo34 and water vapour) was chosen according to the prevailing temperature levels. A numerical tool was developed and a dedicated test rig assembled for the material selection. Critical components have been discussed extensively. A custom adsorber design has been developed, including adsorbents as coating and as granules. The performance of this design was compared experimentally to two other adsorber designs, based on coating and direct crystallization, and found to be superior. The evaporator/condenser was dimensioned accordingly in a compact way, and examined experimentally in a dedicated test rig. Various designs have been discussed for the vacuum vessel using finite element calculations, and a rectangular shaped was suggested with vacuum forces carried by the heat exchangers. A functional module of the storage system was assembled and assessed in experiment, where a cooling power peak of 2 kW and an average power of 1 kW for a total energy of 0.55 kWh was measured. Assuming an optimized system design including compact vessels, this translates into key performance indicators (KPIs) of about 27 Wh/l resp. 27 Wh/kg and 55 W/l resp. 55 W/kg for cooling. For heating, we propose a novel operation mode, where no external heat source is coupled to the evaporator during evaporation. Instead, we allow part of the water to freeze, such that the crystallization enthalpy serves as evaporation enthalpy. The concept hence combines TCM with phase change material as latent heat storage, where

the latter is used as a buffer to provide the evaporation enthalpy. This process was demonstrated in experiment, yielding heating KPIs of 34 Wh/l resp. 34 Wh/kg and 68 W/l resp. 68 W/kg for heating. Simultaneously to the experiments, a simulation model was developed. The thermal storage was modelled in Trnsys and the vehicle with all other components in Simulink. A co-simulation interface has been constructed to couple these models. Detailed system simulations have been performed for five distinct realistic scenarios. These have shown energy savings of 60% for cooling the battery during fast charging, 11% for cooling the combustion engine while regenerating the thermal storage compared, saving 80 seconds for heating a chilled battery up to 20°C and saving 26 seconds for preheating the combustion engine up to 80°C.

2.1.3 Development Line C

The aim of this development line is to develop an improved and experimentally verified thermal storage concept for the conditioning of the railway passenger compartments by adding functionality of thermal storage devices to the system. Three applications are studied in this development line: Optimized underground heat rejection of subway trains and enhanced part-load behaviour of conventional conditioning systems by the use of PCM storages. The third application deals with the improvement of Air-Cycle-Cooling (ACS) systems by the use of adsorption materials. In order to simplify readability, and to establish cross-connections, the three applications were subdivided into two parts concerning the different storage concepts:

- Improvement of underground heat rejection of subway trains, improvement of part-load behaviour of conventional conditioning systems by the use of PCM storages
- Improvement of Air-Cycle-Cooling (ACS) systems by the use of adsorption materials

2.1.3.1 Part-load behaviour of conventional conditioning systems (Objective Ca) and Underground heat rejection of subway trains (Objective Cb)

Concerning the improvement of underground heat rejection of subway trains, improvement of part-load behaviour of conventional conditioning systems by the use of PCM storages were done. These improvements of the part-load behaviour can be accomplished by using a storage evaporator assembled to the air condition system. The usage of an evaporator with integrated PCM is one possibility to reduce or even avoid the part-load operation of the refrigerant compressor resp. the whole air conditioning system. As the part load operation is inefficient using a fixed speed compressor, this leads to a higher system efficiency. The storage evaporator is being discharged during the operation of the air conditioning system and being charged during the standstill of the compressor by the cabin air. For the later on simulation model adjustment and validation, an off-the-shelf storage evaporator for automotive applications was evaluated resp. measured. The measured data lays the foundation for a scalable simulation model in the future. The automotive storage evaporator grants an air outlet temperature lower than 15 °C for $t = 109$ s with a previous PCM discharge time of 4 minutes (@200 kg/min air mass flow and ambient air temperature of 30 °C). This means an average cooling capacity of 1055 W is available during this 109 s.

Additionally, different PCM/Aluminium modules were tested to determine thermal power and storage density. For this RT5HC was used as storage material. It is a PCM with a melting area from 5 to 6 °C and a heat storage capacity of 250 kJ/kg (in a temperature range from -2 to 13 °C). The heat conductivity of both phases is 0.2 W/(m K). Several charging and discharging cycles with different mass flow rate,

different geometry of the modules and different hydraulic concepts were performed. From these experiments measured data were used to parametrize a TRNSYS storage model for further system simulations. For these investigations Dymola was used for the HVAC system and the TRNSYS storage model was integrated using the co-simulation tool BCVTB.

2.1.3.2 Improvement of Air-Cycle-Cooling (ACS)(Objective Cc)

Regarding the improvement of Air-Cycle-Cooling (ACS) systems by the use of adsorption materials the aim of this report is to describe the consequences derived from material characterization on the concept and dimensioning of the components needed to integrate storage functionality into the Air-cycle-cooling system (ACS). To reach a most realistic data base, a second step of air conditioning was built to test some selected materials in the adsorption and desorption simultaneously. Therewith more reliable data were found. Additionally some components already existing were tested. These components show somehow similar functionality compared to the required desiccant unit for the ACS application.

In particular, a finned air heat exchanger, coated with a kind of adsorbent material (SAPO34, produced by MITSUBISHI PLASTICS/JP) and a desiccant wheel with incorporated silica gel (produced by SCHEUCHL/D) were tested. The development of the air dehumidification unit was made by further experimental studies of selected sorption materials as packed bed specimen as well as component tests of existing devices. Simulation studies were performed by LIEBHERR internal Software.

In the ideal case a dehumidifying capacity of 10 g/kg can be reached with the Material Y zeolite, which results in a power saving of 22 % of the unit with constant cooling capacity. The technique results in an additional process air cooling capacity of up to 17 kW. The additional cooling process parameter is an essential feature that must be considered in the detailed design and construction phase.

2.1.4 Development Line D

The goal of Development Line D is to develop a thermochemical energy storage system (TCES). The aim is to work on different aspects of the technology simultaneously, namely on the construction and initial operation of a fluidised bed reactor for hydration and dehydration reactions, the development of a method for modelling TCES, the process design and integration of TCES in waste heat recovery applications. In addition, the evaluation of the economic feasibility of such systems was investigated and the base materials are optimized in order to improve material properties that are of high importance for the process like reactivity and thermal conductivity.

A fluidised bed reactor for testing $\text{MgO}/\text{Mg}(\text{O})_2$ was set into operation and extensive material testing has been performed. The results were summarised in the diploma thesis of A. Bartik, 2018.

A model of the reactor including all peripheral systems was implemented in the software gPROMS. The work is presented in an article published in *Energy (Int. J.)*, which uses methods from chemical engineering and reaction kinetics and applies it to thermochemical energy storage. Also it extensively discusses the limitations of a TCES process and the issue of the supply of the reactant gas on the overall process. Furthermore a process utilizing 3 different reaction pairs arranged in a cascade of reactors was investigated.

A study based on the overall factor method of Lang was done in order to evaluate the economic viability of TCES. The resulting values of the mass and energy balances from the simulation are used in order to yield the size of the utilized equipment. Via this method it is possible to obtain the total capital investment of a TCES system.

In order to enhance the reactivity of the $\text{MgO}/\text{Mg}(\text{OH})_2$ system calcium doping of magnesium oxide was performed. This procedure results in insignificantly increased water dissociation rates, thus enhancing the hydration rate and the completeness of hydration compared to pure MgO .

2.1.5 Development Line E

The goal of this development line is to develop novel medium-temperature PCMs based on sugar alcohols. Within the project, we completed the organic PCMs synthesis efforts. Within the class of sugar alcohols new chemical modifications (acetylations) and chain elongations have been investigated revealing not-yet-known candidate organic PCMs. In addition, thermal stability investigations were performed in DSC and larger volume samples ($\sim 1 \text{ dm}^3$) clarifying the situation for different atmospheric conditions. Erythritol was found to be the most stable compound with a high melting enthalpy. The systematics of melting range and enthalpy with regard to carbon backbone chain length was investigated in great detail for dicarboxylic acids and diamids. We found that there is an appropriate compound for every few degrees Celsius over a phase change range of $100 - 230^\circ\text{C}$. Among the newer investigated substances, we found three interesting organic PCMs in the NN-bis group with enthalpies up to 375 kJ/kg . Finally, we investigated the ease of production which, of course, directly relates to PCM costs and identified sulfuramide, azamide and sebacamide as interesting candidates in addition to sugar alcohols.

On the application side, we found two new industrial use cases for our organic PCMs storages related to solar cooling in food and chemical industries. They will be investigated up to demonstration level within the EU project HYCOOL (Grant Agreement 792073) which was successfully submitted and started in mid-2018.

In a final step we developed two lab-scale storages to demonstrate the feasibility of our organic PCMs on a 100 kg scale. Fast and versatile Dymola/Modelica models were implemented which allow a proper storage design. The models can be combined with different HVAC system libraries in order to simulate the behaviour of our PCM storages on a system level.

Different heat exchanger concepts were evaluated with regard to their economic and technical performance. Fin-tube and tube bundle heat exchangers were finally selected to serve within the lab-scale demonstrators. Erythritol was chosen as the most promising PCM which was compounded with graphite to increase its thermal conductivity and fumed silica to stabilize the mixture against sedimentation.

A dedicated storage test rig was developed at AIT and the storages were characterized in great detail demonstrating a total storage capacity in the range of 50 kWh . Various charging and discharging experiments revealed storage powers in the range of 30 kW . In addition to even allow for constant-power-(dis)charging a dedicated mass flow control strategy was developed and proven.

3 Line A: Novel seasonal solar sorption storage for buildings

Goal

The goal is to develop a system for the seasonal storage of solar heat for room heating and hot tap water in a single family house, based on a novel type of dedicated solar thermal collector and sorption storage vessels, working under low pressure.

The technology used for this application is based on the exothermic and fully reversible sorption process with the material pair zeolite 13XBF (or silicagel) and water vapour. The main advantage of this technology is that the energy is stored in form of a thermochemical reaction and therefore has no losses/self-discharge during the storing period. In addition, the energy density of this technology is 3-5 times higher on material level compared to a sensible water storage.

To further improve the sorption storage system an innovative component the so called “Sorption Collector” was developed. The aim of the new collector type is to increase the efficiency of the charging process and hence, increase the energy density

The technology is based on the “charge boost” technique which uses the pressure difference between two storages at different temperature levels to achieve higher efficiencies. The seasonal sorption storage system is applied in a single-family house (140 m²) in Graz. The heating demand of the single-family house is simulated and has the following boundary conditions:

The sorption storage system is investigated experimentally and in an annual simulation. For the experimental investigation different setups were tested. The first setup is a smaller sized prototype to test the working principle of the main system components (main storage tank, evaporator/condenser heat exchanger, water reservoir, first functional model of sorption collector (single evacuated tube filled with sorption material), the second setup is to test the room storage and the third setup is a realistic scale sorption storage system containing all components necessary for implementation in a real house.

The main KPI's which will be investigated and determine the performance of the storage system will be input and output power, energy density, material properties and costs.

3.1 Experimental results on the sorption collector

The main storage of the system consists of two modules with different designs. One cylindrical tank containing about 1000 l (700 kg) sorption material and a prismatic-shaped module containing 240 l (154 kg) sorption material.

The sorption collector is used as ‘charge boost’ storage. It is used when the state of charge of the main storage tanks has reached a level where it cannot be desorbed/charged any more due to limitations of the temperatures delivered by the collector. As the adsorption vessel is integrated in the collector, higher temperatures can be achieved as in the main storage tanks. The possible reduction of water concentration (= increase of state of charge) depends strongly on the achieved temperatures in the bed – lower water concentrations are possible in the sorption collector.

The sorption collector is operated in a day/night cycle. During the day the collector is used to heat up the main storage by transferring heat via the hydraulic system and the fixed bed heat exchanger in the sorption storage module. At the same time the sorption material in the collector is heated up and the released water vapour is condensed at the condenser heat exchanger. The main advantage during this step is that the collector sorption material is directly desorbed in the collector and therefore reaches the highest possible temperature. Additionally, no extra containment is needed and the system can be built in a compact way.

During the night the charge boost mode can be applied. Therefore, the high radiation losses of the collector are used to cool down the collector sorption material, which also induces a pressure drop. The resulting pressure difference between sorption collector and main storage is used to further desorb water vapour from the hot main storage to the cold sorption collector. This means that during the charge boost step the vapour is shifted to the sorption collector and the heat is released to the ambient. On the next sunny day, the sorption material in the collector can be desorbed again and the process can be repeated. The main advantage during this step is that the main storage can be desorbed to a higher state of charge, compared to a conventional desorption, without increasing the desorption temperature. The sorption collector provides the ideal boundary conditions for applying as charge boost storage because it enables the highest and lowest temperatures in a day/night cycle.

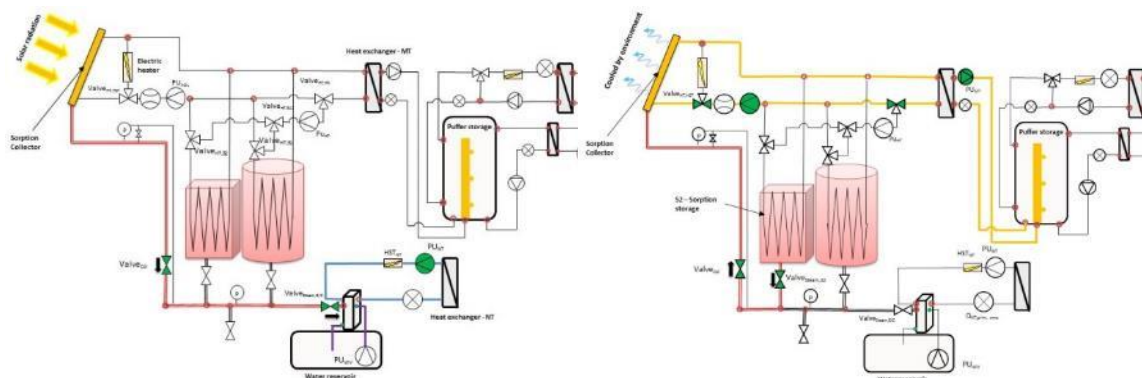


Figure 1: Heat flow diagram for desorption (left) and charge boost (right) of sorption collector

For the sorption collector prototype sorption material zeolite 13XBF was filled into stainless steel pipes with a diameter of 97.8 mm. In the centre of the stainless steel pipe a perforated sleeve is placed to keep a free space to improve the vapour transfer within the zeolite bed. Five stainless steel pipes are welded to a vacuum manifold which is connected to the storage system. On the steel pipes, double copper pipes are placed which are connected to the hydraulic system and enable the conventional use of the collector. On the copper pipes a Sydney-type glass pipe is placed and fixed on the top and bottom of the collector because of the relatively high weight. In addition, the sorption collector is equipped with mirrors on the backside to increase the collector performance [Köll R. et al, 2017]. The design is shown in Figure 2. In total the collector has an aperture area of 3.05 m² and contains 35 kg of zeolite 13XBF in the inner vacuum pipe, which is used for charge boost purposes.

Energieforschungsprogramm – 4. Ausschreibung

Klima- und Energiefonds des Bundes – Abwicklung durch die Österreichische Forschungsförderungsgesellschaft FFG

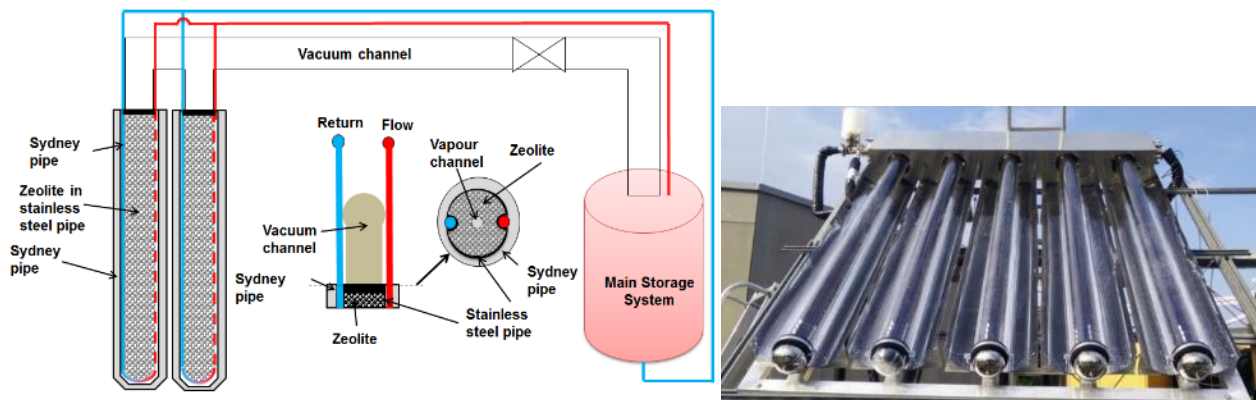


Figure 2: Concept of sorption collector applied as charge boost storage

The performance of the sorption collector is tested experimentally under variation of the boundary conditions. First test results show that the thermal performance of the collector is not negatively influenced by the sorption material in the construction, but the storage system performance can be improved. Due to the charge boost technique the storage capacity of the zeolite could be used more efficiently and hence the energy density can be improved significantly. In Figure 3 the potential of improvement of the energy density by repeating the charge boost is shown.

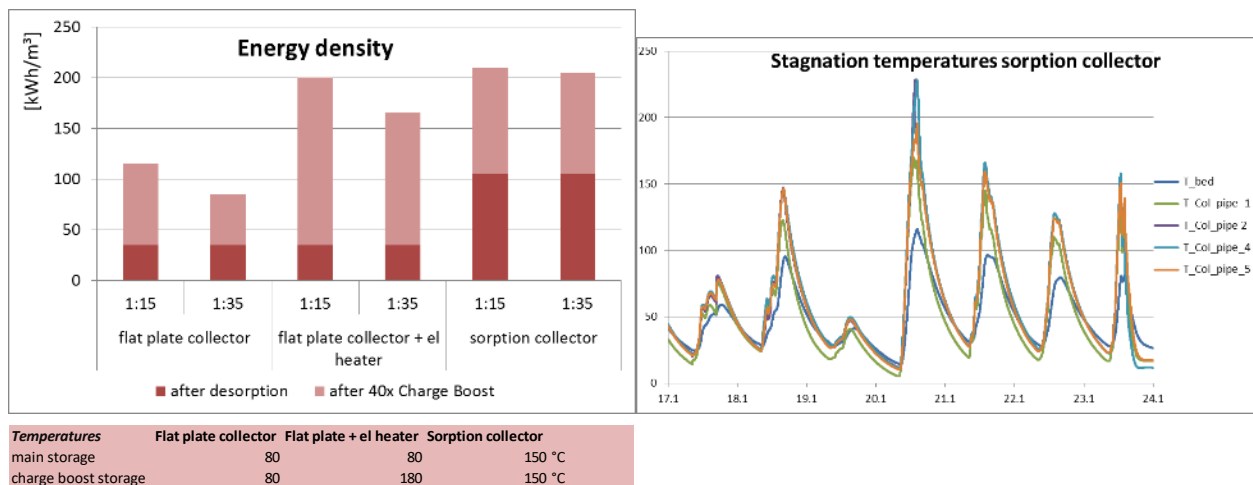


Figure 3: Left: Improvement of the energy density based on repeating the charge boost mode compared to the conventional desorption at the same temperature under different mass ratios between charge boost storage/sorption collector and main storage and different use cases (temperatures). Right: Measured stagnation temperature of the prototype sorption collector

In any use case the energy density can be doubled at least. The highest energy density can be achieved with the sorption collector combination, which achieves an energy density of > 200 kWh/m³. Also the combination of a flat plate collector and an electrical heater driven e.g. by PV electricity, is also a good alternative, achieving between 170 – 200 kWh/m³ (depending on the size).

The measured stagnation temperatures (Figure 3) show a temperature drop to 20 – 30 °C in the bed, due to the high radiation losses of the collector during the night and hence also a significant pressure drop is occurring, which is the ideal condition to perform the charge boost process. This way the day-night cycle can be used most efficiently.

On the outer side of the zeolite bed temperature peaks of $> 220\text{ }^{\circ}\text{C}$ and inside zeolite bed of $115\text{ }^{\circ}\text{C}$ could be observed. The temperature difference between inside and outside is due to the low heat conductivity of the material. This is the reason why a lower amount of water vapour could be removed than expected in the calculations (see Figure 4), meaning that the heat conductivity in the collector is an important issue to improve to achieve high performance.

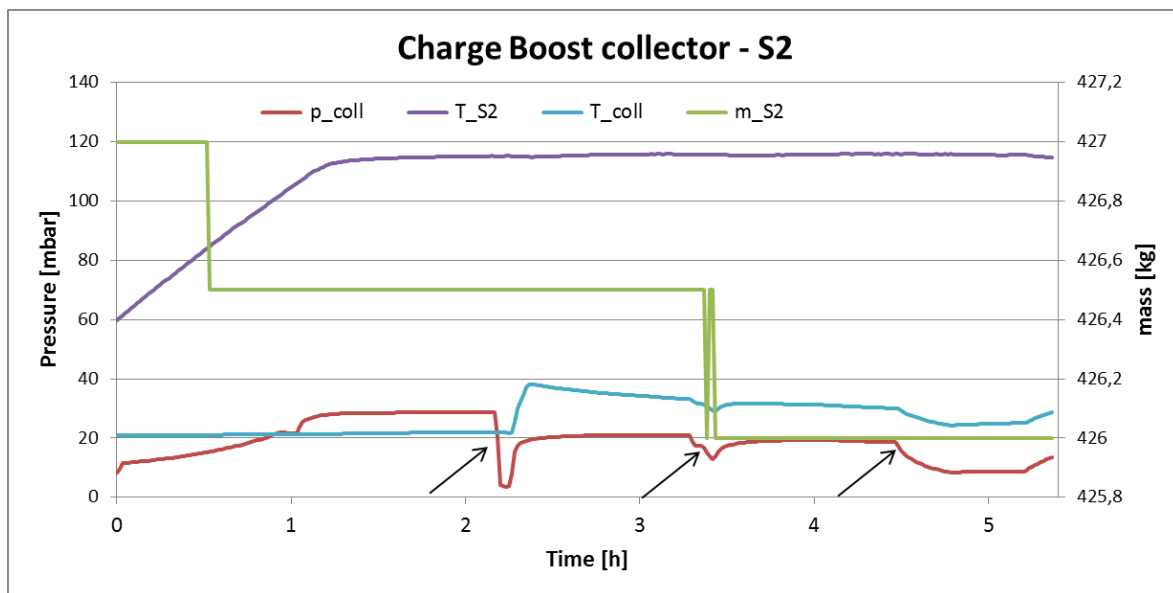


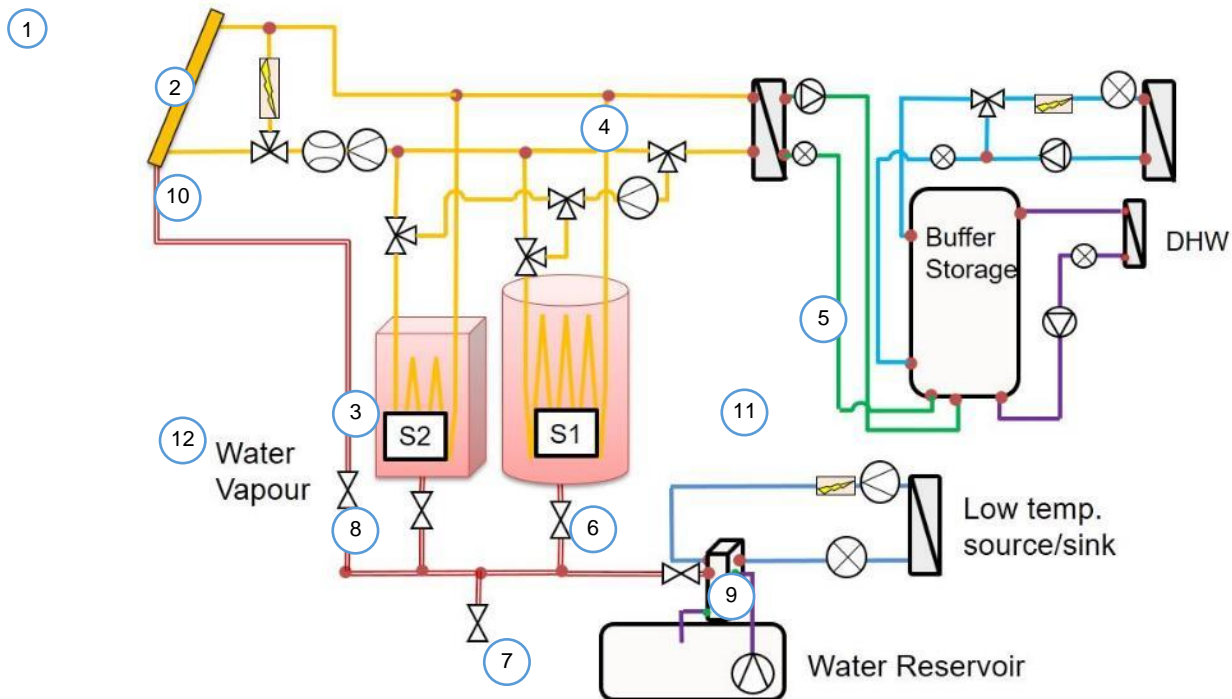
Figure 4: Charge boost experiment of collector and S2

Figure 4 shows the result of once charge boost process (about 40 are planned per year) that with starting conditions of $T_{\text{coll}}=20\text{ }^{\circ}\text{C}$, $p_{\text{coll}}=9\text{ mbar}$, $T_{\text{S2}}=115\text{ }^{\circ}\text{C}$, $p_{\text{S2}}=20\text{ mbar}$ the water concentration of $x_{\text{S2}}=18.4\text{ }%$ could be reduced to $17.74\text{ }%$ ($\pm 1\text{ kg}$ water vapour). The charge boost is applied about 40 times per year and decreases the water concentration level of the main storage (increase of state of charge) systematically. Nevertheless, the feasibility was proven successfully, the full performance could not be achieved. To achieve better performance, the construction has to be optimized to improve the heat transfer in the sorption material, and in a way that no condensed water stays in the pipings between sorption collector and main storage.

In addition, it was observed that a proper construction is necessary to prevent any damage to the glas Sydney-pipes used for the sorption collector.

3.1.1 System setup

The design of the storage system can be seen in Figure 5. The main system components are named below. The different colours in Figure 5 indicate the different loops. Whereas the red line indicates the vapour loop which is under vacuum, the other loops are hydraulic loops. The complete system combines all storage elements necessary in a real house. For system tests, it was focused on the interdependency of main storages and sorption collector. The room storage was not included for the system tests and annual simulations.



- | | |
|---------------------------|-------------------------|
| 1) Sorption collector | 2) Electric heater |
| 3) Sorption storage tanks | 4) Heat exchanger |
| 5) Buffer storage | 6) Evaporator/Condenser |
| 7) Water reservoir | 8) Pressure sensor |
| 9) Heat meter | 10) Flow meter |
| 11) Pump | 12) Valve |

Figure 5: System design of laboratory storage system and its main components.

The working principle is explained in the following:

Desorption (charging):

- The collector heats up the fluid in the solar circuit (Figure 6 yellow loop), which is pumped into the fixed bed heat exchanger of the main storage tank.
- The material inside the tanks heats up and water vapour in the material releases. Due to the lower pressure in the Evaporator/Condenser (E/C) unit the vapour flows through the vapour circuit (red) to the Evaporator/Condenser.
- The water condenses with help of the low temperature heat sink and flows into the water tank.

Adsorption (discharging):

- Water from the water tank is pumped up to the E/C, where it evaporates, again with the help of the low temperature heat source
- The main storage is on a very low pressure level due to the dry and cold sorption material. Therefore, the vapour flows from the E/C to the main storage
- As soon as the vapour gets in contact with the material the adsorption process starts and heat is released. This heat is transferred to the fluid in the solar circuit via fixed bed heat exchanger and then further transferred to the buffer storage.

- From there the heat is used for space heating or domestic hot water preparation

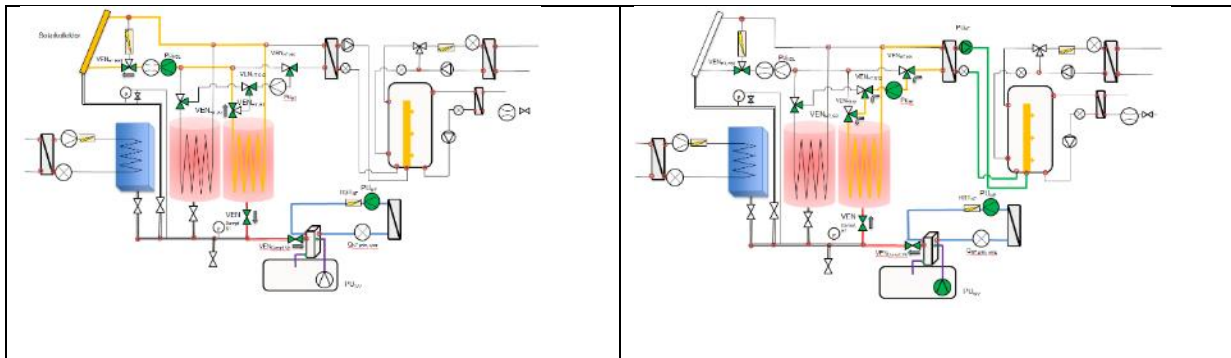


Figure 6 : Schematic flow during desorption (charging) process on the left side and schematic flow during adsorption (discharging) process on the right side

Charge boost:

The charge boost method is used to further dry (desorb) the main storage and to increase adsorption capacity of the material by using the pressure difference of two storages at different temperatures. Therefore, the system is extended by a second, so called charge boost storage.

- The method is applied after full dehydration of both storages
- The charge boost storage is cooled down while the main storage is kept at high temperature
- Due to the much lower pressure in the dry and cold charge boost storage than in the dry and hot main storage the pressure difference is used to further dry the main storage. This is possible until the pressures of the storages are equal
- The charge boost storage gets adsorbed during the process, and needs to be desorbed again to bring it to the initial conditions
- The charge boost process can be repeated

The sorption collector, which is filled with the same material as the main storages zeolite 13XBF, acts as an external charge boost storage to further dry the main storage. During charge boost the hot main storage is releasing water vapour, which flows to the cold, dry collector material, because of the pressure difference. On the next sunny day, the material in the collector is desorbed again directly in the collector. This way the main storage can be further dried step by step. One complete cycle of desorption of the collector material and charge boost lasts 24 hours and can be repeated several times. The result is a higher state of charge, resulting in a higher amount of stored energy.

The sorption collector has the advantage that the sorption material is directly desorbed in the collector, which means that it is desorbed at the highest possible temperature resulting in a high state of charge. Tests proved that the thermal performance of the collector remains high also when the collector is filled with sorption material.

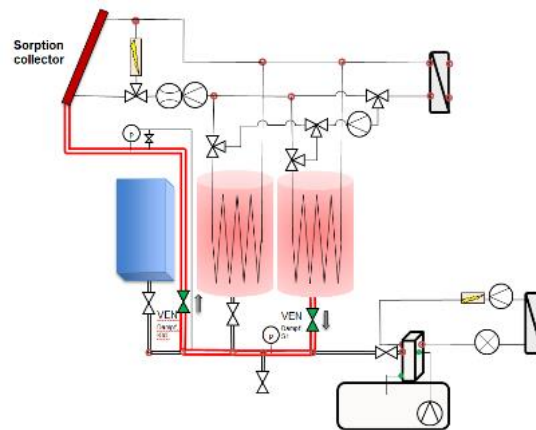


Figure 7 : Schematic vapour flow during charge boost of the main storage by the sorption collector on the left side

3.2 Control Strategy

For the system operation a sophisticated control strategy was developed to automatically operate the storage system. In total 11 different operation modes are possible and to guarantee a proper operation they have different priorities shown in Figure 8.

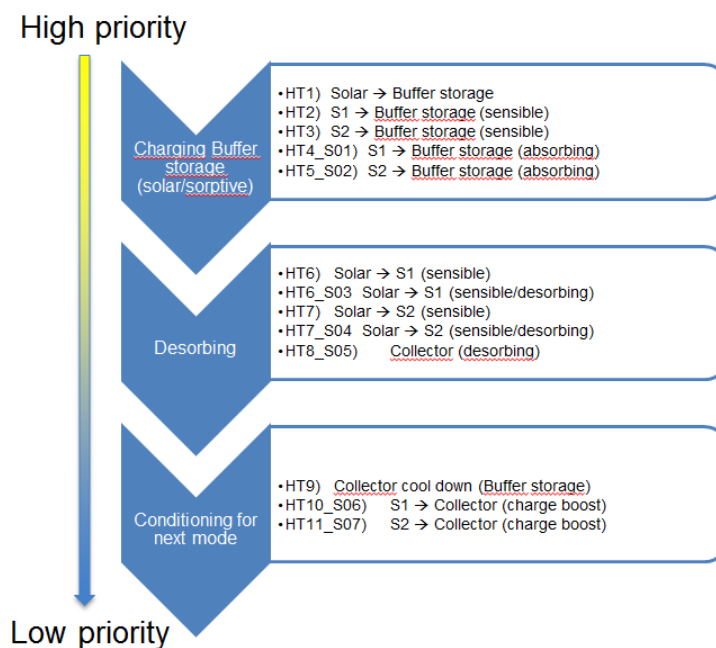


Figure 8: Priority List of operation mode for automated control

The highest priority of all operation modes is the charging of the buffer to guarantee a high level of comfort and reliability. First operation mode is direct charging of the buffer with heat from the collector. If no heat is available from collector then one of the sorption storage modules is discharged (adsorbed) and the heat is extracted to charge the buffer.

If there is solar heat available and the buffer already heated up to a certain temperature level, the surplus is used to charge the sorption storage. It is charged with sensible heat and as soon as the

pressure in the storage p_{S1} or p_{S2} is higher than the pressure in the condenser p_{cond} , the vacuum valve opens and the desorption starts. As soon as $p_{cond} = p_{S1}$ (or p_{S2}) the valve is closed again. After charging of the storage modules S1 and S2 it is possible to desorb (charge) the sorption material in the collector. During day the sun heats up the collector material and as soon as $p_{coll} > p_{cond}$ the vacuum valve is opened and the collector is desorbed. As soon as the collector is dried and $p_{coll} \leq p_{S1}$ the valve closes. The charge boost starts by opening the vacuum valves between storage module S1 or S2 and the collector. **Simulation results**

The control strategy described in the previous section was implemented in the simulation model for annual simulations in TRNSYS.

The annual energy balance for the basic configuration (20 m² collector area, 2 sorption stores with a total volume of 4 m³) is shown in Figure 9. With the definition in Equation 1 this system achieves a solar fraction of 80.9 %. The electrical heaters have to provide auxiliary energy Q_{aux} of 1061 kWh, in order to cover the total useful energy demand for heating Q_{SH} and domestic hot water Q_{DHW} of 5158 kWh.

$$SF = 1 - \frac{Q_{aux}}{Q_{SH} + Q_{DHW}} \quad \text{Equation 1}$$

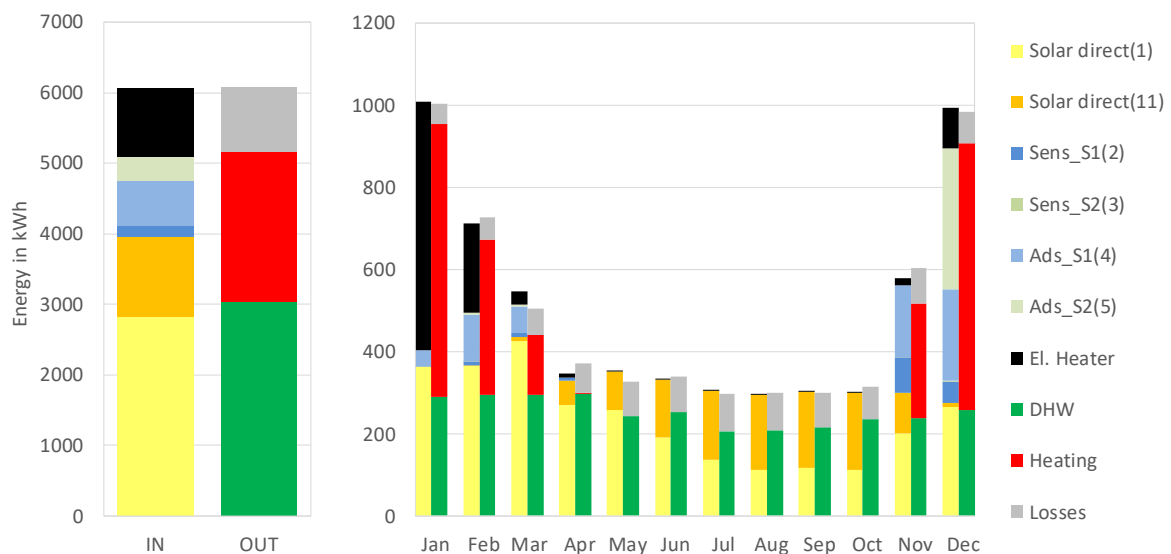


Figure 9: Annual (left) and monthly (right) energy balance for the system (basic configuration, SFH15)

Figure 9 shows that from April to October the energy demand can be almost fully covered by direct solar operation (modes 1 and 11 as described in Figure 8). Also from November to April a large fraction of the demand is contributed by direct solar. In November and December it is possible to cover the majority of the remaining energy demand with the two sorption stores¹, whereas their contribution is lower from January to March.

This is also reflected in Figure 10, which shows the course of the temperatures and water concentrations of the two sorption stores. Charging (drying) takes place from March to August, and discharging mostly

¹ Ads_S1, Ads_S2, Sens_S1, Sens_S2 → the operation modes as described in **Fehler! Verweisquelle konnte nicht gefunden werden.** are indicated in brackets in the legend of the figure

in November and December, whereby both stores are almost discharged at the end of the year. The water concentration reaches about 4 % (fully charged) and about 31 % (fully discharged) in both stores.

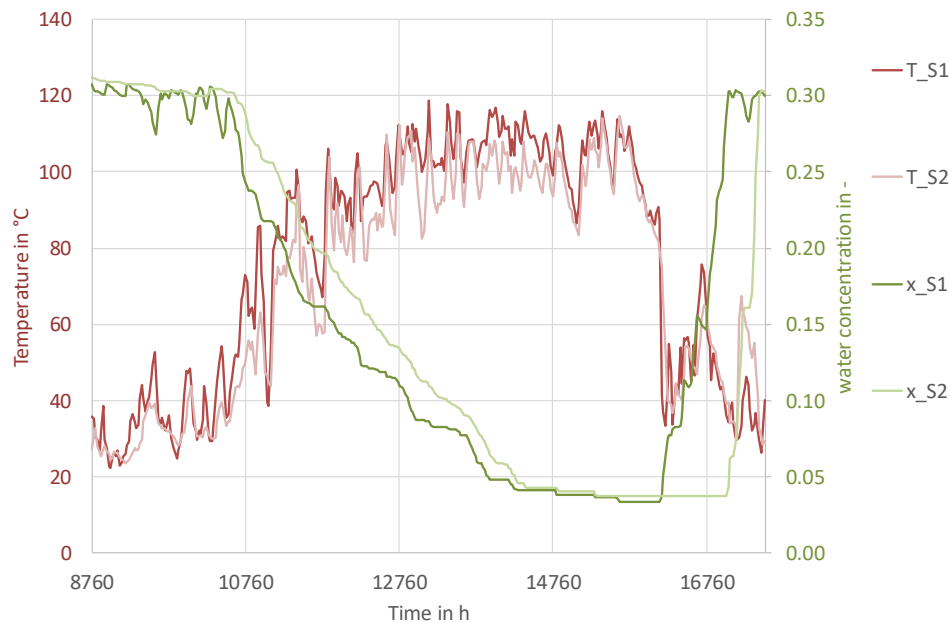


Figure 10: Temperatures and water concentration in the two sorption stores (daily average values) for the basic configuration, SFH15

The energy balance of sorption store S1 is shown in Figure 11. It can be seen that a large fraction of the drying of the store (ca. 69 %) is done via the charge boost mode (HT12), while about 31 % is done via “conventional” desorption (HT6).

Parameter variation for SFH15

In order to analyse the influence on the system efficiency a variation of different parameters was performed.

The collector area and the storage volume were varied from 25 to 40 m² and from 4 to 8 m³ respectively for SFH15, the results are shown in Figure 12. It can be seen that the solar fraction increases both with the collector area and the storage volume. The maximum solar fraction achieved with the simulated configurations is 98.6 %. As an example, Figure 11 shows the energy balance for the system with 30 m² collector area and a storage volume of 8 m³. Compared to the basic configuration (Figure 9) a larger fraction of the total heat demand can be covered by direct solar heating (70 % compared to 65 %). The sorption storage can cover the majority of the remaining heat demand during the winter months (29 % of the total heat demand compared to 19 % in the basic configuration).

Energieforschungsprogramm – 4. Ausschreibung

Klima- und Energiefonds des Bundes – Abwicklung durch die Österreichische Forschungsförderungsgesellschaft FFG

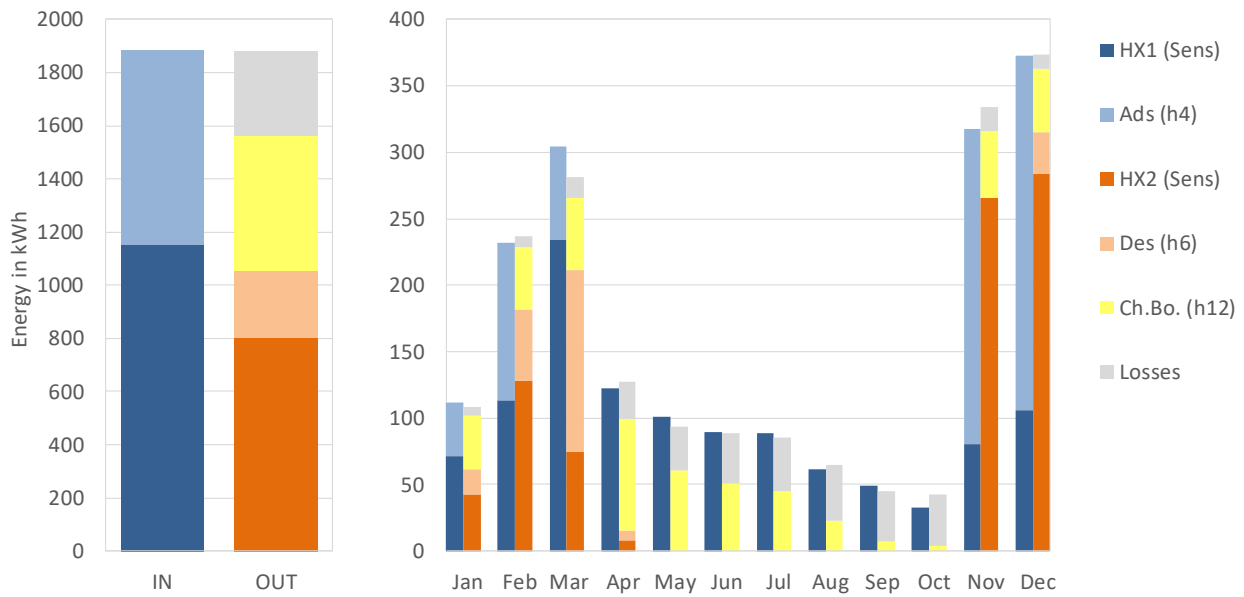


Figure 11: Annual (left) and monthly (right) energy balance of store S1 (basic configuration, SFH15)

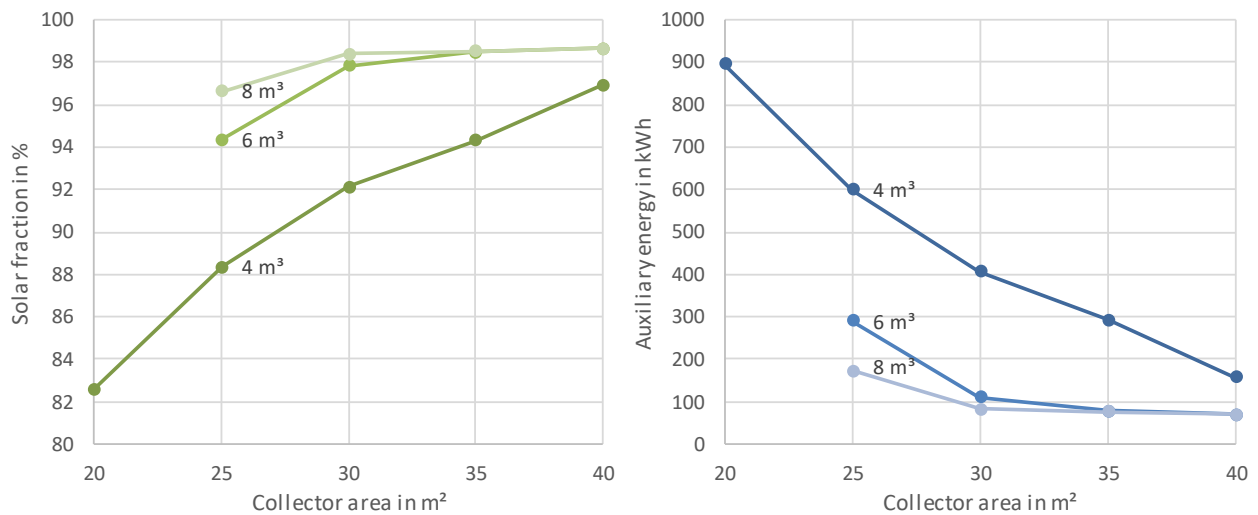


Figure 12: Solar fraction (left) and auxiliary energy (right) for different collector areas and sorption store volumes for SFH15

4 Line B: Heat storage for car battery temperature conditioning

The goal of Line B is to develop a thermal management for batteries in electric or hybrid vehicles based on sorption thermal storage technology. We focused on hybrid vehicles, where waste heat of the combustion engine can be re-used to charge the thermal storage. The work in the project included definition of the boundary conditions and of the requirements on the thermal storage, tool and test rig development for material selection, design of critical components (adsorber, evaporator/ condenser and vacuum vessel), system design, dedicated experiments for the critical components and the entire storage system, modelling of the components, construction of a co-simulation interface and simulation of the thermal storage integrated in the vehicle.

4.1 Boundary conditions and system design

4.1.1 Battery- Definition

Within the battery development and integration, automotive manufacturer faces two main challenges in order to guarantee thermal safety of battery systems. First, the perpetuation of lifetime and performance targets at low ambient temperatures. Second, the limitation of temperature rise due to cell heat losses at high ambient temperatures. Because of the wide possible temperature range of the environment (-20°C to 40°C in the scope of this project), the main application areas have to be extracted in order to focus on defined operating points and strategies. This approach is essential for the target definitions of the heat storage system.

In the beginning, targets of the thermal storage system requirements have to be elaborated and components have to be dimensioned, for e.g. the capacity of the thermal storage that fits actual requirements of the battery system itself and its management. To simulate and validate a proper behavior of the overall system, including powers and heat flows as they occur in reality, it is necessary to define boundary conditions and requirements. Therefore, the battery system should be able to fulfill the following specifications.

Driving range: 200km

Mean energy consumption 14kWh/100km

4.1.2 Requirements of the Components

There is a need to define all components, which are used in a coolant circuit of a BEV, RX or a vehicle powered by a conventional powertrain. It is possible to use a lot of components in all kind of different vehicle concepts. All requirements regarding the A/C circuit needs to be defined within the SiL simulation, due to a huge amount of dependencies of the cabin model and the ambient temperatures

Cooling system battery:

max. power: 3kW

Inlet temperature coolant: 10°C

Volume-flow: 20 l/min

Outlet temperature coolant: 12,5°C

Evaporator (coolant/refrigerant):

Inlet temperature coolant: 12,5°C

Outlet temperature coolant: 10°C

max. power: 3kW

Volume-flow coolant: 20 l/min

Refrigerant: R134a

H1 (HEX ambient, coolant/air):

max. power: 4kW

Inlet temperature air: 30°C

Outlet temperature air: 40°C (as low as possible)

Volume-flow coolant: 20 l/min

Waste Heat HX (coolant/coolant):

max. power: 4kW

Inlet temperature coolant (Input from ICE): 95°C

Outlet temperature coolant (output to thermal storage): 90°C

Volume-flow: 20 l/min

Thermal storage HX:

max. power: 4kW

Inlet temperature coolant: 90°C

Volume-flow: 20 l/min

4.2 Materials selection and development

Work package 2 started with an extensive literature research on candidate materials. Since heating and cooling is required, phase change materials can be excluded, and the literature research focused on thermochemical materials (TCM), in particular on sorption materials. This is because most other kinds of TCM are either not yet sufficiently explored / difficult to handle in small system setups (e.g. fluidization is usually performed on larger scales), and/or come with significant security issues such as toxicity or corrosion. Since material properties are reported in literature in different ways, where the essential properties for the considered application are difficult to extract and compare, a calculation tool was built up in Python. This tool takes any equilibrium data on sorption material pairs and fits the characteristic curve according to the Dubinin theory, an example is shown in Figure 13, right hand side.

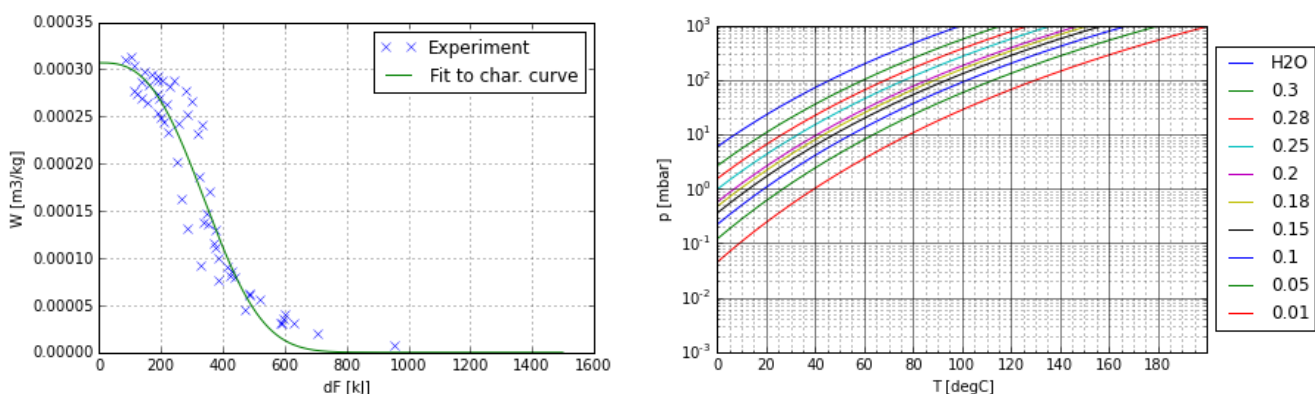


Figure 13: Experimental data on SAPO-34 and water from literature, and fit to the characteristic curve (left) and calculated isosters for this system (right). The legend for the isosters gives the corresponding water loads.

The literature data and the tool were applied to evaluate candidate material for the following three scenarios:

- Scenario 1 (**S1**): Plug-in hybrid; Exhaust gases of combustion engine used for desorption
- Scenario 2 (**S2**): Plug-in hybrid; Fuel-cell provides temperature for desorption

- Scenario 3 (**S3**): All-electric vehicle; Thermal storage electrically desorbed when battery is charged

In Table 1 the temperature levels for this operation mode for the different scenarios are summarized.

Table 2 shows the corresponding calculated adsorption capacity and energy density for a short list of promising candidate materials.

Table 3 gives further details such as costs.

Table 1: Temperature levels of different scenarios for cooling purposes in summer

Scenario	T _{des}	T _{cond}	T _{ads}	T _{evap}
S1	60	30	30	10
S2	90	30	30	10
S3	150	30	30	10
S3a	180	30	30	10

Table 2: Adsorption capacity and energy density for short list for material selection

Name	Adsorbate	Ads. capacity (S1/S2) [kg _{fluid} /kg _{mat.}]	Energy density (S1/S2) [Wh/kg _{mat.}]	Ads. capacity (S3/S3a) [kg _{fluid} /kg _{mat.}]	Energy density (S3/S3a) [Wh/kg _{mat.}]	Source
MB3A	Water	0,07/0,145	46/95	-	-	[1]
RD2060	Water	0,08/0,15	52/98	-	-	[1]
Sorbead R	Water	0,08/0,14	55/97	-	-	[1]
Sylobead SG B 127	Water	0,06/0,125	41/86	-	-	[2]
RD-type silica*	Ethanol	0,04/0,09	-	-	-	[3]
AQSOA Z02	Water	0,03/0,23	25/181	-	-	[4]
AQSOA Z05	Water	0,04/0,04	31/31	-	-	[4]
13XBF	Water	-	-	0,15/0,2	145/193	[5]
13XBF	Methanol	-	-	0,055/0,085	43/66 [▲]	[5]
13XBF	Ethanol	-	-	0,05/0,06	37/44 [◇]	

*...general RD-type silica gel, no producer defined, serves only as rough comparison to the silica gel-water pair

[▲]...binding energy of about 1700 kJ/kg_{methanol}

[◇]...due to higher mole weight than methanol a binding energy of 1800 kJ/kg_{ethanol} is assumed

[1] Ng K.C., "Experimental investigation of the silica gel-water adsorption isotherm characteristics", Applied Thermal Engineering, no. 21, pp. 1631-1642, 2001

[2] Wagner W. et al, "Modularer Energiespeicher nach dem Sorptionsprinzip mit hoher Energiedichte (MODESTORE), Gleisdorf, 2006.

[3] Arnoldsson J., "Adsorption chillers - uptake of Ethanol on Type RD Silica gel", Linköping, 2012.

[4] Kayal S. et al, "Adsorption characteristics of AQSOA zeolites and water for adsorption chillers", International Journal of Heat and Mass Transfer, no. 92, pp. 1120-1127, 2016.

[5] Jänchen J. et al, "Adsorption of water, methanol and acetonitrile in ZK-5 investigated by temperature programmed desorption, microcalorimetry and FTIR", Thermochimica Acta, no. 379, pp. 213-225, 2001.

Table 3: Further details for short list for material selection

S	Material	Name	Producer	Shape	Thermal Cond. [W/m*K]	Stability (number of cycles)	Price**
1,2	Silica gel	MB3A	Fuji Silysia Ltd.	Beads	0,174	permanently stable*	~12[€/kg] [◇] ~11[€/kg] ¹⁰⁰⁰
1,2	Silica gel	RD2060	Fuji Silysia Ltd.	Beads	0,198	permanently stable*	~10[€/kg] [◇] ~9[€/kg] ¹⁰⁰⁰
1,2	Silica gel	Sorbead R	BASF SE	Beads	0,2	permanently stable*	12,5[€/kg] 7,95[€/kg] ¹⁰⁰⁰
1,2	Silica gel	Sylobead SG B 127	Grace Davison	Beads	0,14-0,2	permanently stable*	~6[€/kg] ^Δ 4,15[€/kg] ⁵⁶⁰
1	SAPO-34	AQSOA Z02	Mitsubishi Plastics	Powder/ Pellets	0,13	>~1.000.000	120[€/kg] [▲] 89[€/kg] ¹⁰⁰⁰
2	AIPO-18	AQSOA Z05	Mitsubishi Plastics	Powder	0,12	>~200.000	120[€/kg] [▲] 89[€/kg] ¹⁰⁰⁰
3	Zeolite	13XBF	CW Bad Köstritz	Pellets	0,58	>~2.000	4[€/kg] ¹⁰⁰⁰

*...considered as permanently stable due to low working temperatures and highly stable structures

**...manufacturer's data

◇...min. purchase of 20kg (MB3A)/25kg (RD2060)

Δ...min. purchase of 140kg

▲...plus 120€/10kg delivery costs; Facility for commercial production in operation since short time -> price is expected to decrease in future

¹⁰⁰⁰...price per kg when purchasing 1000kg

⁵⁶⁰...price per kg when purchasing 560kg

It can be seen that the obtained results for scenario 1 ($T_{des}=60^{\circ}\text{C}$) are relatively poor for all examined materials, indicating that this configuration possibly won't be able to fulfill the performance requirements of the considered application. Alternatively it should be clarified whether the boundary conditions e.g. on T_{evap} could be relaxed somehow. For scenario 2 ($T_{des}=90^{\circ}\text{C}$) nearly all materials using water as adsorbate are advantageous for the cooling purpose. Especially AQSOA-Z02 seems favorable. Due to the specific shape of the isotherms of AQSOA-Z05 only a small amount of water is adsorbed at the defined framework conditions. For example, if the evaporation temperature is increased, much higher values could be reached. Looking at scenario 3 ($T_{des}=150^{\circ}\text{C}$) and 3a ($T_{des}=180^{\circ}\text{C}$) the 13XBF-water pair also shows acceptable results for the adsorption capacity and high energy densities. In comparison to that, the adsorption capacity is very low when using methanol or ethanol as fluid. Based on these results, AQSOA-Z02 and water as fluid have been selected as baseline TCM for further developments in the project.

For some material properties, in particular those related to kinetics, the data present in the literature are too poor, also because of missing standards. Since kinetic aspects are directly related to the power of the system, a dedicated material test rig was constructed, the scheme of which is shown in Figure 14.

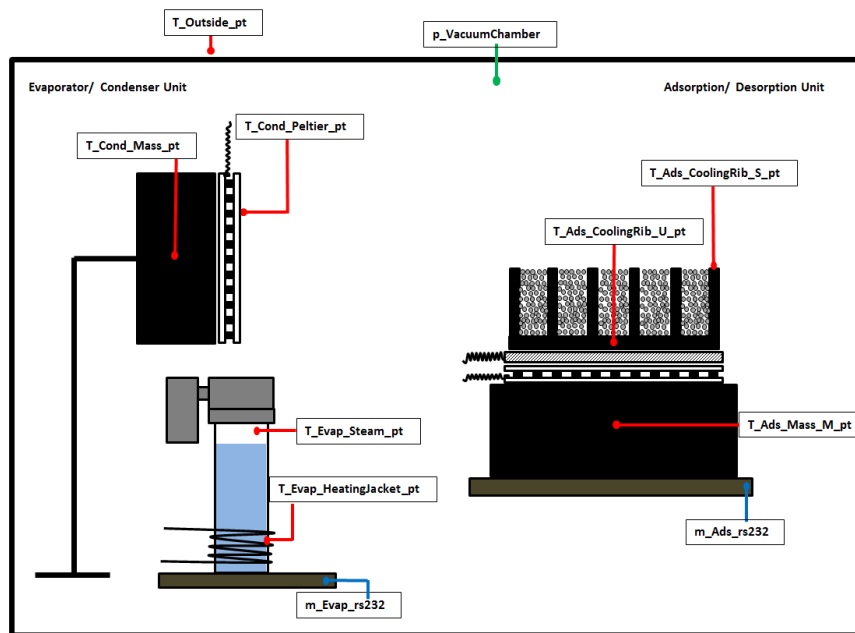


Figure 14: Scheme of the material test rig.

A second motivation is to assess the material's performance at an intermediate scale. The results serve to understand the difficulties in up scaling from lab reactor to demonstration systems. A closed sorption test rig with continuous temperature and state of charge measurement for about 100 g adsorbens was designed and assembled. The main challenge is to achieve sufficient precision considering measurement and control, in particular as these two often contradict each other. For example, controlling the temperature requires to remove the generated heat. If doing so with a heat exchanger and a heat transfer fluid, these piping will affect the scale and hence the measurement of the state of charge. In parallel to these investigations, the adsorbens Aqsoa Z02 was ordered from Mitsubishi and pelletized by AMMAG in synergy with Development Line C. The goal was to have these granules available in a suitable size distribution, to be able to fill them inside the coated fin heat exchanger in Work package 3, for a possible improvement of the performance.

AQSOA® Z02 zeolite powder has been pelletized by vacuum spray drying in fluidized bed using 10 % PVP (w/w) as a binder. PVP is stable up to 130°C and can be used in medium temperature applications. Resulted granules are shown in Figure 15.



AQSOA®-PVP < 1.2 mm

AQSOA®-PVP 1.2 – 2 mm

AQSOA®-PVP > 2 mm

Figure 15: Size fractions of AQSOA®-PVP pellets prepared in fluidized bed palletization.

4.3 Component Development

4.3.1 Component Design

The optimal component design depends on many boundary conditions given by the application, but also on material selection and the specific system design choice. For the present application, we choose a closed sorption system design, since this setup is in general able to provide heating and cooling without the need to refill process fluid. Correspondingly, the component design includes a fixed bed adsorber, an evaporator/condenser, a vacuum valve and the vacuum vessels.

Simply put, the performance of a thermal storage system is given by its energy and power capacity normalized to volume, mass or costs. The theoretical (equilibrium) energy content can be calculated in a straightforward manner by the amount of storage material and the boundary conditions for charging and discharging. For a thermochemical storage, the so-called four-temperature approach is a common method for that goal, which is performed based on the tool developed in Work Package 2. In practice, the actual energy content of the storage is somewhat lower, caused by different effects, all of which are related to non-equilibrium dynamics. In particular, requirements on a lower bound on the extracted power imply that only a fraction of the equilibrium energy content will be extracted in practice. The corresponding amount of reduction of the energy content may be estimated by adjustment of the boundary conditions corresponding to design calculations for the power to be extracted, and its lower bound.

The power which can be extracted from the storage system at certain boundary conditions is determined by its ability for sufficient heat and mass transfer. For the special case of a sorption thermal storage, three mechanisms are crucial for the dimensioning of the sorption heat exchanger: (i) mass transfer of the vapour through the bulk to the pores where the sorption takes place, (ii) sorption kinetics (mass transfer through the solid medium to the sorption site and binding process) and (iii) heat transfer from the sorption process to the heat transfer fluid. Similar aspects are important to be considered for an evaporator/condenser in a closed system (and the connecting vapour channel).

In general, a fixed bed adsorber design can be based on (A) filling a heat exchanger with adsorbents, (B) coating surfaces (e.g. the fins) of a heat exchanger with adsorbents, (C) direct crystallization of adsorbents on surfaces of a heat exchanger or (D) combinations thereof.

Calculations for the heat transfer in case of (A) have shown that the power requirements imply very small fin distances, such that only little volume is left for the actual TCM. In order to be able to provide both high energy and high power density, we therefore decided to choose a coated fin heat exchanger as baseline adsorber. Such an adsorber with coating of the TCM AQSOA-Z02 is manufactured by Mitsubishi Plastics, Inc.. This will in the following be considered as adsorber design (1). In order to increase the energy density, we investigated the effect of additional filling of granules between the coated fins, which will be called adsorber design (2). For a comprehensive comparison, we also consider an adsorber with direct crystallization, provided by Fahrenheit, called adsorber design (3).

The filling in design (2) has two effects on the power performance. On one hand, there is more active TCM, which might increase the performance. On the other hand, the tightly packed filling might introduce a pressure drop through the pack, decreasing the performance.

For the evaporator/condenser, several design approaches have been discussed. The main requirement is a large surface and good heat transfer while ensuring little volume and weight. As baseline design, we have chosen a thin lamellar heat exchanger, integrated into the water reservoir and partially flooded with water, when the system is full charged. So for discharging a partly immersed pool boiling occur, which will be enhance due to the many narrow gaps from the heat exchanger. However, during condensation these gaps can trap a certain amount of water in between during due to the capillary forces, so that the available heat transfer surface diminishes. In our case, condensation performance degradation is not expected, because a low water capacity is used for operation and the low capillary forces in the gaps of the heat exchanger, which were also tested in the lab. Beside of that, the heat exchanger has a high heat transfer surface for condensation and evaporation and the tubing's diameter are larger than the liquid level, which are very beneficial for the heat transfer between heating/cooling water and the distilled water. It can be also assumed, that the heat transfer inside the tubes is optimized by the manufacturer. All in all, the combination of compactness, low weight and sufficient performance makes the chosen heat exchanger suitable for the requirements. The design is shown in Figure 16.

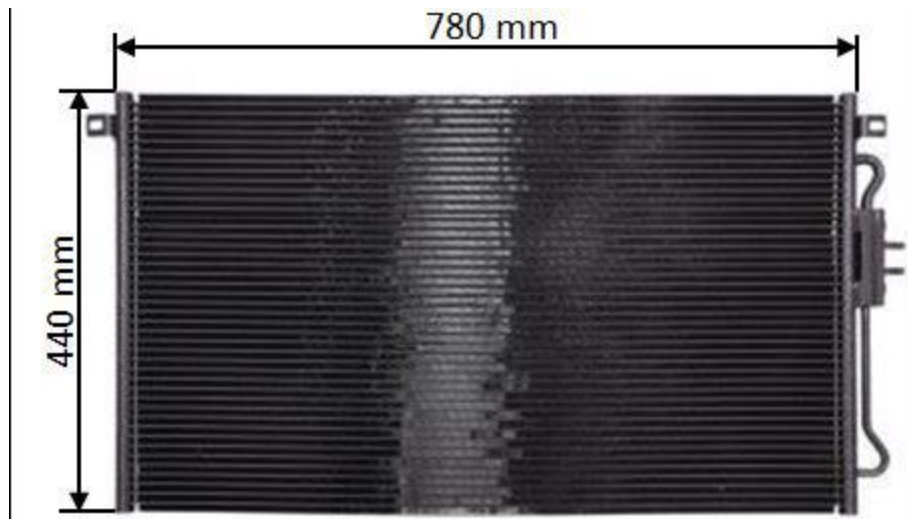


Figure 16: Evaporator/condenser design.

4.3.2 Dedicated Component Experiments

Various evaporator/condenser designs have been discussed and assessed experimentally in a dedicated test rig, targeting at a high power density at system level. Aiming at minimum weight and space consumption, a flat fin heat exchanger was chosen, as shown in Figure 17. As boundary condition in experiment, the vapour pressure has been fixed to 20 mbar, which was realized using an overdimensioned plate heat exchanger and a controller. The results are shown in Figure 18, where a cooling power up to 2.5 kW was observed. The cooling power is fairly constant over time and also over the filling level. For a space efficient system design, the vessels of the functional components play a major role. For this reason, rectangular shaped vessels have been investigated. The main obstacle in this respect are the vacuum forces, which have been assessed using FEM-calculations, as shown in Figure 17, right hand side. The rectangular vessel has been built for the evaporator/condenser and integrated in the thermal storage system.

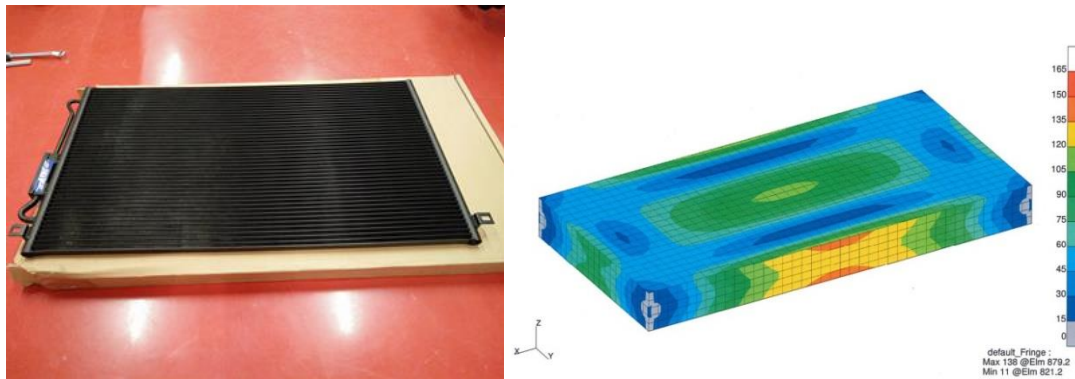


Figure 17: Evaporator/condenser (left hand side) and design of its rectangular vessel (right hand side).

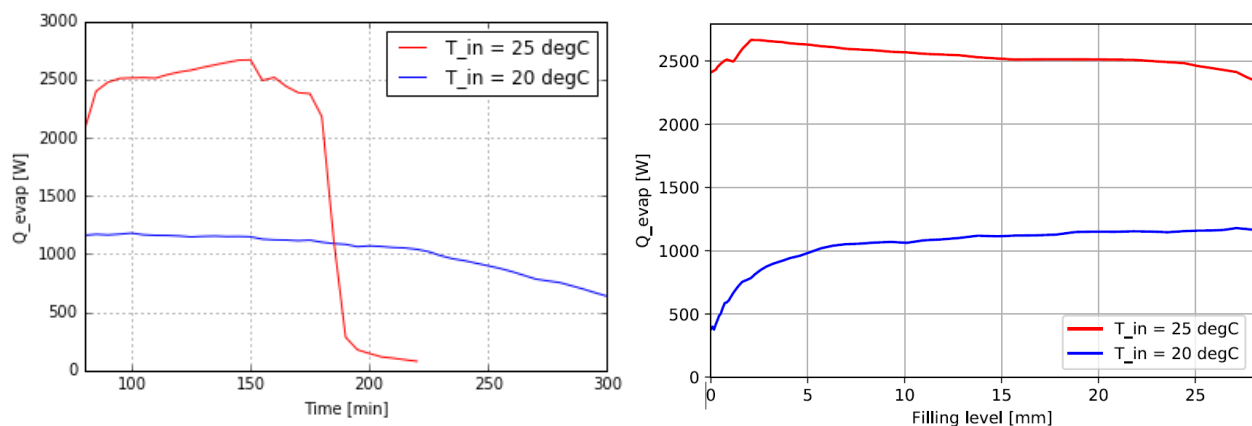


Figure 18: Experimental results for the evaporator. The cooling power provided by the evaporator is shown for a given environmental pressure of 20 mbar and two different inlet temperatures of 20°C and 25°C, respectively. The power is shown versus time (left hand side) and versus the filling level (right hand side).

The heart of the sorption storage system is the adsorber. The requirement for high power calls for efficient mass and heat transport, such that in any design, all adsorbents must be very close to the heat exchanger and vapour channels must be available in abundance. Three designs are investigated in this project (see Figure 19): (1) A coated fin heat exchanger; (2) the same coated fin heat exchanger including an granulated adsorbents filling; (3) metal fibers with direct crystallization. Design (1) is manufactured by Mitsubishi Plastics, Inc.; for design (2) the matching adsorbents AQSOA-Z02 was orderd from the same company, and pelletized within the project consortium; design (3) was provided by Fahrenheit, which is a world-leading company for this kind of adsorber design.

As already mentioned the granules for design (2) have been pelletized by AMMAG in synergy with Development Line C. The corresponding adsorbents in powder form was delivered by Mitsubishi Plastics Inc. and is therefore the same as in the coating of design (1) and (2), while the binder is expected to be different. The adsorbents in design (3) is a SAPO34 as well, however, manufactured by Fahrenheit in the process of the direct crystallization. Slight differences can thus be expected in the material performance. The three adsorbers have been assessed in the storage system test rig, including the evaporator described above. The experimental results indicate that design 2, the coated filled adsorber, shows the best performance in terms of high energy and power. We conclude that the pressure drop introduced by the packed bed of the granules has a minor effect on the power. We further note that design (3) targets at a longer stable power output instead of a high brief one. Further results are shown in the context of system experiments.

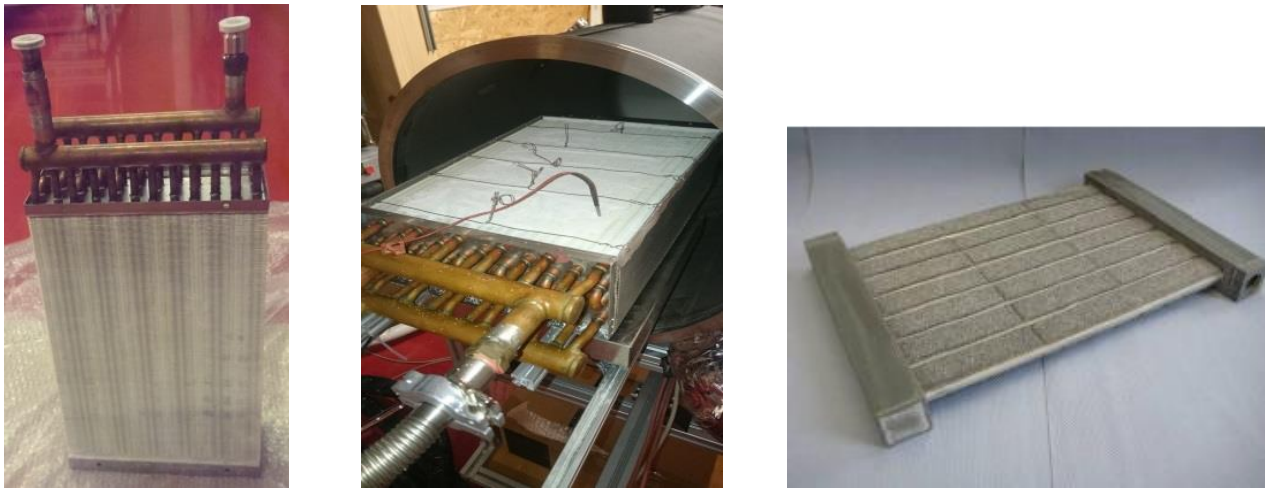


Figure 19: The three adsorber designs investigated. Left: Plain coated fin adsorber provided by Mitsubishi Plastics Inc.; center: the Mitsubishi coated adsorber filled in addition with granulated adsorbents; right: schematic picture of an adsorber with direct crystallization of adsorbents, provided by Fahrenheit.

4.4 Storage system development

4.4.1 Storage system design

The storage system considered here is a closed vacuum storage system with a water reservoir, in order to have water available for cooling through vaporization and vapor for heating through adsorption, both in discharge mode. It can be distinguished between different types of systems according to their number of thermal storages (= vessels). In this project one or two vessel systems have been designed and are examined in more detail. Both concepts provide specific advantages and drawbacks which are discussed in the following sections. Further on, the different modes of operation are presented and explained with the help of graphics. Finally an alternative system, which focuses a so called direct evaporation method is briefly introduced.

The one-vessel system consists of one thermal storage (S1) in which the adsorption material is stored (see Figure 20). The adsorption heat is extracted with an integrated fixed bed heat exchanger. The connected evaporator/condenser unit which is coupled to an adsorptive reservoir serves as low temperature heat source or heat sink during operation. An ambient air heat exchanger (H1) is used to dissipate or supply the heat for the adsorption process. The electrical battery is connected to the secondary circuit of a liquid-liquid heat exchanger (H2) which transfers heat or cold to the cells. In case of a plug-in hybrid, a liquid-liquid heat exchanger (HW) that is coupled to the internal combustion engine or to the fuel cell delivers the required energy for regeneration. It has to be mentioned, that this heat exchanger is not required in all-electric cars. In that case, this task is carried out by an electrical heating device (HD). Nevertheless, for a comparison of the different designs and to show the maximum complexity, only the entire systems are illustrated.

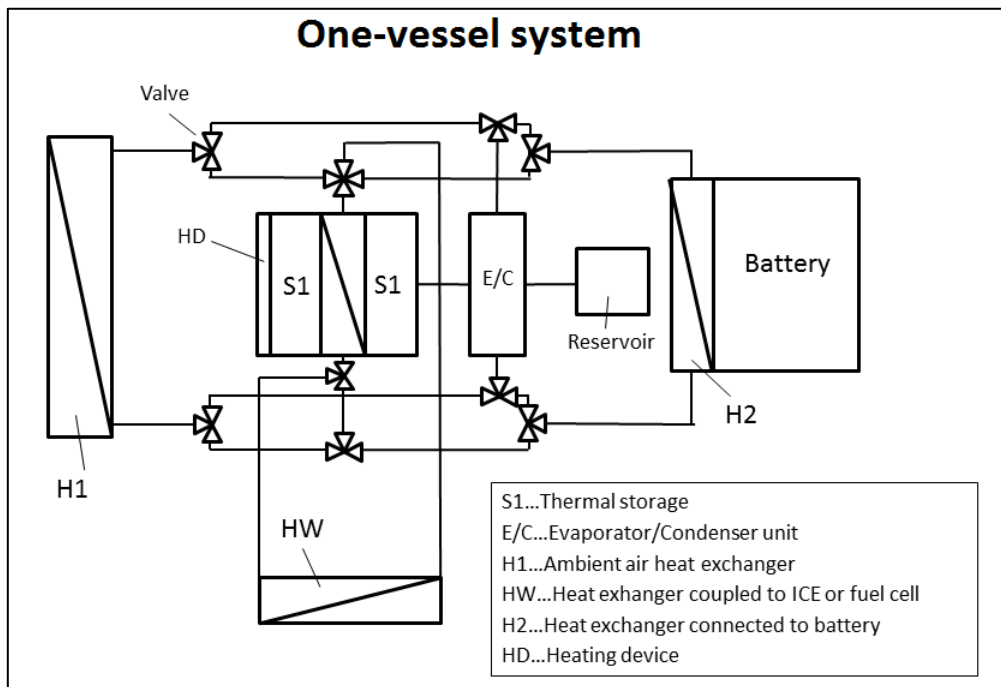


Figure 20: One-vessel system

Another possible design is the two-vessel system. It enables simultaneous cooling or heating and regeneration by the installation of a second sorption thermal storage which is in alternating operation to the first one. The system as it can be implemented in a vehicle is shown in Figure 21.

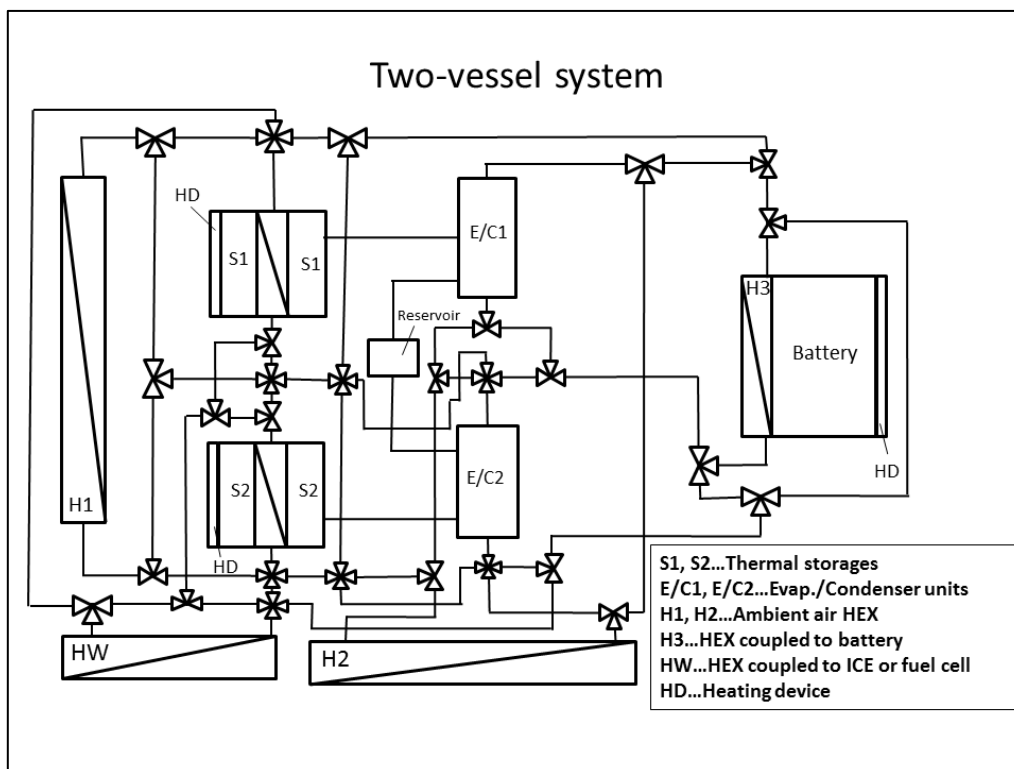


Figure 21: Two-vessel system

As it can be seen in the picture above, the complexity of this concept enhanced dramatically in comparison to the one-vessel variant. Several valves and circuitries as well as a comprehensive control concept are necessary to set up a functioning system. Besides the potential error rate the space requirements are increasing as well. Additionally to the second sorption storage, a second evaporator/condenser unit and a third heat exchanger has to be mounted.

Nevertheless, this configuration offers advantages as well. As an example, as already mentioned, one vessel can be charged while the other one is discharged simultaneously. As a consequence, the needed amount of adsorption material per storage and thus the capacity is reduced by a continuous alternating operation. The utilization of different types of adsorption material is also conceivable with such systems.

4.4.2 Storage system experiments

The storage system includes the adsorber, the evaporator/condenser, their vacuum vessels and a vapour channel including a valve between them. The storage system test rig includes heat and cold supply for both adsorber and evaporator/condenser and a control for the temperatures/power and the valve. A vacuum pump and a strategy to remove inert gases is also required. Such a system test rig was assembled in the third year, a picture of which is shown in Figure 22. The test rig is equipped with numerous temperature sensors, a scale to estimate the state of charge and pressure sensors at adsorber and evaporator. Charging and discharging experiments have been performed for various sets of boundary conditions.



Figure 22: Test rig for the storage system including adsorber, evaporator/condenser and rectangular vessel.

For charging, we considered a desorption temperature of 95°C and a condenser temperature of 15°C. Such boundary conditions are encountered, e.g., in the case of thermal management for hybrid vehicles, when the waste heat from the ICE coolant is used for desorption and the condenser is coupled to the ambient in winter or cooled by an AC device in summer. The vapour valve was closed at first, but opened when the adsorber temperature would exceed 70°C in order to avoid damaging the interior scale with the high humidity.. When opening the valve, a narrow power peak up to 20 kW is indicated by the

scale. This leads also to a drop of the adsorber temperature, since the heat supply cannot counter react sufficiently.

For discharging various scenarios have been considered, here results for evaporation temperatures of 25 °C. As already mentioned, such boundary conditions can be encountered, e.g. when the adsorber is coupled to the ambient in summer and the evaporator is used to cool the battery or the cabin. The opening of the valve at roughly 8:10 triggers the adsorption, which aligns the pressures in the system, increases the adsorber temperature level and decreases the evaporator temperature level. The various and heating/cooling powers respectively heat flows are shown as well. The operating window of useful cooling power is here defined to start by opening the valve and to end when the cooling power falls below 200 W. For the boundary conditions considered here, this window encompasses a period of 25 minutes, within which the maximum cooling power extracted was almost 2 kW, the total cold energy extracted was 400 Wh, and an average cooling power of almost 1 kW was found.

Thermal management in E-mobility requires not only cooling, but also heating capabilities. In winter the batteries should be pre-heated before starting the vehicle when the ambient temperature is below zero. A charged TCM storage can in principle provide both cold and heat. However, it acts like a heat pump with a time delay. Correspondingly, when discharging it for heating applications, heat is required (at somewhat lower temperature) for evaporation. Taking the latter from the ambient proves difficult when the ambient temperature is low, i.e. when the heat is most needed. This is a difficulty yet unsolved for this application.

We suggest to buffer the evaporation heat, exploiting a phase change of the process fluid. Evaporation and freezing takes then place at the same time, and the freezing enthalpy serves as evaporation enthalpy, which enables the storage to be discharged. Clearly, it is necessary to prevent spontaneous freezing of the process fluid before the discharging is triggered, which can be realized either by sufficient insulation, additives to change the freezing point, or supercooling.

We performed experiments using water as process fluid, which freezes at 0°C, providing a saturated vapour pressure of 6 mbar. This pressure suffices for discharging the heat storage and enables it to provide heat at 10-20°C. The experimental setup is defined by a preconditioning of all components to 10°C, opening the vapour valve and extracting heat at 10°C the adsorber while supplying no heat to the evaporator. We observed freezing in the evaporator during the process, in accordance with the temperatures and pressure measured.

*Table 4: Specifications and performance of the storage system corresponding to the three different adsorber designs. * denotes that the required volume and weight was estimated, assuming a compact vacuum vessel corresponding to the FEM calculations shown for the evaporator/condenser.*

	SAPO-34 [kg]	Volume [l]	Weight [kg]	Power average [W]	Total energy [Wh]
Empty Mitsubishi	2.5	(15.7) *	(9.8) *	958	415
Filled Mitsubishi	3.3	(15.7) *	(10.8) *	1067	549
Fahrenheit	2.5	15.4	15.5	482	337

Defining again a window by requiring a minimum heating power of 200 W, we observe a total extracted heat energy of 680 Wh, an average heating power of 1.35 kW and a peak heating power of 2.3 kW. The temperature of the adsorber increased up to 20°C.

For a scaling evaluation on system level, we determine the volume and weight of the entire system, or rather estimate these values assuming a compact vacuum vessel corresponding to the FEM calculations shown for the evaporator/condenser. This allows also for a comparison of the performance of the three different adsorber designs at system level. We define Key Performance Indicators (KPIs) corresponding to the energy/power density on the system level, i.e. all auxiliary components are accounted for. These measures are given in Table 4 and Table 5.

Table 5: Key Performance Indicators (KPIs) defined as energy/power density on the system level, i.e. all auxiliary components are accounted for.

KPIs	per volume	per weight
Cooling energy density	27 Wh/l	27 Wh/kg
Cooling power density	55 W/l	55 W/kg
Heating energy density	34 Wh/l	34 Wh/kg
Heating power density	68 W/l	68 W/kg

4.4.3 Storage system simulations

In order to re-use simulation models developed in Trnsys and Simulink, a co-simulation interface is necessary. A novel interface was constructed in the course of the project, exploiting an existing interface between Trnsys and Matlab “Type155” provided in the Trnsys standard library. Different versions of the interface have been constructed and compared to each other and to the openly / commercially available interfaces BCVTB and FMI. A simple case study involving the sorption storage was considered, and accuracy and computational performance as well as user friendliness and flexibility was discussed. An overview of the results is shown in Figure 23.

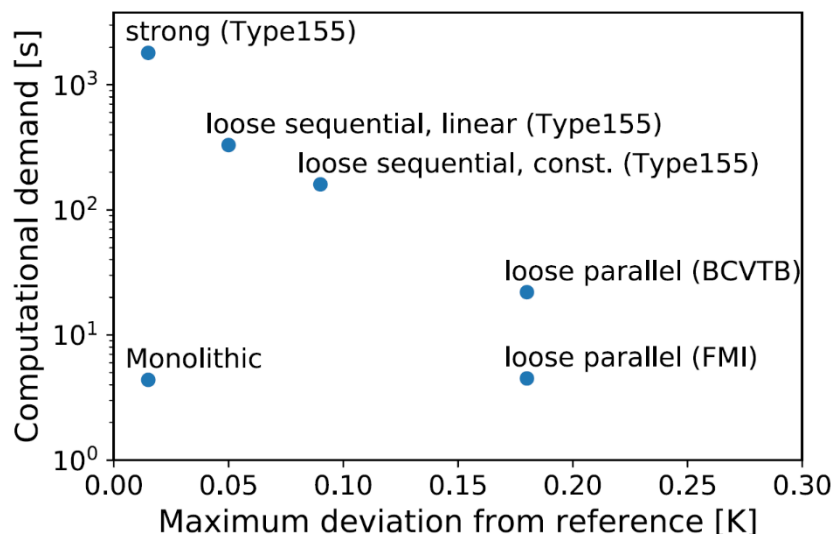


Figure 23: Overview of the performance of the different co-simulation interfaces and setups discussed for a simple case study involving the thermal storage.

For the actual system simulations, we decided to use FMI, as this interface is world-wide the most accepted standard for co-simulation. The entire system simulation built up in Simulink includes the various thermal components in the vehicle and the master for the co-simulation with the thermal storage.

4.4.4 Operation state of the storage in the simulation cases

1. Discharging of the storage. The cooling fluid that should be heated up flows through the adsorptive storage heat exchanger. The evaporation enthalpy required in the water reservoir needs to be provided by a secondary fluid that is conditioned with ambient conditions and flows through the heat exchanger in the water reservoir (the evaporator/condenser)
2. Charging of the storage. Sufficiently (for desorption) hot cooling fluid flows through the adsorptive storage heat exchanger, to dry the storage. The evaporation energy is provided by this fluid. In the water reservoir the condensation heat is released and needs to be carried away by a secondary fluid that is cooled with ambient conditions.
3. This case is very similar to Case 1. The thermal storage was also discharged but instead of only assuring a fast heating up of the combustion engine the battery was heated up first and afterwards the cabin and the combustion engine were heated.
4. Discharging the storage. The cooling fluid flows through the heat exchanger of the evaporator and loses heat to provide the evaporation with energy. A secondary fluid must carry away the condensation heat in the adsorptive storage and transfer it to the ambient air.
5. Switch between operation mode 2, to charge the storage with waste heat from the engine, and operation mode 4, to cool the battery while charging the storage.

Table 6: Summary of simulation results corresponding to the used cases described above

Used Case	Description	Results	Next Steps
1	Preheating combustion engine (Discharging)	@80°C time saving 26 sec.	Determine Sensitivity of the system
2	Cooling of combustion engine and regeneration of thermal storage unit (Charging)	11% energy saving for fan	Optimize Ratio P/E
3	Heating of a chilled battery (Discharging)	Heat up to 25°C time saving 80 sec.	Optimize Ratio P/E
4	Battery cooling during high ambient temperatures (Charging)	60 % of energy saving	Optimize Ratio of P/E through Simulation
5	Battery cooling during long-term driving applications (Charging and Discharging)		Optimize Ratio P/E, Operational Strategy

Different operating conditions for the storage were defined. In order to define at which point the thermal storage should be discharged to cool the battery and in what circumstances should it be charged.

For this, the following variables were monitored:

- battery temperature
- engine temperature
- state of charge of the store (water load)

Another problem is the small interval at possible coolant mass flows for the battery model where a solution of the model is possible. Therefore, no regulation for the coolant mass flow for the battery cooling could be implemented.

In order to keep the battery temperature at a maximum possible cooling capacity below a certain point would also be necessary to regulate the distribution of the load, between the combustion and electric motor. Again, there was a problem with the switching logic.

4.5 Control development

A sophisticated control is essential for an efficient thermal management involving many components. The main operation modes of cooling/heating of the battery and regeneration of the thermal storage are described in the former chapter covering the simulation results. The four operation modes defined in Deliverable D1B1 read:

- Mode A: Avoidance of extensive battery temperature rise during fast charging or at high ambient temperatures (see Case 4 during driving cycle)
- Mode B: Battery cooling for long-term driving applications (see Case 5)
- Mode C: Temperature rise of chilled battery. (This case was only tested at AEE Intec)
- Mode D: Regeneration of thermal storage unit (see Case 2 utilizing waste heat of the combustion engine)

The most important input variables for the system control are the battery state of charge (SOC), the thermal storage SOC and the various temperature levels in the system. The design of the system control depends on the achievable power and capacity of the thermal storage as well as on the chosen system concept.

Table 7: Temperature levels in vehicle

Battery	35°C
Power Electronics	70°C
Engine	95°C
Turbocharger	100°C
Driver/Passengers	20°C
Electrical Machine	80°C

Thermal systems in electric and hybrid vehicles operate with a higher number of components than equivalent systems in conventional vehicles. While thermal management of the combustion engine, transmission and the passenger cabin are implemented in well-known and proven way, the integration of electric motors, power electronics and the battery introduces new challenges for thermal management in automotive industry. The battery for example needs to operate at its well-defined temperature level. The electric motor on the other hand operates at different temperature level and the power electronics operates at yet another temperature level. The temperature and the humidity in the passenger cabin must assure a suitable comfort. This requires an air conditioning system, which again operates at different temperature level. Multiple levels of operational temperatures as shown in Table 7, require an effective thermal management of the overall vehicle. It must also assure that components operate at high efficiency in order to provide the best trade-off between the mileage and the passenger comfort. Since thermal processes are nonlinear in nature, the thermal management is a complex process Gregorčič et al. (2013).

Maximization of the various benefits of alternative propulsion systems can only be achieved by improving the entire system, i.e. overall vehicle operation. This can only be achieved by developing new breakthrough approaches and methodologies, which can be efficiently implemented first to electric passenger cars and then consequently to global transportation system. Alternative thermal storage systems can play a major role in achieving these ambitious goals. Integration of new thermal storage systems on its own will not provide the overall efficient operation. A new, model-based control strategies need to urgently be developed. This vision requires mergence of methods from a wide range of disciplines. These include techniques from computer science, machine learning, artificial intelligence, systems theory and their integration with established engineering design methodologies. Paradigms above all assume some form of model of the system and its operation. It is therefore of highest importance to develop suitable modelling procedures for modelling of storage systems.

4.5.1 Subsystem battery

The input/output behaviour of battery and its components is in general is nonlinear. This means that the thermal dynamic of the battery must be modelled utilizing nonlinear modelling techniques. Many modelling techniques which can be applied in this area have been proposed over the past years. Due to the complexity of thermal processes first principle models and their analytical approximations cannot be efficiently applied and hence a more flexible type of model needs to be utilized Gregorčič et al.(2017). It is common that black-box and grey-box models are used in thermal applications. A useful approach

similar to Wiener/Hammerstein principle has proven to provide good results. Wiener/Hammerstein assumes the nonlinear static part of the model, where the dynamic part is assumed to be linear. In practice this structure needs to be extended where the dynamic part of the model is also assumed to be nonlinear. Local Model Network (LMN) paradigm has shown good results in sufficiently capturing nonlinear dynamics. Hence the general representation of the nonlinear model structure is shown in Figure 24.

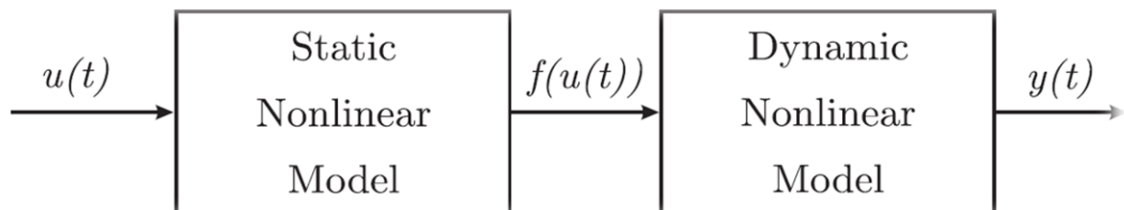


Figure 24: General representation of the nonlinear model structure.

4.5.2 Subsystem thermal storage

The storage system considered here is a closed solid sorption storage system including a water reservoir, in order to have water available for cooling through vaporization and vapour for heating through adsorption, both in discharge mode. It can be distinguished between different types of systems according to their number of sorption storages ("vessels" called in the following). System designs including one or two vessel and have been set up and examined.

4.5.3 Objective and system simulation design

The simulation environment in Matlab / Simulink is modular and completely parametric. The basic structure and data streams are shown in Figure 25 as a simplified block diagram. The vehicle model includes the important thermal components of the internal combustion engine, the battery and the passenger cabin, whereby each of the submodels can be parameterized in such a way that all defined vehicle types can be mapped. Thus, both a VKM, hybrid and electric vehicles can be represented with a total model.

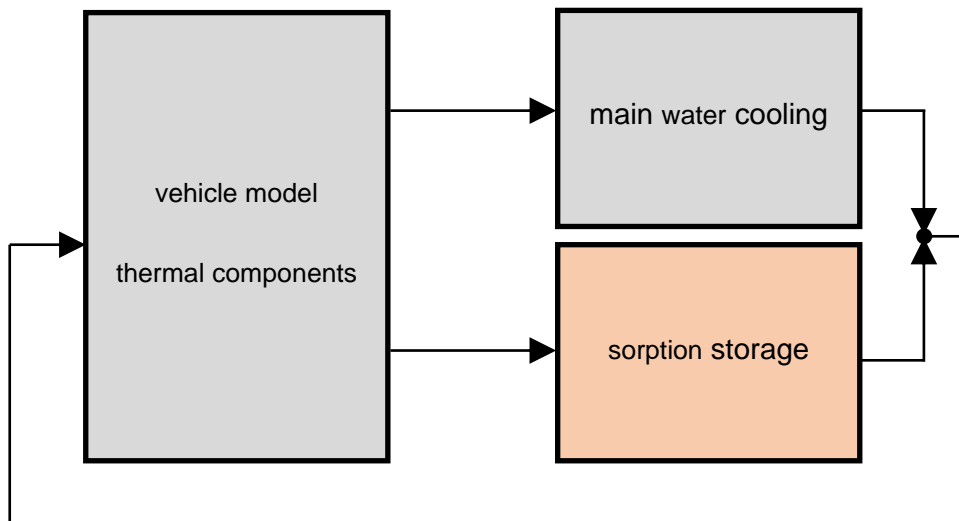


Figure 25: Basic structure and data streams.

An adaptive distribution of the coolant mass flow to sorption storage tank and main water cooler is necessary in order to dissipate any heat which is not required from the sorption storage via the HWK to the environment. In addition, the mass flow in some applications exceeds the maximum possible / sensible of the sorption storage.

5 Line C: Storage for efficient energy systems in railway vehicles

The general aim of DL-C is to develop an improved and experimentally verified thermal storage concept for the conditioning of the railway passenger compartments by adding functionality of thermal storage devices to the system. During the first year the application case was developed, the boundary conditions were collected and the basic concept (technical and thermodynamic) was made in WP1. During the second year, work in WP2 was conducted, testing environments were built and experimental verification of the selected storage materials together with basic (structural or functional) component parts tested (like storage material plus heat conducting structure). In the last two project years more measurements were done in the laboratory with the focus on the system and control strategies. Especially in this period also system simulations were performed.

5.1 Boundary conditions and system design

Boundaries for HVAC systems for railway applications

As for railway applications of HVAC (heating, ventilating, air conditioning) systems knowing the relevant regulations for the railway sector is necessary, they shall be mentioned in the following.

The boundary conditions are defined by:

- Passenger comfort
- Environment
- Reliability, maintainability and safety
- Fire protection
- Handling of refrigerants (HFKW) - halogenated fluorocarbons

Afterwards is a listing of the relevant regulations for the railway sector:

- EN 13129-1 Railway applications - Air conditioning for main line rolling stock - Part 1: Comfort parameters
- EN 14750-1 Railway applications - Air conditioning for urban and suburban rolling stock - Part 1: Comfort parameters
- EN 14813-1 Railway applications - Air conditioning for driving cabs - Part 1: Comfort parameters
- UIC 553 Heating, ventilation and air-conditioning in coaches
- EN 50125-1 Railway applications - Environmental conditions for equipment - Part 1: Rolling stock and on-board equipment
- EN 45545-1,2,5,4 Railway applications - Fire protection on railway vehicles
- EN 13313 Refrigerating systems and heat pumps - Competence of personnel
- EN 378-4 Refrigerating systems and heat pumps - Safety and environmental requirements - Part 4: Operation, maintenance, repair and recovery
- EN 378-2 Refrigerating systems and heat pumps - Safety and environmental requirements - Part 2: Design, construction, testing, marking and documentation
- REGULATION (EU) No 517/2014 on fluorinated greenhouse gases and repealing Regulation (EC)

- REGULATION (EU) No 303/2008 Minimum requirements for the certification of companies and personnel as regards stationary refrigeration, air conditioning systems and heat pumps containing certain fluorinated greenhouse gases as well as the conditions for mutual recognition of the relevant certificates

Remarks on System Design (Ca and Cb)

Prior to the design process, some general system setups were discussed. Aim of the discussion was to collect arguments for combined or separate solutions for the requirements of Ca & Cb and the proposed concepts. As a result of this discussion concerning the up- and downsides, a concept was designed with a refrigerant cycle that has an additional storage evaporator and a larger PCM storage integrated in an additional coolant cycle. This concept was discussed in WP1 because changes in the refrigerant cycles would make necessary completely new developments of HVAC systems at all.

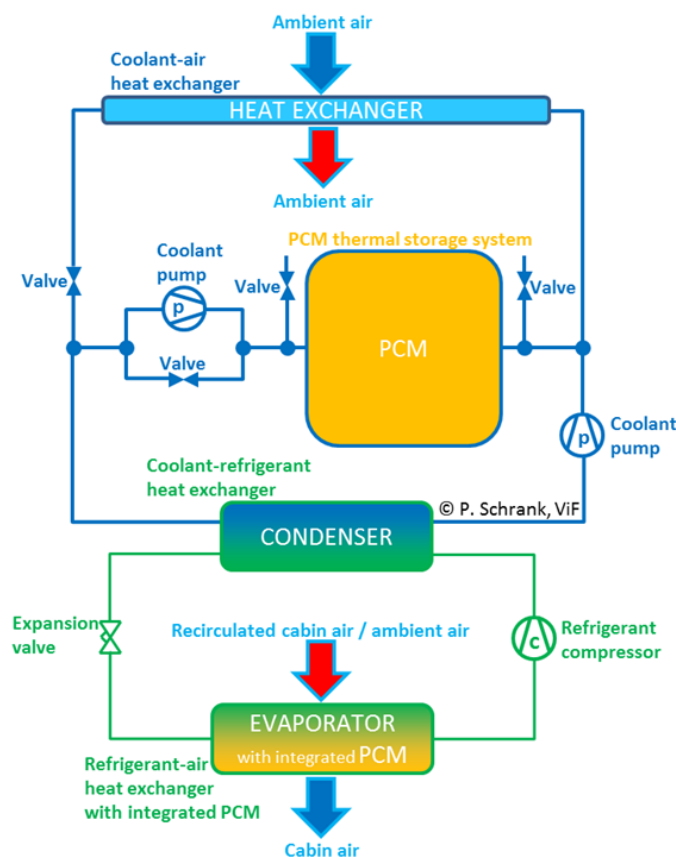


Figure 26: Air conditioning concept v2.2b

The system working in “tube-mode” means that the in yellow shown PCM thermal storage system stores the heat and the light blue heat exchanger is not working, which means that no heat is rejected to the ambient. Outside the tunnel it is possible to reject the heat from the PCM and the condenser of the refrigerant circuit via the heat exchanger in the “outdoor-mode”. Because of the installed valves and a second pump in the coolant circuit a discharge of the PCM thermal storage system during standstill at end of line station is also possible.

To also address the tasks of Ca it is coupled to a refrigerant circuit with an evaporator with integrated PCM shown in the bottom part of the figure by the system connected with green lines.

Main advantages of the Air conditioning concept:

- Charging of PCM thermal storage system in „tube-mode“ (objective Cb).

- Simultaneous discharging of PCM thermal storage system and conditioning of the cabin in „outdoor-mode“ (objective Cb).
- Less part-load operation of the refrigerant compressor due to evaporator with integrated PCM. (objective Ca)
- Little adaptations to the standard HVAC system on top of the wagon. (see section Ca)
- Possibility to discharge PCM thermal storage system during standstill at end of line station. (objective Cb)

Storage Material Data

Different kind of storage materials are available on the market; most of them are paraffins and salt-hydrates. The usability of the PCM is most dominated by properties like melting-temperature and reliability (corrosion and thermal stability). Storage density, heat conduction, and several others are influencing the design of the storage cell.

If the storage should be included on the low temperature side of the system a temperature range around 0°C is required. PCM Materials for this purpose are for example: RT5HC/RT8

RT5 HC

The most important data:		
Melting area	5-6 main peak: 6	[°C]
Congeeing area	6-5 main peak: 5	[°C]
Heat storage capacity ± 7,5%	240	[kJ/kg]*
Combination of latent and sensible heat in a temperatur range of -2 °C to 13°C.	67	[Wh/kg]*
Specific heat capacity	2	[kJ/kg·K]
Density solid at -15°C	0,88	[kg/l]
Density liquid at 20 °C	0,76	[kg/l]
Heat conductivity (both phases)	0,2	[W/(m·K)]
Volume expansion	13	[%]
Flash point (PCM)	115	[°C]
Max. operation temperature	30	[°C]

RT8

The most important data:		
Melting area	6-9 main peak: 7	[°C]
Congeeing area	9-6 main peak: 8	[°C]
Heat storage capacity ± 7,5%	180	[kJ/kg]*
Combination of latent and sensible heat in a temperatur range of 0 °C to 15°C.	50	[Wh/kg]*
Specific heat capacity	2	[kJ/kg·K]
Density solid at -15°C	0,88	[kg/l]
Density liquid at 15 °C	0,77	[kg/l]
Heat conductivity (both phases)	0,2	[W/(m·K)]
Volume expansion	14	[%]
Flash point (PCM)	116	[°C]
Max. operation temperature	40	[°C]

Case Study:

Boundary Conditions of London-Underground (Bakerloo Line)

Operation inside tunnel (design point)		
Tamb=30°C; pax=160; no sun; no loss in air-ducts, etc.		
cooling load at evaporator	kW	19
temperature after HX	°C	17
Operation outside tunnel (design point)		
Tamb=28°C; pax=160; sun; no loss in air-ducts, etc.		
cooling load at evaporator	kW	29
temperature after HX	°C	11

Operation inside tunnel (design point)		Tamb=30°C; pax=160; no sun; no loss in air-ducts, etc.	
load at HX	W	23760	estimated using Wlast
time in tunnel	min	48	estimated from timetable of respective line
cooling load energy	kWh	19.0	
average COP of HVAC	1	2	estimated average (assumption)
energy to be stored in condenser	kWh	28.5	condenser waste heat -> heat storage desing capacity

Operation outside tunnel (design point)		Tamb=28°C; pax=160; sun; no loss in air-ducts, etc.	
load at HX	W	33030	estimated using Wlast
average COP of HVAC	1	2	estimated average
waste heat at condenser	kW	49.5	due to air-conditioning in overground section
time outside tunnel for discharging	min	56	estimated from timetable of respective line
mean storage discharge power	kW	30.5	
total power to be transferred	kW	80.1	for HVAC operation and condenser storage discharge in overground operation

Cc: Air-Cycle-Cooling (ACS)

The main goal of development is to de-humidify the inlet air and to cool in order to reduce the enthalpy and enhance the ACS performance therefore. In principle two different solutions are possible for enthalpy reduction: Since a significant temperature increase is expected due to the condensation of air humidity in the adsorption cycle (a) cooling of the process air between dehumidification and the turbine inlet is possible by external cooling with ambient air but also (b) internal cooling by process air from the low pressure path before the compressor inlet (approx. 25°C between HX and compressor). The cooling concept (a) or (b) and the consequences to the system efficiency has not been evaluated yet. Experimental data (i.e. adsorption enthalpy and temperature shift) have to be collected first.

Boundary conditions:

Ambient Conditions		Design point:		
Amb. pressure	1013 mbar	Cooling Power	31,9 kW	El. Power 43,6 kW
Amb. Air Hum.	50% (x=18g/kg)	Cabin Air Temp.	27°C	Speed 38880 rpm
Amb. Air Temp.	35°C	Cabin Air Hum.	50%	OutTemp.130°C
Process Air Flow	0,65 kg/s	Cabin Air Flow	1 kg/s	

Numerical process simulation can highlight the benefit of humidity and enthalpy reduction of the inlet air:

- **Calculations with**
 - Constant cooling power 32,7kW
 - Constant mixed air conditions 32°C/44%
 - constant liquid water quantity before heat exchanger (note: not possible for extreme low process air humidity of 10g/kg)
 - liquid water from TRB + additionally sprayed condensate from supply air path
 - Condensate is limited → spray limitation

5.2 Materials selection and development

Ca: Improvement of part-load behaviour of conventional conditioning systems;

Cb: Improvement of underground heat rejection of subway trains

Concerning the improvement of underground heat rejection of subway trains, improvement of part-load behavior of conventional conditioning systems by the use of PCM storages an overall air conditioning

concept was chosen. It consists of an evaporator with integrated PCM, furthermore condenser of the refrigerant circuit is coupled to a thermal PCM storage system using coolant as heat transfer fluid. Figure 26 shows the chosen air conditioning concept. It is about an overall concept, which represents a solution not only for the improvement of underground heat rejection of subway trains but also for the improvement of part-load behaviour of conventional conditioning systems.

The usage of an evaporator with integrated PCM is one possibility to reduce or even avoid the part-load operation of the refrigerant compressor. As the part load operation is inefficient using a fixed speed compressor, this would lead to higher system efficiency.

Therefore, a concept of a refrigerant circuit with an evaporator with PCM was designed. The evaporator shown in green/yellow is able to deliver cooled air for a defined period of time while the compressor is switched off. To address the tasks (lower/avoid underground heat rejection) the condenser of the refrigerant circuit is coupled to a thermal storage system using coolant as heat transfer fluid. It is able to store heat by charging a PCM thermal storage while driving in a tunnel. This system and its coolant circuit are shown in the upper part (blue lines). For the task concerning improvement of part-load behavior, the part load operation of the compressor could be reduced or even avoided because the compressor runs in full-load operation to cool down and solidify the PCM material in the evaporator as well as to cool down the air for the cabin.

Since the early 1990's metallic foams are widely known as a class of multifunctional materials that presents attractive thermal, electrical and acoustic properties. Moreover, several studies highlight their excellent specific mechanical properties they do have. They are especially quoted for their random topology, high open porosity, low density and high thermal conductivity and large accessible surface area per unit volume. Metallic foams have been already successfully applied in numerous applications such as heat exchangers, vehicle traction batteries conditioning and catalytic field application such as fuel cells systems.

Specimen Design:

In order to determine the material properties of PCM infiltrated aluminium foam (AlSi10) several specimens have been manufactured. The specimens consist of a bare or corrugated tube in the center (inner tube) surrounded by a PCM infiltrated aluminium foam tube. The specimens are covered by an additional steel tube to prevent leakage and both ends are sealed with metal plates. Figure 27 shows a longitudinal section of a specimen without the outer steel tube enclosure.



Figure 27: Longitudinal section of a specimen with a corrugated inner tube

For experiments and simulations the storage material RT5HC from Rubitherm (www.rubitherm.eu) was selected. This material was selected because it was decided to integrate a thermal storage on the cold side (evaporator) of the HVAC system. RT5HC is a pure PCM, this heat storage material utilizing the processes of phase change between solid and liquid (melting and congealing) to store and release large quantities of thermal energy at nearly constant temperature. Phase change materials (PCM's) provide a very effective means for storing heat and cold, even when limited volumes and low differences in operating temperature are applicable.

Properties:

- high thermal energy storage capacity
- heat storage and release take place at relatively constant temperatures
- no supercooling effect, chemically inert
- long life product, with stable performance through the phase change cycles
- melting temperature range: 5-6 °C

Measurement setup:

The measurement setup to characterize the material properties (shown in Figure 28) consists of the heat source, an internal pump in the return stream, a magnetic flow meter as well as a bypass valve to set volume flows between 630 and 5500 l/h. 2 PT100 temperature sensors measure the flow and return temperature to the PCM tube, and 2 times 5 Thermocouple sensors are used to measure surface temperatures of the specimens. The heat source is capable of providing a heating temperature of +9°C at 9 kW and a cooling temperature of +1°C with a power delivery of 1.5 kW. To prevent freezing of the heat transfer fluid, a mixture of 65% water and 35% Antifrogen N was filled inside the system.

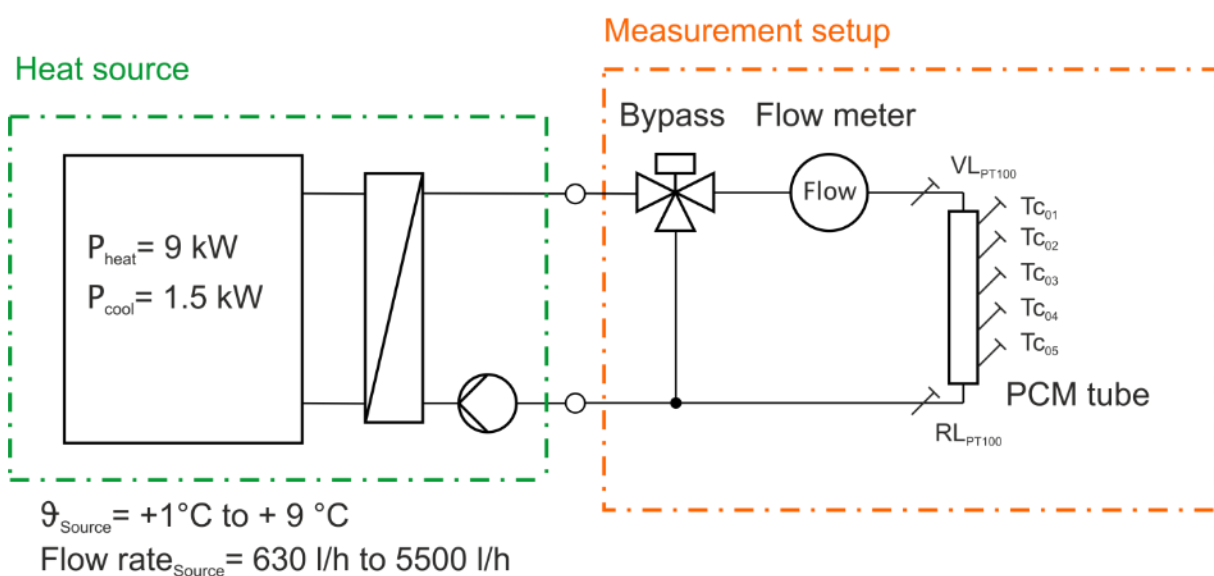


Figure 28: Measurement setup

Measurement of PCM/Aluminium modules

As the thermal behaviour and the power performance of the combination aluminium foam and PCM is not determined yet, an optimum operating area, where maximum power delivery occurs, has to be

worked out. With the outcome of the measurements it is intended also to parametrise a TRNSYS model (type842) for the system simulations. Numerous geometric variations can then be performed within the simulation with the benefit of reduced costs and time. As the necessary measurement data has to be collected prior to the simulation, several prototype storage modules have been manufactured and prepared for the measurements. These experimental PCM modules have either the shape of a tube, representing an “elementary cell” within a compound of surrounding paraffin, as well as a storage box design with 14 parallel tubes through a cuboid housing. These PCM/Aluminium modules have been measured and analysed in the laboratory of the Institute of Thermal Engineering TU Graz. To give a quick overview, Figure 29 shows both measured experimental modules.

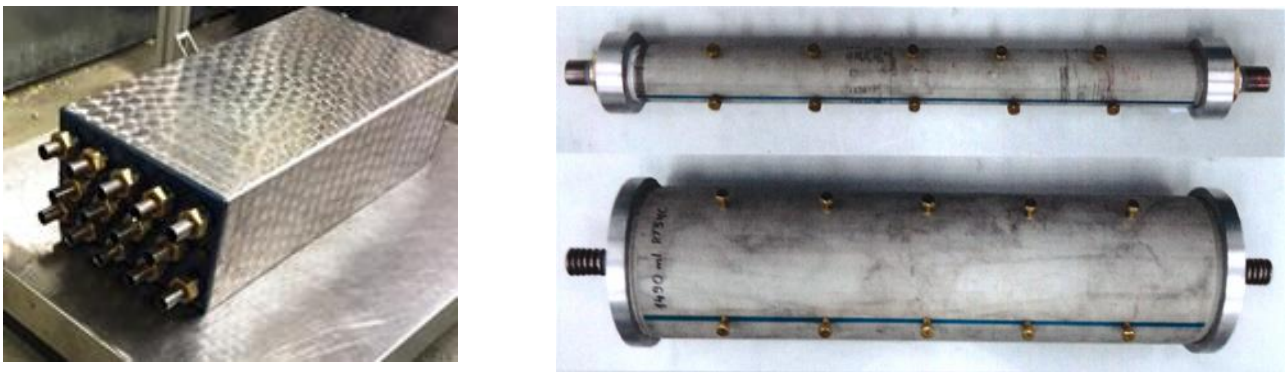


Figure 29: Experimental box and experimental tube

As there is a difference in power delivery as well as varying charging/discharging durations when circulating through the experimental box with different hydraulic settings, it is intended to flow through the experimental box either in parallel or serial direction. It has to be mentioned that all test tubes have been equipped with surface temperatures and are covered with a proper insulation.

Cc: Improvement of Air-Cycle-Cooling (ACS)

Regarding the improvement of Air-Cycle-Cooling (ACS) systems by the use of adsorption materials, the main goal of the development is to de-humidify and to cool the process- inlet air in order to reduce the enthalpy and enhance the ACS performance therefore. The process air treatment unit must be placed beneath or inside the inflow box respectively outflow box. The process- outlet air should be used to dehumidify the desiccant in the process air treatment unit.

For aim of adsorption measurement, the construction of an air conditioning unit was necessary to provide a constant flow of air (at design point condition DP) to the adsorption specimen. The ambient conditions at DP are:

$T_{\text{ambient}} = 35^{\circ}\text{C}$, Humidity is 48%relH ($x=17\text{g/kg}$)

This condition is relevant for the adsorption process when air is guided over the sorbent material in order to get dehumidified. For the desorption process other conditions are relevant namely the exhaust air from the compressor. This air stream exhibit

$T_{\text{exhaust}} = 130^{\circ}\text{C}$, Humidity is ca. 2%relH ($x=22\text{g/kg}$)

The exhaust air will be used to drive the desorption process. Since it is unclear at the moment how the dehumidification will influence the process efficiency (decrease of exhaust temperature) the experiments

concentrate only at the adsorption process. Materials will be desorbed in a drying-oven overnight. During a second stage the desorption conditions will be integrated to the test stand also.

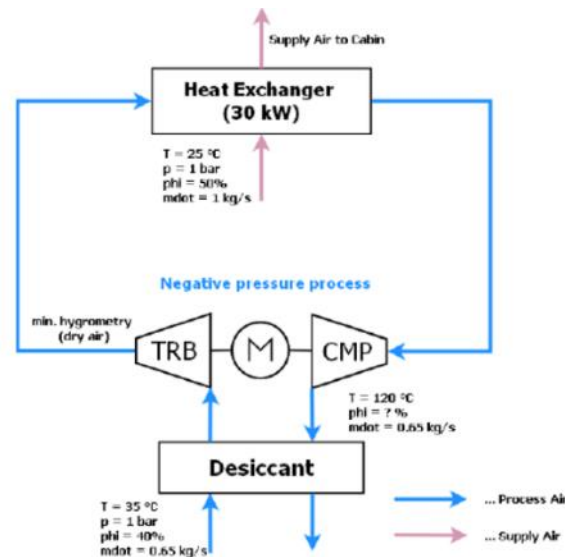


Figure 30 : Working principle of the ACS with values for air condition

The schematic drawing in Figure 30 shows the working principle and the relevant air conditions at each step of the process. For a practicable realization a certain factor of downscaling was used. Air channel dimensions were reduced to 40% of the real design, air stream to 16%. Therefore, the air velocity in the channels (and specimen) is kept constant. The typical velocity at the entrance box of the existing ACS design was assumed to reach around 3.5 m/s. Even if the design of a final desiccant unit is unforeseeable at the moment air velocity are assumed to be in a comparable range.

Desiccant unit design may be like a sorption- wheel (continuous adsorption-desorption process) like a pair of boxes with changing operation (adsorption- desorption changing bed reaction). For experimental measurements the changing fixed bed reaction was chosen since the reaction principle has the advantage of an easy to construct specimen and containment type. The specimen will be placed in the adsorption-box and the desorption-box (or drying oven) in a consecutive way by performing adsorption-desorption cycles.

Specimen design:

The specimens that perform dehumidification should be able to attract and store air humidity by the amount of 16% of the realistic design (16% of 0.65kg/s). The specimen should exhibit a rather low pressure drop to the air stream (not quantified yet) that means large channels but good dehumidification rate (large reactive surface). The sorption material should heat up as low as possible since temperature increase will decrease efficiency. Since “low heating” substances (low adsorption enthalpy) show low hydrophilic character these substances are not suitable. Therefore, the ability to cool the ingoing air is assumed in order to reduce the overall enthalpy of the ingoing air (temperature and humidity). Effective cooling can be reached with ambient air since the temperature will reach remarkable increase during desorption. Even in case of isenthalpic changes of the air condition, a reduction of the water content from 17g/kg to 7g/kg will result in a temperature increase from 35°C to 62°C due to the condensation enthalpy of the water inside the sorptive material. Since the use of capable sorptive materials introduce

additional enthalpy to the adsorption process (released heat due to binding of the water molecules= adsorption enthalpy) a temperature gradient even steeper (up to max 75°C) is expected. (During the experiments the temperature increase will be lowered by the heating of the sorbent itself, this means heating of the specimen will absorb energy, an unstable temperature development is expected).

To realize a specimen with channels as reactive surface, a stack of activated plates, shown in Figure 31 are built, both sides of the plates coated with sorbent materials. Silicon resin was chosen as heat resistant glue for the granules and plywood sheets (impregnated with lithium waterglass) as substrate materials. Several different materials available in granular form were tried.



Figure 31 : ACU1 air conditioning unit to provide air at 35°C and 50%relHum (left) and specimen stacks (right).

The construction of the stack specimen is rather elaborative and it takes several hours for impregnating, coating, and mounting of the plates. Since several materials have to be tested the use of easier available specimen design seems preferable. Therefore, and due to the fact that the blower of the ACU is able to reach pressure ranges of about 800-1000Pa (8-10mbar) a packed bed design was used for further experiments. For this a separate holder was constructed that allows filling on the workbench, Flow area 27x27 cm², bed width (thickness) 4-7 cm.

Sorbent materials used for ACU test rig:

Materials (long list) were selected according to their suitability due to their known thermo-physical properties. Available materials are:

- BASF KC-N drying agent (silica based, resistant to fluid water)
- Köstrolith 4A (Linde-type) zeolite (molecular sieve, grains 1,6-2,5 mm)
- Köstrolith 3A zeolite (molecular sieve, grains 1,6-2,5 mm)
- Köstrolith Y zeolite (molecular sieve, grains 1,6-2,5 mm)
- SILKEM 4A zeolite
- OKER-Chemie Siogel (microporous silica gel, grain size 2-4mm)
- LiCl salt impregnated onto textile cloth
- Li-Y (modification of Y zeolite, ion exchange Na to Li)

The first six are commercial available materials, the last two modifications.

5.3 Component Development

Ca: Improvement of part-load behaviour of conventional conditioning systems, Cb: Improvement of underground heat rejection of subway trains

Storage Evaporator

As already mentioned, improvements of the part-load behaviour can be accomplished by using a storage evaporator assembled to the air condition system. The usage of an evaporator with integrated PCM is one possibility to reduce or even avoid the part-load operation of the refrigerant compressor resp. the whole air conditioning system. As the part load operation is inefficient using a fixed speed compressor, this would lead to a higher system efficiency.

The storage evaporator is being discharged during the operation of the air conditioning system and being charged during the standstill of the compressor by the cabin air.

For the later on simulation model adjustment and validation, an off-the-shelf storage evaporator was evaluated resp. measured.

The passenger car storage evaporator is used in models like BMW F10 (5 series) or BMW F01 (7 series) and manufactured by Behr-Hella. These air condition systems run on R134a refrigerant. Especially this kind of evaporator is used in air condition systems for “mild-hybrid” applications with automatic engine start-stop control. Within its build-in dimensions of 307x245x60 mm a thermal storage material is cased to provide passenger comfort during engine standstill. A third row of multi-port-extrusion tubes (MPE) equipped with fins is added to a standard two-row evaporator. The third row of MPE-tubes is shrouded with a phase change material (PCM). According to the Behr-Hella patent the PCM is presumably composed of Decanol, Tetradecan or similar substances of the alcohol or paraffin group or a mixture of these. All of them come with nucleating agents to improve the solidifying process.

The aluminium body of the evaporator has a total mass of 2,2 kg. Not considering the jointed tubes as useful thermal storage mass, the amount of $m_{\text{Alu}} = 2,0$ kg Aluminium and $m_{\text{PCM}} = 0,168$ kg (measured) PCM could be taken into account. To calculate the thermal energy stored within the storage evaporator, a temperature range (ΔT) from 4 °C to 15 °C was considered. In sum the thermal energy stored in the evaporator considering this temperature range is 62 kJ.

Measuring procedure of Storage Evaporator

To determine the behaviour of the storage evaporator, a refrigerant cycle with R134a was set up inside a climate chamber. Various operation points, considering air inlet temperature (ambient temperature), air humidity and air mass flow through the evaporator were tested.

Following measuring points, concerning the storage evaporator, were used:

- Air temperature and its relative humidity (in- & outlet)
- Pressure drop of air and refrigerant R134a
- Mass flow of air and refrigerant R134a
- Evaporator aluminium body temperature (inside/outside)

A flow straightener located upstream of the evaporator was installed to eliminate turbulences and provide orthogonal inflow. Due to the uncertainty of measurement of the humidity sensor ($\pm 2,5$ %rh) and the high enthalpy of vaporization of water, calculations based on this specific measurement data come

with a higher inaccuracy than others. Also the reaction time of the sensor and the measurement frequency of 1 Hz influenced the precision of the transient measurements.

The air outlet temperature was measured with the help of a thermocouple measurement grid within the airflow. The grid is made of 20 equally spaced thermocouples within the 300x280 mm air duct, approx. 300 mm downstream the evaporator.

The measurement grid is able to determine an uneven temperature distribution, but not an uneven air flow velocity resp. air volume flow.

The air outlet temperature mentioned in the following chapters is an arithmetic average of these 20 measuring points. The temperature within the evaporator was measured by means of two thermocouples mounted on the aluminium PCM-housing wall (shown in Figure 32). Also the calculated saturated vapour temperature (evaporating temperature) of the refrigerant specifies the temperatures inside the evaporator.

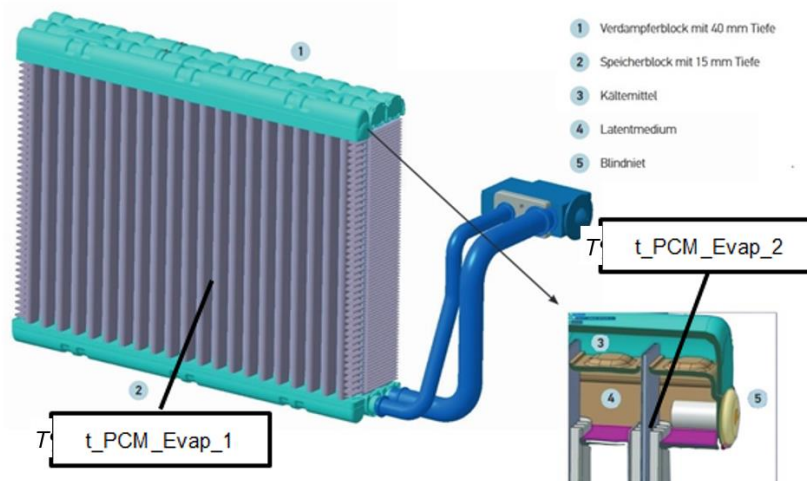


Figure 32: Location of the two surface temperature sensors on the evaporator

Typical measuring cycle

The main focus during measurements was set to the transient, thermal behaviour of the evaporator. After compressor standstill the storage evaporator provides a certain cooling capacity due to its thermal mass and the phase change of the containing PCM. A typical measuring cycle comprises different, sequential phases (shown in Figure 33):

1. Steady compressor operation 1 to 4 minutes: discharging / solidifying the PCM
2. Compressor stopping procedure:
 - a. Closing the expansion valve
 - b. Slowing compressor speed (frequency controlled)
 - c. Compressor standstill
3. Transient measurement of the evaporator behaviour
4. Drying-up the evaporator
5. Start compressor and new measuring cycle

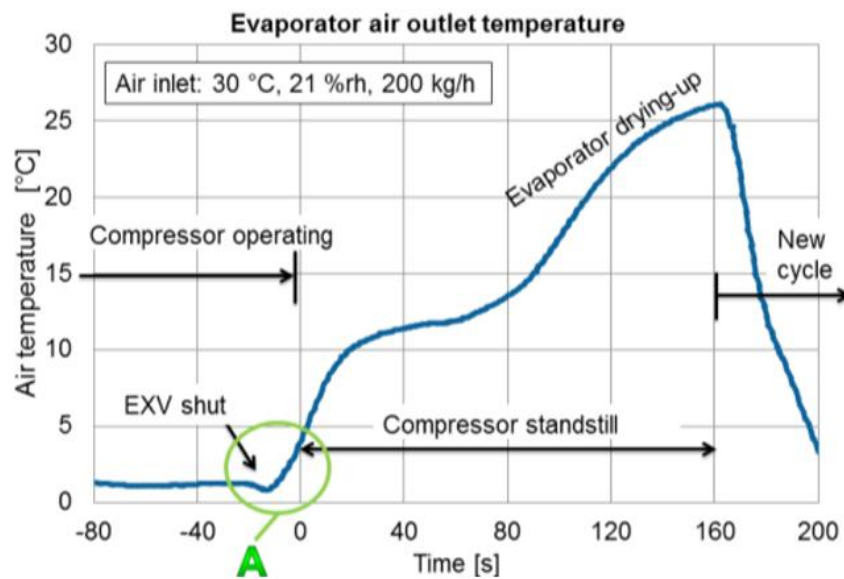


Figure 33: Typical measuring cycle

Experimental PCM/ Aluminium box measurements

An exemplary charging/discharging cycle in parallel flow direction shows Figure 34. The charging cycle takes about 180 minutes and the discharging cycle takes about 120 minutes. The mass flow rate was about 1500 kg/h and the initial temperature of the box prior to the measurement was set to 8.7 °C. From time interval 185 minutes to time interval 193 minutes the heat exchanger fluid was set to +9 °C via the bypass channel.

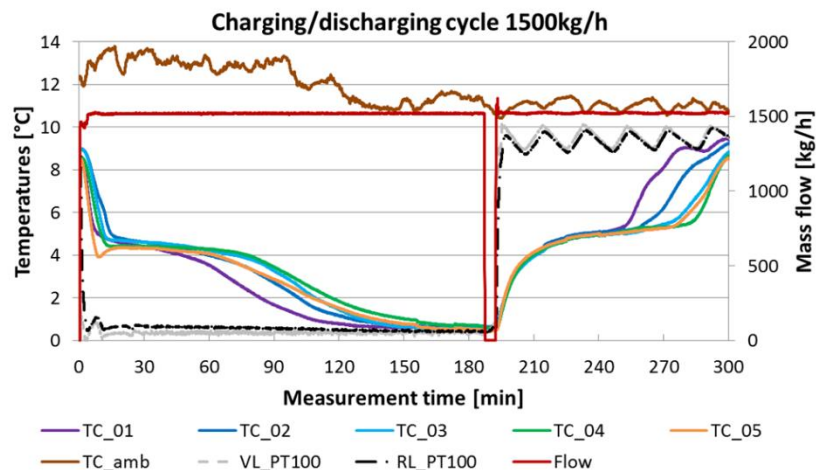


Figure 34: Exemplary charging/discharging cycle of parallel box measurements

It has to be mentioned that the discharging cycle is highly influenced by the slow behaviour of the controller of the heat source, as the temperature of flow stream is varying about $\pm 0,6$ K. But as the charging cycle is more relevant for the HVAC subway application the discharging cycle can be neglected.

The power delivery can be estimated by measuring the temperatures of flow and return stream and the mass flow rate. As the specific heat capacity of the glycol/water mixture is well known the power delivery can be calculated. The power delivery to the experimental box is low due to the small temperature

difference between flow and return stream. This small temperature difference does not change significantly throughout all measurements, despite changing mass flow rates. Also due to laminar flow situation inside the pipes (according to the corresponding Reynolds number) power delivery is limited.

Experimental PCM/ Aluminium tube measurements

Measurements to specify the size and influence of several “elementary cells” within an experimental box have been performed in addition to the tests of the experimental box. For this purpose, PCM/Aluminium tubes have been designed and fabricated. As the measurement cycle is expected to be much faster than the measurements of the box, much more measurement data can be collected with the same amount of time. Also manufacturing this tubes can be performed in much shorter time and in addition this tubes are much cheaper and less complicated. This PCM/Aluminium tubes have then been measured and analysed in the laboratory of the Institute of Thermal Engineering TU Graz.

After the first measurements a very small temperature difference between flow and return stream ($\pm 0,07$ K) was detected. As the temperature difference was within the measurement uncertainties it was evident that a power estimation would lead to unsatisfying results. Luckily the dimensions and masses of the tubes as well as the thermal properties of the paraffin are well known. So the total energy content can be calculated by defining a specific temperature boundary where the phase change, and therefore the main energy conversion occurs. Analysing the thermal properties of the used paraffin Rubitherm RT5HC (<https://www.rubitherm.eu/>) the phase changing process (from liquid to solid state) starts at temperatures below $+6$ °C within a temperature range of 3 K. In addition, the analyse of the measurements show that the thermal conductivity below $+3$ °C increase dramatically due to elongated charging durations (despite the aluminium matrix) and the specific enthalpies within this area are small in comparison to the specific enthalpies between $+6$ °C and $+3$ °C. Therefore, energy contents of temperatures below $+3$ °C are not being considered for estimating average power delivery. An illustration of defining the boundary temperature is shown in Figure 35.

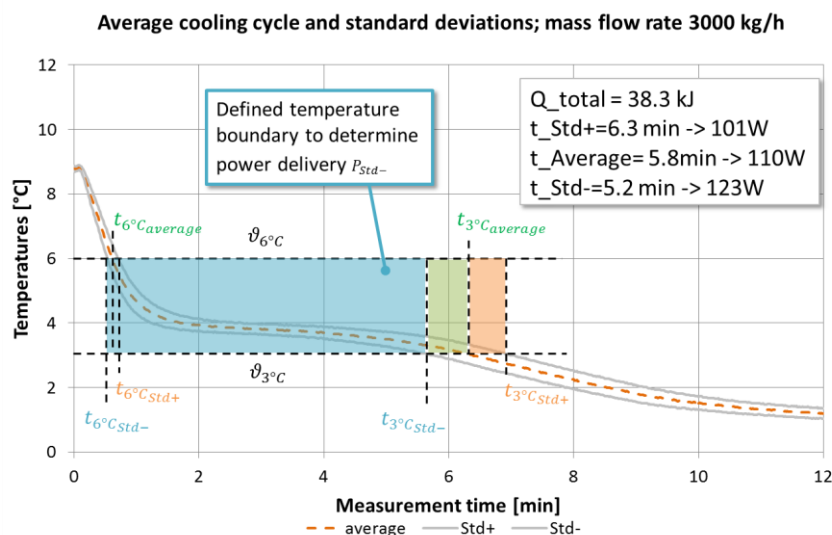


Figure 35: Definition of temperature boundary for estimating average power delivery

Estimating charging durations is slightly more relevant in terms of usage of PCM/Aluminium storage systems for technical applications as the main intention is to cool down the PCM modules as fast as possible. Discharging durations are shorter because ambient losses enhance melting of the paraffin

leading to increased average power delivery. By calculating the total energy content and dividing it through the time it takes to undergo the temperature boundary an average power delivery for the average cooling curve and the according standard deviations Std- and Std+ can be calculated. Using the numerical model developed to characterise the thermo physical properties for the power estimation of the tube tests shows comparable results regarding the power estimation as the estimation method described above.

Cc: Improvement of Air-Cycle-Cooling (ACS)

The procedure to get a preliminary design can be summarized as follows:

- Measurement of stack specimens for first results regarding dehumidification rate and temperature lift
- Measurement of packed bed specimens as an easier available specimen design for several materials and its modifications.

For these measurements the changing fixed bed reaction was chosen since the reaction principle has the advantage of an easy to construct specimen and containment type. The specimen will be placed in the adsorption-box of the test rig, desorption was currently done in a drying oven.

- Extending of the test rig in order to integrate the desorption step

For these measurements different specimen designs (stacks, packed bed and finally sorption wheels) were used. The measurements were always performed in an alternating operation.

Test rig modification :

The adsorption test rig was modified in order to integrate the desorption step (dehumidification of the sorbent material):

- second step for air heating
- additional air humidification
- desorption temperature 130 °C
- separate ad- and de-sorption box
- adsorption @ 35 °C / 17 g/kg
- desorption @ 130 °C / 22 g/kg
- Changing-bed experiments

The test rig construction was finished in Dec 2016 and is shown in Figure 36.

The principle design requirements are as follows:

- low mass
- low installation volume
- low pressure drop
- operation under steady conditions
- possibility for external cooling
- shock resistant
- low maintenance and consistent performance



Figure 36 : Test rig extension (ACU2) for simultaneous ad- and de-sorption of the desiccant specimen

The external cooling function could be achieved by ambient air or via an intermediate circuit which introduces the energy into the process. Depending on this, a rotary or a plate heat exchanger must be installed behind the sorption wheel.

The exact requirements for the sorption wheel are Maximum dehumidifying performance (>10 g/kg), low temperature lift (possible rinsing zone) pressure drop <10 mbar. Maximum diameter 0,3 m, maximum length 0,25 m.

5.4 Storage system development and numerical simulation

Ca: Improvement of part-load behaviour of conventional conditioning systems, Cb: Improvement of underground heat rejection of subway trains

For transient system simulation an existing TRNSYS model is used. This type842 was developed at the Institute of Thermal Engineering Graz University of Technology².

The TRNSYS type842 represents a classic heat air exchanger, which is not exposed to air as heat transporting fluid, but to PCM between its aluminium fins. When the type842 is parametrized with the physical properties of paraffin and the used aluminium foam it basically replicates the Aluminium/PCM matrix which has been used within the tested experimental modules³. Additionally, the TRNSYS type842 has been validated within the PhD of Andreas Heinz and also used in several simulations prior these experiments. It is intended to abstract the porosity level of the aluminium foam with the build in parameter t_f (distance between each fin) and s_f (thickness of each fin), as the aluminium foam consists of cavities, absorbing the paraffin, and a thin aluminium shell representing the aluminium fins. The distance between the heat transporting tubes can be adjusted by the parameter t_l (vertical distance

² Andreas Heinz, Application of Thermal Energy Storage with Phase Change Materials in Heating Systems, PhD, TU Graz, 2007

³ see also Christian Brandstätter, 2017

between the pipes) and t_q (horizontal distance between the pipes). After adjusting the mass of the PCM, the mass of additional thermal capacities of the experimental modules, density of the PCM and the Aluminium foam, and the thermal conductivity parameters of PCM and Aluminium the TRNSYS type842 is physical equivalent to the experimental modules. Figure 37 gives a quick overview of the modified PCM/air heat exchanger as well as the most important parameter used within the simulation.

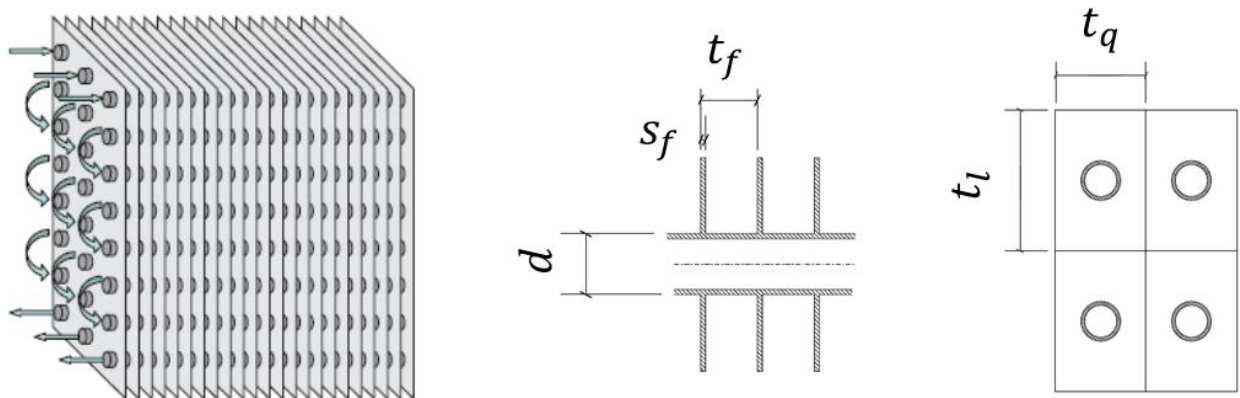


Figure 37: TRNSYS type842 and basic geometric parameters

Length t_l and width t_q of the “elementary cell” of the surrounding tube area are equal to the average distance between the tubes of the experimental box in vertical and horizontal direction. Unfortunately, the thermal conductivity of the PCM cannot be separated in thermal conductivity of solid and liquid state but only as general parameter for both phases. This seems to be the only disadvantage of using this simulation model.

A description of all parameters as well as the numerical abstraction of the TRNSYS type842 can be found in the PhD of Andreas Heinz (A. Heinz, 2007).

Inputs to the TRNSYS simulation are the measured flow and return temperature, as well as the mass flow rate and the ambient temperature. Also the surface temperatures of the box are transferred to the simulation to check for charging/discharging progress and for comparison with the PCM node temperatures of the simulation. As the experimental box measurements in parallel flow orientation are provided with the flow distributor in flow and return stream the simulation has to be adapted to these additional masses. This can be done by abstracting the flow distributor by using a water storage tank model (type4c) which has to be parametrized with the physical properties of the heat exchanger fluid and the individual volume of 6,75 dm³. All simulated values and results (PCM node temperatures, calculated power deliveries, return flow temperature of the simulation...) have been collected with an online plotter (type65c) and written to an output file for further analysis and data visualization. The time steps of measurements and simulations have been 1 second. A quick overview of the TRNSYS components within the simulation in TRNSYS STUDIO gives Figure 38. In general, the components of both parallel and serial simulations were kept untouched, only the volume of the flow distributor has been changed.

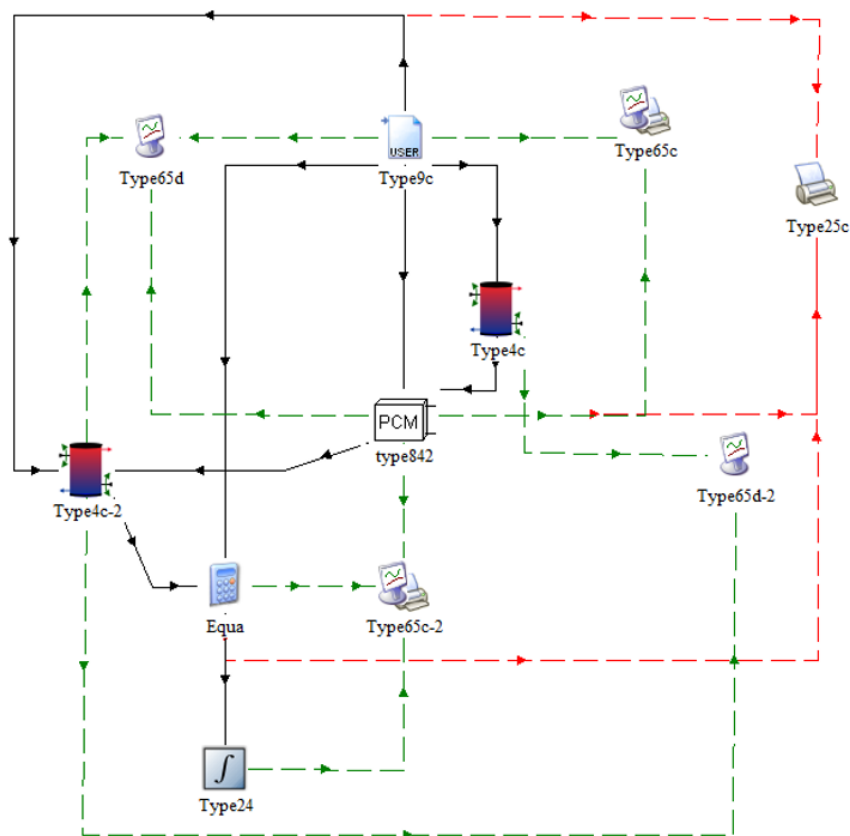


Figure 38: Overview of the used components within the TRNSYS simulation in TRNSYS STUDIO

Transient system simulations:

The main focus in the last period of the project was on system design and system simulation. The built model in Dymola with the ViF-in-house library “ViF-Lib” is shown in Figure 39. A “ports translator” model ensures the communication of the “bcvtb” model⁴ (for co-simulation with TRNSYS and thus with the PCM storage) with the built system model.

Due to the defined cooling capacity demand ($\dot{Q}_{\text{inside_tunnel}} = 19 \text{ kW}$ and $\dot{Q}_{\text{outside_tunnel}} = 29 \text{ kW}$) the number of refrigerant systems resp. units will obviously be determined by about 4 to 5 because one unit delivers a cooling capacity of $\dot{Q}_{\text{dot}} = 8 \text{ kW}$ in the worst case scenario (full load: 167 persons and full solar heat input). The lower cooling capacity (8 kW) compared to the base model (9,55 kW), is due to the subject of an additional heat transfer. The simulation resulted in a 180 dm^3 (gross) PCM storage per refrigeration system/unit to guarantee a 48 minutes underground operating. Consequently an approximately 1000 litre PCM storage per wagon has to be installed.

Cc: Improvement of Air-Cycle-Cooling (ACS)

The evaluation of the process behavior of a desiccant unit integrated into an Air-cycle-cooling-system (ACS) was performed by Company LIEBHERR with own simulation tools. The simulation system is based principally on the thermodynamic change of condition of the process air completed with pressure changing elements (turbine, channels, heat exchanger, and compressor).

⁴ BCVTB, Building Control Virtual Test Bed“, <https://simulationresearch.lbl.gov/bcvtb/FrontPage>

Definition of boundary conditions include: Air inlet temperature, air inlet humidity, pressure drop on turbine, internal air spray, internal heat exchange, internal pressure drop, pressure and temperature increase by compressor.

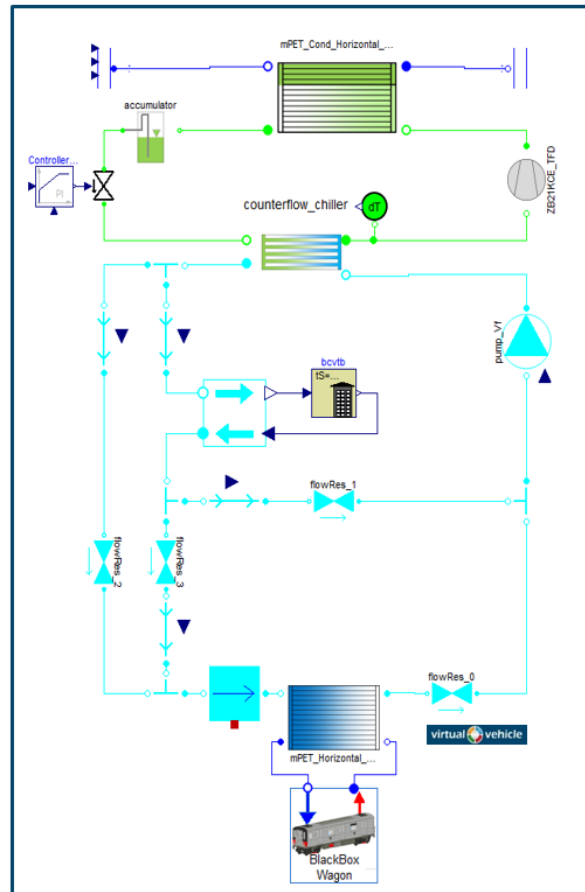


Figure 39: Overview of the system built in Dymola (including ports translator and bcvtb-interface to TRNSYS PCM storage model)

In addition, the desiccant unit provides dehumidification and temperature increase prior to inlet, additional pressure drop before inlet and after outlet.

The boundary conditions of the simulation were changed in such a way like a desiccant unit would do and the resulting cooling power and efficiency were taken as an assessment of possible improvements of the system. The simulation was carried out with the Liebherr internal ACS software, which allows to modify individual process parameters. The following parameters were taken into account:

- Operation of the plant in the Design Point ($T_{\text{ambient}} = 35 \text{ }^{\circ}\text{C}$, relative humidity is 50 %, $x = 17 \text{ g/kg}$)
- The desiccant material sample reduces the humidity and increases the temperature of the process inlet air
- The additional cooling performance of a supplementary heat exchanger is considered as an input value
- The main results are electric power saving and process outlet temperature of the unit at variable process-air cooling parameters and sample pressure drops

Table 8 shows the experiments, the measurement results as input for the simulation studies.

Table 8: Measurement results as input for the simulation studies

	Simulation Study 1	Simulation Study 2
Material	Y zeolite	SAPO (Mitsubishi AQSOA)
Specimen form	packed bed	packed bed
Material mass	0,804 kg	0,78 kg
Grain surface	2,75 m²	3,04 m²
Pressure drop	10 mbar	10 mbar
Exposure time for averaging	4 Minutes	5 Minutes
Dehumidification performance	-10 g/kg	-6,8 g/kg
temperature lift	26,6 K	16,9 K
Desorption	airflow, 130 °C	airflow, 130 °C
additional cooling	5,1 to 17 kW	2,3 to 13,5 kW

The figures below show the results of the simulations. In Table 9 the legend entries are explained in detail.

Table 9: Legend entries for the simulation results

T_CPR_out_estimated	°C	Estimated outlet temperature of the process air, which is used to dry the sorbent
T_TRB_in	°C	Process inlet temperature resulting from adsorption process and additional cooling
P_el,MACM	%	Reduction of the required electrical power at the same cooling capacity of the ACU unit

Figure 40 gives an overview of the main results regarding the materials Y Zeolite and the SAPO Material. With Y zeolite a minimum additional cooling effort of 9,5 kW is required to achieve electrical power savings. The maximum power saving amounts to 22 %, resulting in an additional process air cooling capacity of 17 kW. The process outlet temperature drops therefore to a value of 106 °C. The results for the SAPO material show a lower additional cooling need, but also lower electrical power savings.

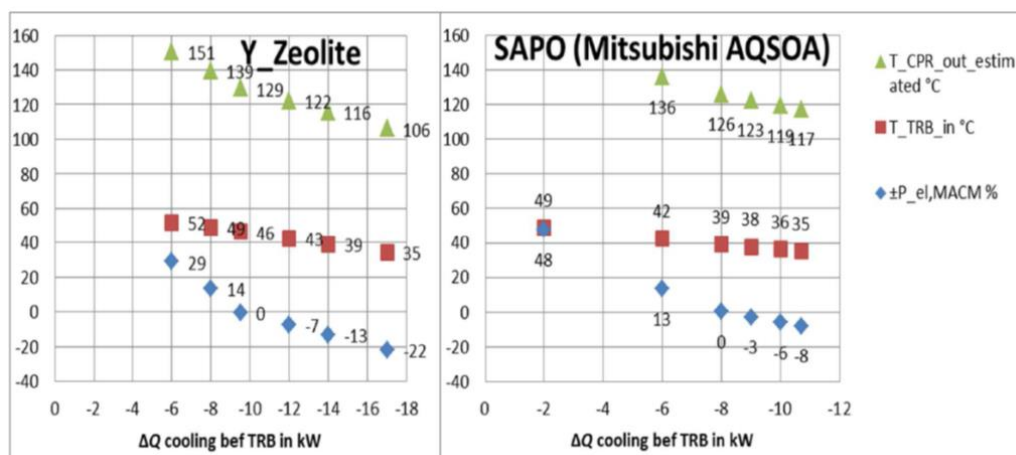


Figure 40: Y Zeolithe / SAPO: Power saving with ideal additional cooling of adsorption heat

The pressure loss of 10 mbar (worst case) at the ACS process inlet and outlet, caused by the sorption material, reduces the power savings slightly. Therefore, Figure 41 shows a maximum power saving of 19 % at 17 kW maximum external cooling load, concerning the material Y Zeolite. The minimum external cooling capacity to achieve savings is 11 kW.

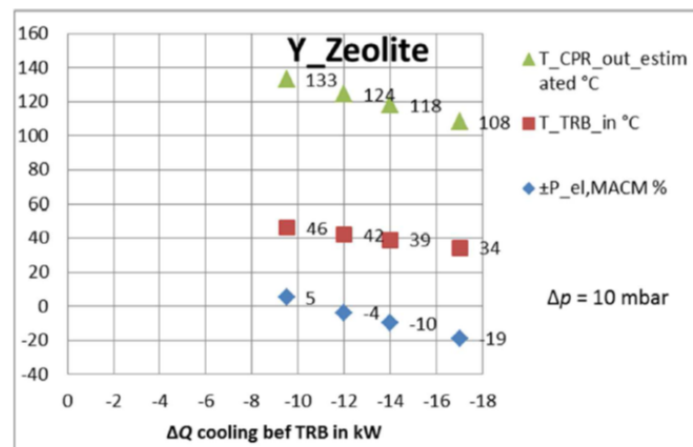


Figure 41: Power saving considering pressure drop of desiccant, ideal additional cooling

Figure 42 shows the parameters, when the whole additional cooling load is fed into the process air circuit. Considering a pressure loss of 10 mbar in the case of the Y zeolite and additional cooling exclusively in the process circuit no savings can be achieved. Additional cooling to 100 % in the process air circuit is therefore not followed up.

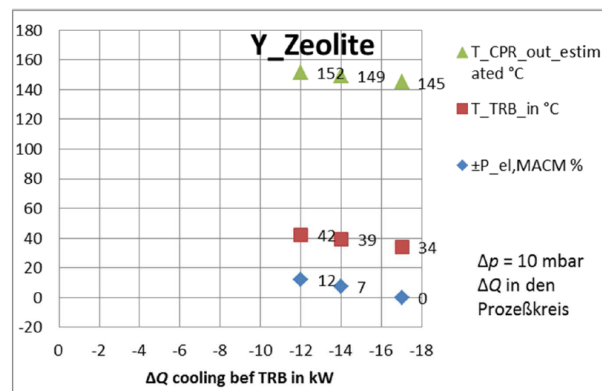


Figure 42: Power saving considering pressure drop of desiccant, additional cooling in process loop

Figure 43 shows the idea of a partial additional cooling with process air (so that heat exchanger for the ambient air remains in a practical size), so that the dehumidification is approximately isothermal. The power savings decreases, and the process outlet temperature increases with increasing additional cooling in the process loop.

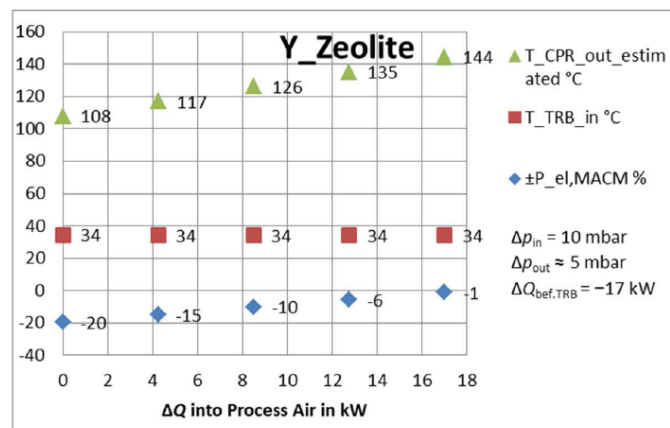


Figure 43: Power saving considering pressure drop of desiccant, partly additional cooling in process loop

The general prospects can be summarized as follows:

- The dehumidification performance achieved by furnace desorption is also obtainable by airstream desorption
- The temperature lift is a process parameter (no material characteristics value)- further experiments should show the correlation
- The occurring time course and average determination of the changing bed measuring results has strong effects on the simulation results
- The pressure drop occurring with all specimen designs is generally < 10 mbar
- The additional cooling process parameter is an essential feature that must be considered in the detailed design and construction phase
- Further evaluations with other desorption conditions should be carried out before the detailed design and construction phase can start

5.5 System Integration and Control

5.5.1 Study 1: Integration Concept and Demonstration of a PCM Storage in a Rail HVAC Application

Introduction

Employing a PCM storage in a rail HVAC system basically aims at the following two objectives:

1. [Ca]: Increase system energy efficiency by enabling on/off-operation of the compressor instead of using a conventional refrigerant bypass as a means of part-load control.
2. [Cb]: Bridge phases of cooling demand, when the compressor cannot be operated or may only be operated in a derating mode due to external limitations. Applications include the reduction of heat rejection in a tunnel (e.g. in deep tube lines of London) and the reduction of noise emissions in a railway stations: The cooling demand shall be (largely) covered by a thermal energy (cold) storage while the train operates in a tunnel or stops at a station.

The demonstration aims at testing the PCM storage developed by project partner i2m within an HVAC system architecture relevant for a rail application as outlined above and under close-to-reality operating conditions.

System architecture and boundary conditions

Figure 44 schematically shows the overall system architecture of the HVAC system and the rail vehicle. Fresh air from the ambient is mixed with return air coming from the rail vehicle. The resulting mixed air is cooled and dehumidified in the brine-air heat exchanger. Finally, the air is supplied to rail vehicle as supply air. The PCM storage is integrated in the brine cycle, which is cooled with a refrigerant cycle. A bypass valve allows continuously varying the brine mass flow rate through the PCM storage. The system architecture enables the main operating modes summarized in Table 10.

In the demonstration focus was put on the application bridging compressor shutdown/derating operation at stations. Table 11 summarizes related key parameters with respect to a typical moderate operating point (ambient air temperature: 25°C, ambient air relative humidity: 45%, solar radiation: 496 W/m², passenger occupancy: 50%).

Realistic operating conditions (e.g. ambient temperature, passenger occupancy) as well as an appropriate rail vehicle (with parameters on geometry, insulation, passenger capacity, etc.) were chosen to obtain the required cooling capacity, air mass flow rates, and corresponding air states (temperature, humidity) by means of a model on thermal loads. By multiplying the required cooling capacity with the duration of cooling from the PCM storage yielded the required PCM storage capacity.

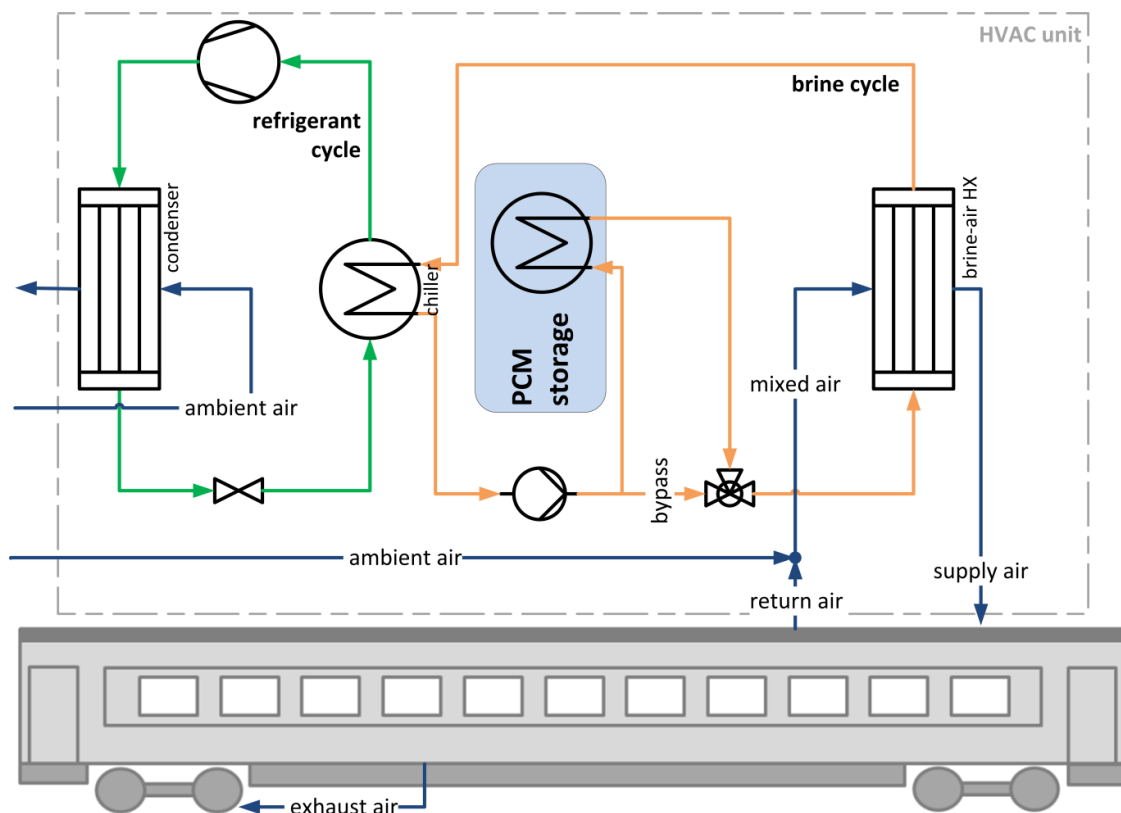


Figure 44: Overall HVAC system architecture

Table 10: Main operating modes of the system

operating mode		refrig. cycle	brine cycle	PCM storage	supply air fan
1	regular cabin cooling	on	on	disabled	on
2	regular cabin cooling + PCM charging	on	on	enabled	on
3	cooling from the PCM storage	off	on	enabled	on
4	PCM charging only	on	on	enabled	off

Table 11: Key parameters of the considered application including air state and volume flow at the virtual brine-air heat exchanger

quantity	Unit	value
required cooling capacity	kW	16.3
duration of stop at station	Min	3
required storage capacity	kWh	0.815
mixed air mass flow rate	m ³ /h	3730
mixed air temperature	°C	22.7
mixed air relative humidity	%	49.4

Demonstrator Hardware and Software

The test set-up featuring hardware-in-the-loop (HiL) simulation basically allowed high flexibility to study different applications of the thermal energy storage by appropriately scaling virtual system components. Figure 46 shows the scheme of the PCM storage demonstrator. Figure 45 depicts a full plant top view of the implemented PCM storage demonstrator. A thermal conditioning unit by Liebherr with a nominal cooling capacity at the evaporator of 8 kW was used in the demonstration. A Matlab/Simulink program was developed to control the test bed and to acquire data from various sensors.

The PCM storage module was developed by project partner i2m and is composed of an aluminum foam matrix (for a sufficient heat transfer rate into/from the PCM) and the PCM RT5HC from supplier Rubitherm. Details on the PCM storage module are given in section WP3-Component Development.

As an application-specific test of the PCM storage was in the focus, it was important to include the thermodynamic behavior of the brine-air heat exchanger. A conventional fin-and-tube heat exchanger of supplier Sierra was selected and dimensioned with respect to a typical design point of Central Europe (ambient temperature: 35°C, vehicle set temperature: 27°C, passenger occupancy: 100%, direct solar radiation: 700 W/m², 30° angle, diffuse solar radiation: 100 W/m²). The brine-air heat exchanger was implemented as a model in a hardware-in-the-loop simulation: It was represented by an electric heater, which was controlled based on simulated characteristics of the heat exchanger.

Energieforschungsprogramm – 4. Ausschreibung

Klima- und Energiefonds des Bundes – Abwicklung durch die Österreichische Forschungsförderungsgesellschaft FFG



Figure 45: Implemented PCM storage demonstrator (full plant top view)

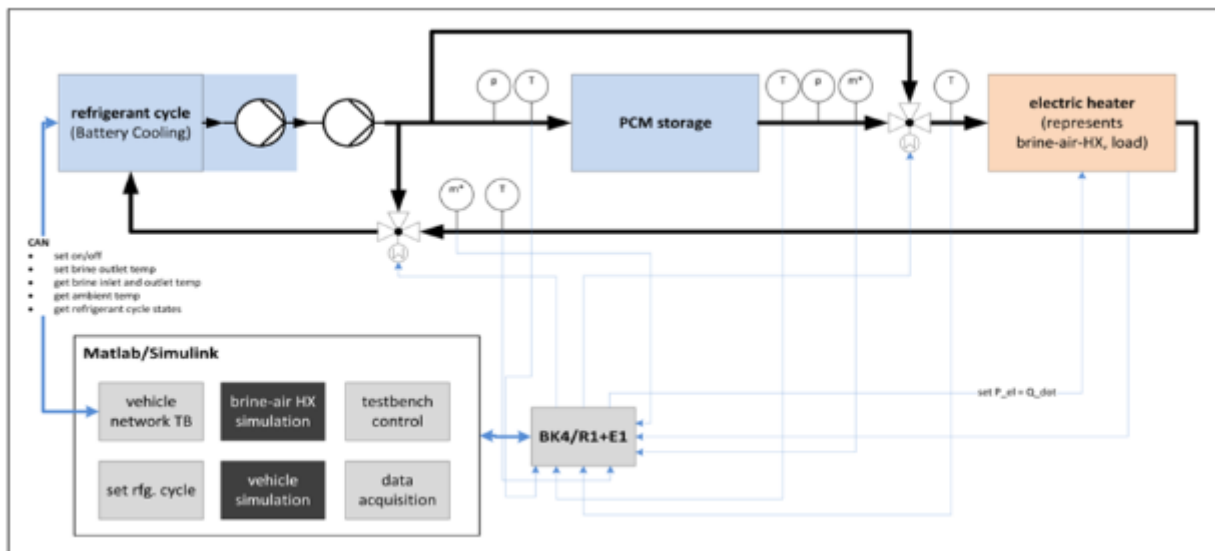


Figure 46: Scheme of the PCM storage demonstrator

Measurement results and discussion

In the following measurement results of a particular test with hardware-in-the-loop simulation of the brine-air heat exchanger are shown. In this test the air state and air volume flow at the brine-air heat exchanger were kept constant with respect to mixed air and the vehicle was not included in the hardware-in-the-loop simulation. The maximum volume flow circulated through the thermal conditioning

unit, the PCM storage, and the electric heater. The test can be divided into three phases as summarized in Table 12.

Table 12: Phases of Test 13

	phase 1 initialization	phase 2 “charging with cold” cooling / solidification	phase 3 “discharging cold” heating / melting
start time	0 sec.	1023 sec.	3424 sec.
end time	1022 sec.	3423 sec.	4273 sec.
duration	17 min	40 min	14 min
TCU operation,	cooling	cooling	off
set temperature	$T_{\text{target}} = 12^{\circ}\text{C}$	$T_{\text{target}} = 0^{\circ}\text{C}$	---
electric heater	off	off	on (model-controlled)

Figure 47 shows the brine temperature at the PCM storage inlet (blue) and outlet (red). In phase 1 of initial cooling the outlet temperature converges towards the inlet temperature relatively fast: In this phase no phase change occurs in the PCM storage. During the initial pull-down of phase 2 (approximately from 1023 to 1378 seconds), the outlet temperature closely follows the inlet temperature. As soon as the transition temperature of about 5-6°C of the PCM is reached, the inlet and outlet temperature curve start to diverge due to the phase change of the PCM. Eventually the set temperature is reached and the TCU activates the refrigerant bypass for cooling power reduction. Enabling and disabling the refrigerant bypass causes the temperature to oscillate around a relatively constant temperature level. As time passes more and more PCM is solidified and the storage outlet temperature converges towards the storage inlet temperature until both temperature levels (almost) coincide. At this point the state of charge is close to 100%.

Based on the brine inlet and outlet temperature, the specific thermal capacity of the brine (as a function of the brine temperature), and the brine mass flow rate derived from the flow meters, the power transferred into or out of the storage could be obtained, as shown in Figure 48. The different phases as discussed for Figure 47 are clearly visible. The electric heating power was limited to approximately 13.4 kW. It can be observed that the power transfer of the storage greatly lags behind the power transfer of the electric heater. The key reason for this is the thermal capacity of various components of the demonstrator.

It becomes obvious that cooling capacity changes drastically throughout discharge operation due to the steadily declining driving temperature difference at the brine-air heat exchanger. Therefore, in a rail application, a controlled discharge of the PCM storage will be needed. This can be realized by adjusting the mass flow rate through the PCM storage with a brine bypass.

The charging/discharging power of the PCM storage was integrated over time to derive the energy transfer to/from the storage. Considering phase 2 of sensible and latent cooling (time range 1023 sec. to

3423 sec.) with the brine inlet temperature range 12.5 °C to 1.6 °C the PCM storage capacity was found to be 0.72 kWh.

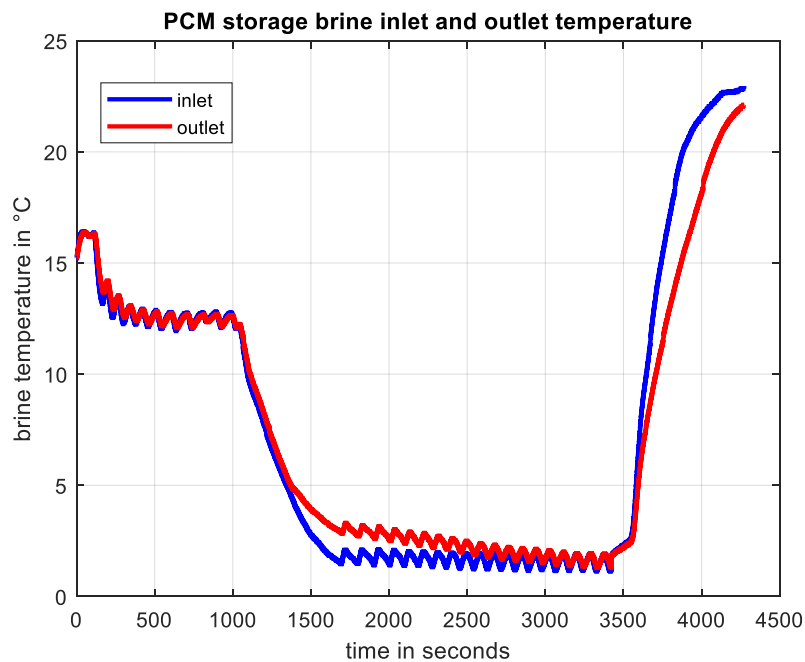


Figure 47: Test 13 – Brine temperature at PCM storage inlet and outlet

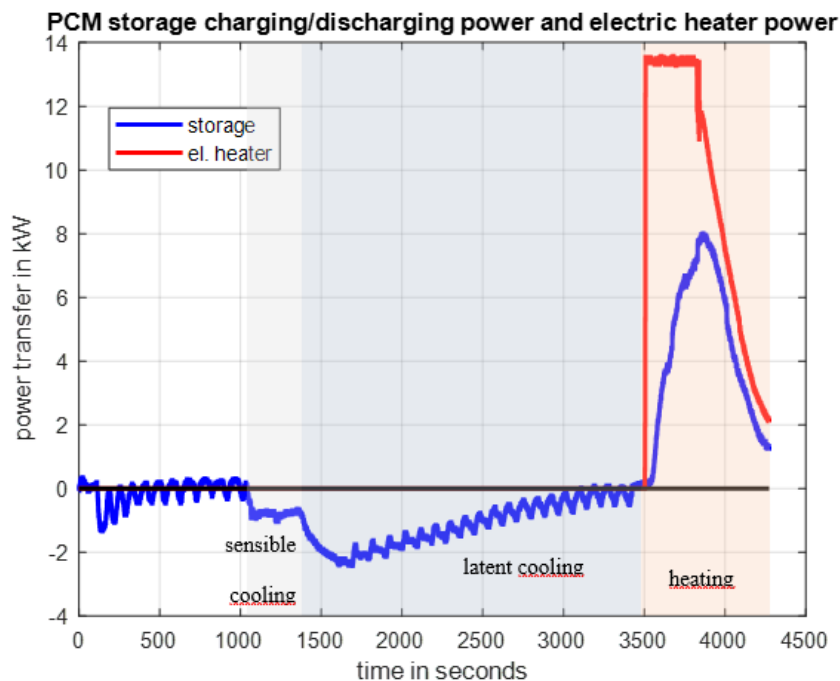


Figure 48: Test 13 – Power transfer to / from PCM storage and electric heater power:
(-) "charge with cold"/solidify | (+) "discharge cold"/melt

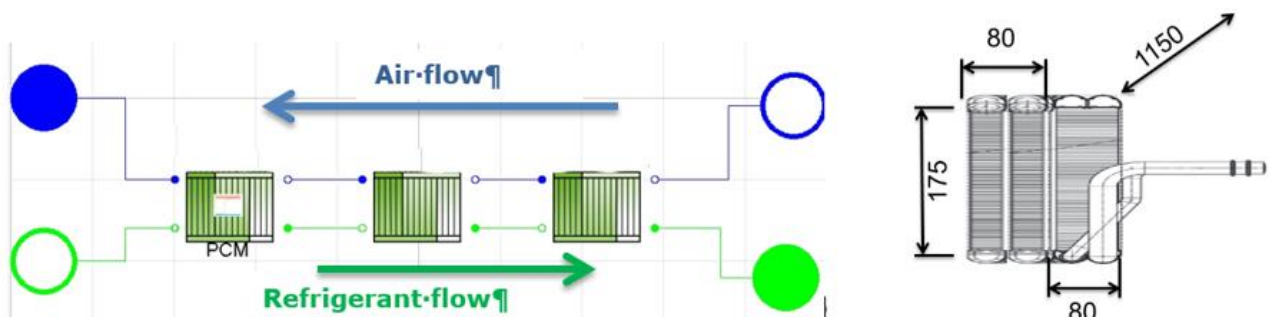
Conclusions of experimental results and outlook

It was the task to measure and assess the performance of the PCM storage from project partner i2m under realistic boundary conditions and integrated into a brine-cycle relevant for a rail vehicle. The tests

showed promising results so far. The measured storage capacity was plausible with respect to theoretical considerations. For future studies it is suggested to assess water as a storage medium and to implement automatic cooling power control.

5.5.2 Study 2: Integration of the Storage Evaporator Model into the Refrigeration System Simulation Environment

The evaporator build-up structure was similar to the storage evaporator on the test rig. Therefore: two normal tube-and-fin layers without PCM and one bigger tube-and-fin layer with encapsulated PCM, was assumed for the storage evaporator (subway size). The three evaporator layers are in series concerning air flow and refrigerant flow, counter flow arrangement (Figure 49). Each layer itself represents the typical cross-flow layout. This arrangement is reasonable to receive the lowest possible temperature at the PCM layer, refrigerant and air side. This is important to cool down the PCM during compressor operation. For the implementation of the PCM within a tube-and-fin evaporator a tube-in-tube design was assumed (see Figure 49). Also important was the quotient of heat transfer area between refrigerant ↔ PCM and PCM ↔ air to ensure early discharge of PCM during compressor operation and adequate melting progress during compressor standstill. This could be a trade-off only, considering different ambient conditions. In this case we focused on a certain part load use case for the A/C system mentioned in the following chapters. The radial PCM thickness x in heat flow direction should not exceed 5 mm to ensure charge and discharge of the PCM within practical time span and temperature level. Only PCM enriched with high thermal conductivity materials (e.g. metal particles, aluminum or copper wires or Boron nitride additive) could avoid this restriction. For the following simulation a radial PCM thickness of 3 mm was assumed. Fins through the PCM reservoir (Figure 49) enhance the thermal conductivity to the PCM by reason of its poor thermal conductivity. As a side effect the thermal resistance between refrigerant and air in this evaporator layer could be lowered. This allows an air-cooling capacity of this “PCM filled”- evaporator layer also during the PCM discharge period. For the following simulations a number of 8 radial fins in the tube-in-tube design was assumed. Lower number of fins led to a significant lower cooling performance during compressor still stand. A similar construction could be seen in the automotive storage evaporator of “Behr-Hella.



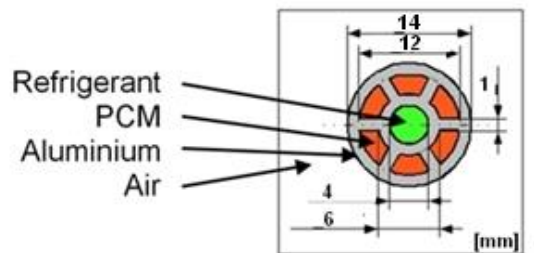


Figure 49: HX configuration (top), tube-in-tube integration of the PCM reservoir (bottom) ⁵

The minimal overall installation space of the assumed storage evaporator was 1150x175x160 mm. This includes the PCM storage layer with 1150x175x80 mm dimensions. This layout allowed implementing max. 1.2 kg of PCM. The PCM filled layer was placed at the air outlet of the heat exchanger, to avoid high heat flux between air and PCM during the cool down.

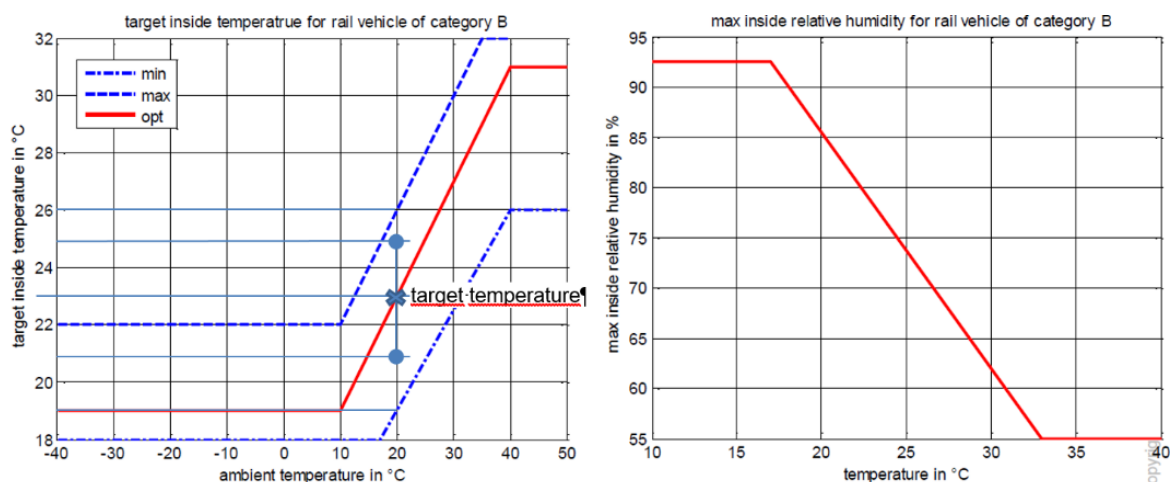
5.5.3 Simulation of required Energy Rates of the Storage System for a defined Use Case

Use case

A use case involves one on-off run of the A/C refrigerant cycle during a part load situation (duration “on-off run”: several minutes). At first a cool-down of the system to a certain minimum air temperature was simulated. Afterwards the standstill period of the compressor and the reheat-up of the system were considered.

The parameters for the simulation, see in Table 13, based on data from Liebherr

“Test1_LoadProfile_LondonUnderground_LVF_0146”, were applied for the simulation. Considered was a load profile during midday, while the subway is driving inside a tunnel. The limits for passenger comfort (Figure 50) were related to the ambient air temperature (outside of the tunnel) of approx. 20 °C. This relation is based on people’s expectation for a certain ambient temperature expressed by their worn clothes.



⁵ Source: Air Conditioning Library (ACL), Modelon AB

Figure 50: Limits for air temperature and humidity for adequate passenger comfort; Sketched in the assumed target temperature $23\text{ }^{\circ}\text{C} \pm 2\text{ K}^6$

Table 13: Main Parameter of the simulation model

Parameter	Unit	Value
air flow rate (A/C module)	m ³ /h	1333
fresh air ratio	%	25
fresh air temperature (tunnel)	°C	28
fresh air rel. humidity (tunnel)	%	43
PCM mass	kg	1.2
fusion temperature PCM	°C	15
fusion enthalpy	kJ/kg	220
heat transfer area refrigerant<->tube (all three layers)	m ²	0.8+0.4+0.4=1.6
heat transfer area PCM<->outer tube +PCM fins (PCM layer only)	m ²	2+1=3
radial thickness PCM	mm	3

The fusion temperature for the PCM was chosen by 15 °C, quite high compared to automotive applications. This is related to the high air mass flow through the evaporator and the higher air outlet temperatures during compressor operation. To surely discharge the PCM during compressor operation the A/C module must be capable to run at an air outlet temperature slightly below the PCM fusion temperature. Also the already mentioned temperature range of a typical phase change of PCM has to be considered. During optimization of geometric parameters of the storage evaporator various trade-offs occurred: e.g. If the melting temperature of the PCM is assumed higher, solidification of the PCM is easier for given amb. conditions. But during compressor still stand the required cooling performance of the PCM evaporator block isn't guaranteed. It should be mentioned here, that the geometrical implementation of the PCM (Figure 49) and the chosen PCM itself was only optimized for one certain ambient condition (see Table 13) in this use case. The heat transfer area of the inner tube (refrigerant side) is summed up for all three heat exchanger layers.

Simple cabin model

For an evaluation more similar to the reality (especially transient behaviour) a simple cabin model was used. Together with ambient conditions and a load profile based on data from Liebherr

“Test1_LoadProfile_LondonUnderground_LVF_0146” this leads to a necessary cooling capacity, on which this simulation is based (Table 14). From this data a mean load profile was derived: partial load, ~90 passengers, 28 °C air temperature (=tunnel), 25 % fresh air ratio; For one subway cabin an amount

⁶ Source: Liebherr-Transportation Systems 2014

of 3 A/C modules installed (refrigerant cooling cycles) were assumed. So for one A/C module only $\frac{1}{3}$ cabin was supposed to be cooled. The assumed compressor for one A/C module comes with following spec sheet data:

max. Compressor connected wattage	kW_e	3
Compressor displacement @ 50Hz	m³/h	8,6

The whole cabin model reflects an air volume and a point mass, consisting of 75 kg air ($c_p=1$ kJ/kgK) and 100 kg of solid material ($c_p=0.85$ kJ/(kgK)). The solid mass only represents the surfaces of the interior involved in the fluctuation of temperature. Both values represent an estimation only, to simulate some transient behaviour.

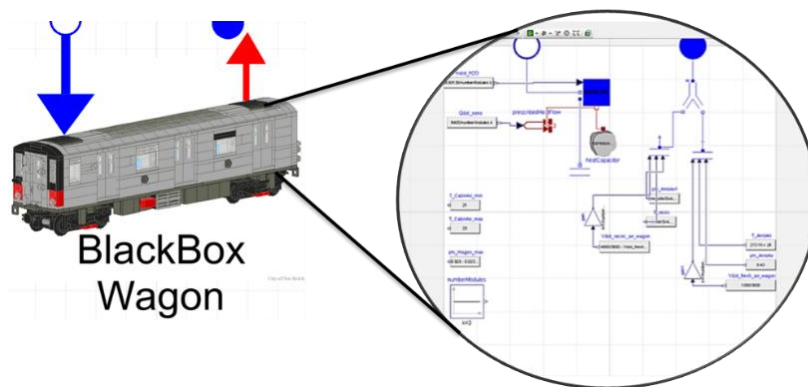


Figure 51: Simple cabin model based on air volume and point mass ⁷

Table 14: Main parameters of the simulation case

Parameter	Unit	Cabin – 3x A/C Modules	1/3 Cabin – A/C Module
sensible Load	[W]	8400	2800
latent load	[W]	3500	1166
latent load (H₂O)	[kg/h]	5	1.66
thermal mass cabin	[kJ/K]	75*1+100*0.85	53.3
min. cabin temp.	[°C]	21	21
max. cabin temp.	[°C]	25	25

5.5.4 Results and Discussion

For the defined use case, fresh air temperature 28 °C (tunnel) and about 90 passengers in a subway cabin (see more in Table 13 and Table 14), were considered. The following graphs show the transient behavior of a storage evaporator system and a standard evaporator system. For both systems (PCM / no

⁷ Source: Liebherr-Transportation Systems 2014; Air Conditioning Library (ACL), Modelon AB

PCM) the compressor operation period and the compressor standstill period were simulated separately. In the simulations the compressor started when the cabin reaches the temperature limit of 25 °C and stopped at a cabin temperature of 21 °C (see passenger comfort limits Figure 50, for a 20 °C day). Due to the heat storage capability of a PCM implement evaporator the compressor running time span could be extended significant. The absolute values of the simulation results include high uncertainty due to simplification of the simulation and assumed settings. Results are more suitable to comparing systems with and without a storage evaporator.

Table 15: Results of Simulation

		time span	mean cooling power (evaporator - air side)	mean cooling power (evaporator – refrigerant side)	mean power (condenser)	PCM mass
	Unit	s	W	W	W	Kg
PCM	compressor operation	130	6000	9000	11000	1.2
	compressor standstill	330	1200	0	0	1.2
no PCM	compressor operation	95 ¹	7000	8100	11000	0
	compressor standstill	120 ¹	850	0	0	0
	compressor operation	<50 ²	7000	8100	11000	0
	compressor standstill	100 ²	~850	0	0	0

¹ only applicable for the 1st “Pull Down” due to high humidity inside cabin

² estimation based on simulation, see Figure 54

Evaporation of attached condensate (water) during the compressor standstill represents an important effect. Due to the high evaporation energy of water (latent heat $h_{fus}=2530$ kJ/kg @ 15 °C) it's a lightweight and cost-free heat storage inside an evaporator. But standard evaporators can hardly use this potential because of the warm and extreme moist air leaving the evaporator. Normally the wet-bulb temperature of the air inflow is not low enough to provide an air outflow (into the cabin) pleasant for passengers. The limit of moisture (related to a certain air temperature Figure 50) is reached quite fast. With the help of an integrated PCM inside the evaporator, it is possible to keep the exiting air temperature lower. As a side effect the evaporation of water (off the evaporator surface) slows down and so the latent evaporation heat of water could help to cool down the airflow at a useable temperature level. Also the relative humidity of the exiting airflow remains below the limits for passenger comfort. The evaluation of a storage evaporator imbedded in an A/C refrigeration system will focus on the cooling capability within the limits for air temperature and especially humidity.

If the single on-off cycles are combined to a one hour cycle the cabin temperature (Figure 53) and the relative humidity (Figure 52) show the cyclical trend as expected. The number of *start* = 8 compressor starts per hour is the result for this storage evaporator system in part load conditions. For the air condition system with a standard evaporator (no PCM) the on-off cycle could not be repeated due to the high humidity inside the cabin. So the number of compressor starts had to be increased to achieve the same passenger comfort level. For the standard evaporator system the number of *start* = 24 compressor starts per hour is the result for this standard evaporator system in part load conditions, see Figure 54. This number of starts is drastically higher than the manufactured recommends for any reciprocating compressor.

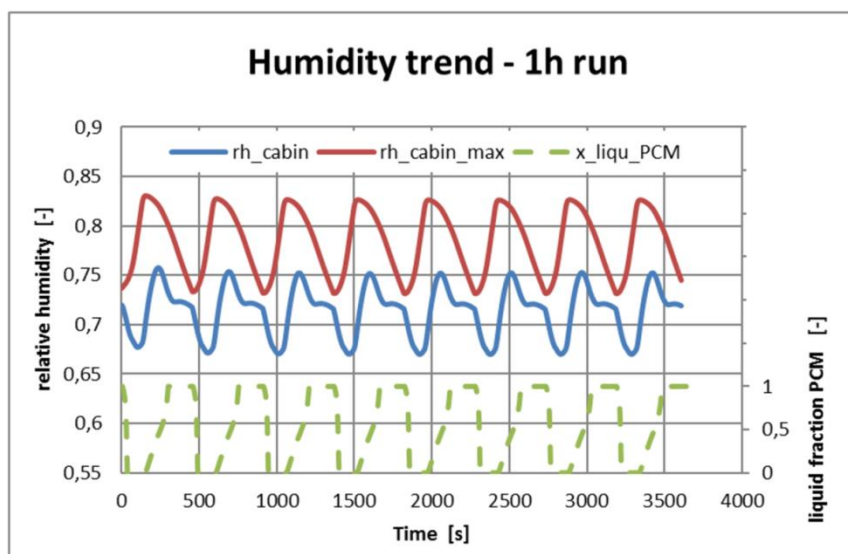


Figure 52: Relative humidity trend inside cabin together with the liquid fraction of PCM during an one hour cycle (PCM evaporator)

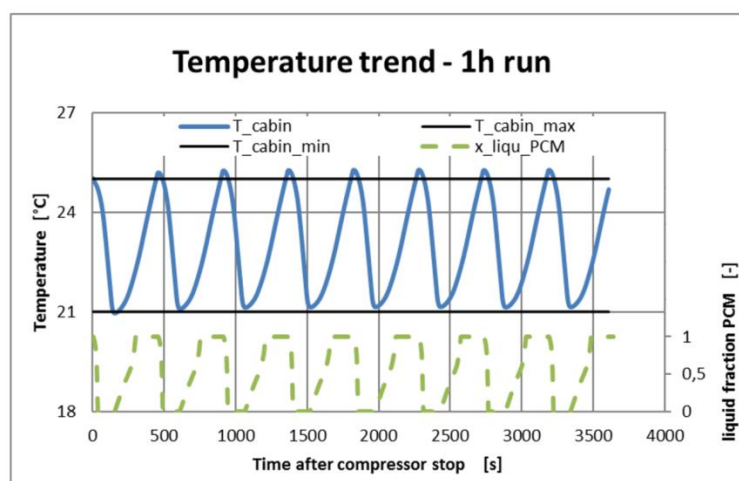


Figure 53: Temperature trend of cabin together with the liquid fraction of PCM during a 1 h cycle (PCM evaporator)

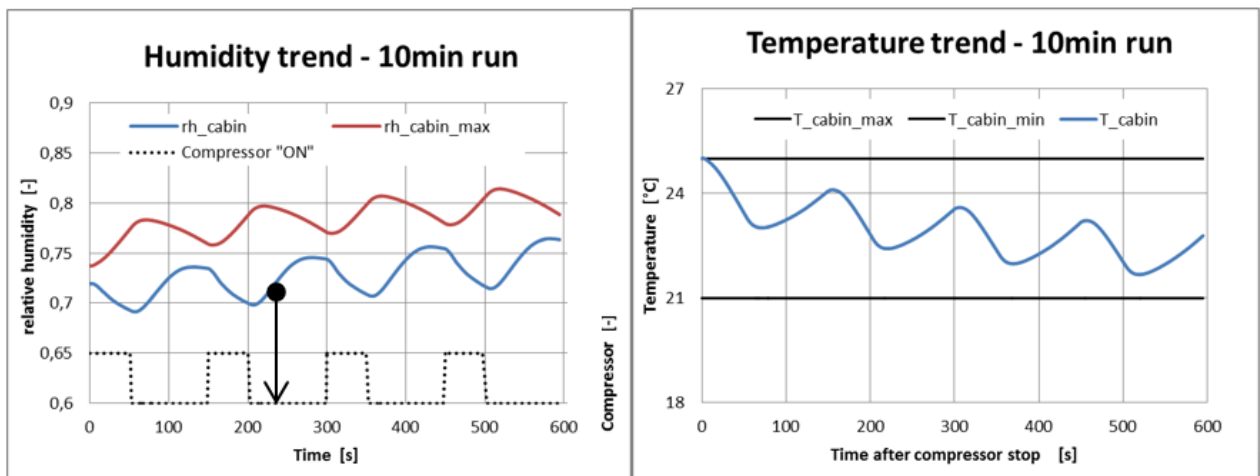


Figure 54: Temperature and humidity trend of cabin during a 10 min cycle (standard evaporator)

Summary Storage Evaporator

With assumed settings in the simulation, a conventional A/C system without PCM isn't able to run in on-off mode during part load, due to the high number of compressor starts per hour, see Figure 54. So an inefficient part load operation mode, called hot gas bypass, has to be run. To avoid this scenario with a fixed-speed compressor the use of an advanced storage evaporator is a possible solution.

For the considered ambient condition (Table 14) a storage evaporator implemented in an A/C module for an underground railway can create an appreciable benefit. By utilising the thermal inertia of the cabin and the energy stored inside the evaporator due to the added PCM it is possible to operate the A/C module in the more efficient on-off mode. The critical number of compressor starts per hour will not be reached in the considered use case. Therefore, the operation strategy for this part load scenario is on-off operation. The implementation of a useful amount of PCM inside an evaporator the installation space required is double at least. To gain benefit of a storage evaporator solution in A/C systems the consideration of further use cases and validation of thermal mass of the cabin in the transient model is mandatory. Optimisation potential for all geometrical parameters and thermal characteristic of the PCM is given at this early stage of development. E.g. the use of additives for the PCM could enhance the low thermal conductivity of this kind of materials.

5.5.5 ACS HVAC Simulation Results – Batch Dehumidification

ACS	air cycle system
HVAC	heating, ventilation, and air-conditioning
HX	heat exchanger
LVF	Liebherr-Transportation Systems GmbH & Co KG
MACM	motorized air cycle machine

To simulate the effect of the dehumidification on HVAC system level the ACS architecture was mapped in Liebherr's internal EOLE simulation software⁸ for this purpose. The simulation software has proven its value in many years of use at Liebherr in various research and customer projects. The model for the turbomachine is based on characteristic maps. Characteristic maps were also used for various heat exchangers. Model inputs were temperature, humidity and mass flow rate of the processed air, the model output was the electric power consumption of the turbomachine. All simulations target was a constant cooling power on the climatic air flow in design point conditions.

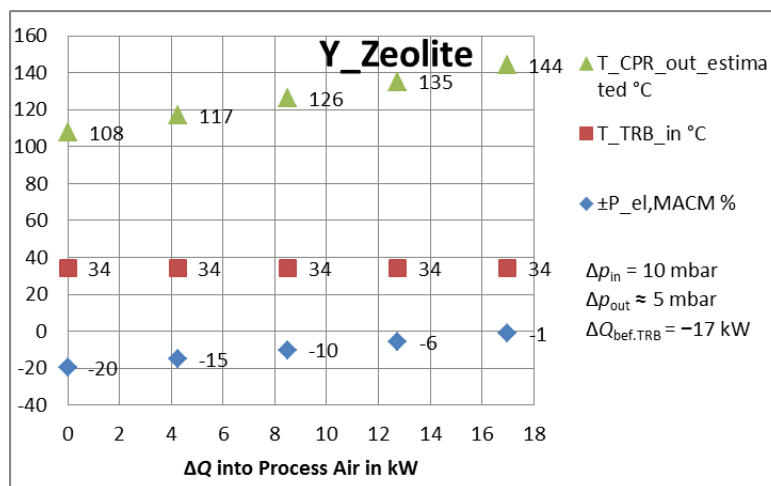


Figure 55: Simulation of power saving as function of the re-cooling performance

According to the material characterization Y zeolite was identified as the most efficient desiccant under the ACS inherent operating conditions:

- $dx = -10$ g/kg (ave)
- $dT = 26.6$ K (ave)
- required cooling 17 kW

Applying these figures on the thermodynamic simulation model of the ACS HVAC shows a resulting power saving potential on the MACM motor of 22%, if the complete temperature increase can be compensated. A positive effect through dehumidification on the power consumption starts at a minimum of 9.5 kW re-cooling capacity (Figure 55).

Considered re-cooling architecture

To gain the best overall system efficiency the re-cooling of the turbine inlet airflow should be done as much as possible using ambient air as heat sink. In a railway HVAC system the installation space is the driving limiting factor for the efficiency of the air/air heat exchangers.

⁸ Liebherr-Aerospace Toulouse SAS. EOLE (version 15.0.0.) - Tool for thermodynamic system simulation for performance assessment of Aircraft and Helicopter Air Conditioning Systems, Bleed Systems, Vapor Cycle Systems, Toulouse 2015 (not published)

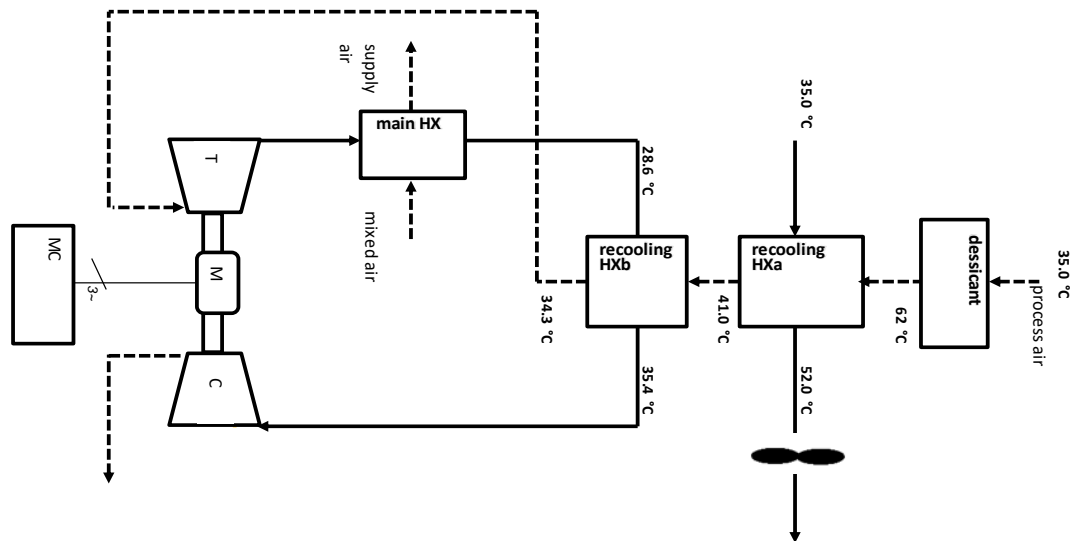


Figure 56: Chosen re-cooling architecture

Table 16: Heat exchanger characterization for re-cooling

re-cooling HX ambient (HXa)			re-cooling HX process air (HXb)		
CFL	390	mm	CFL	150	mm
HFL	400	mm	HFL	200	mm
NFL	540	mm	NFL	2x310	mm
core weight	42	kg	core weight	9	kg
Q	13	kW	Q	4	kW

Limiting the size of the re-cooler to reasonable dimensions for integration in the HVAC unit (assumption max. height approx. 0.4m, max. lateral length approx. 0.5m) shows, that it is not possible to gain a re-cooling capacity of 17 kW, just by using the ambient as heat sink.

Consequently, a concept was chosen for simulation on system level, anticipating that a small part of the re-cooling heat is introduced in the process cycle just upstream the compressor.

With the re-cooling architecture according to Figure 56 and Table 16a total reduction of the MACM power of 15% is reachable. Since the ambient air heat exchanger needs also a fan for the cold air flow the total benefit is decreased to 8.5%, since the fan itself has non-negligible power consumption.

Table 17: Resulting power saving respecting re-cooling equipment

power MACM basis [kW]	35.8
power MACM desiccant dehumid [kW]	30.5
power reduction MACM [kW]	5.3
power fans for re-cooling [kW]	2.3
net power reduction [kW]	3.0
net power reduction [%]	8.5

5.5.6 ACS HVAC Simulation Results – Sorption Rotor Dehumidification

Considering the results of the sorption rotor tests a lower dehumidification rate and increased heat impact was observed:

- $dx = -6.8 \text{ g/kg}$ (ave)
- $dT = 40 \text{ K}$ (ave)
- required cooling 25 kW

The reduced dehumidification performance and the increased heat impact on the processed air flow causes less power saving and the need for an increased heat exchange upstream the turbine stage. Figure 57 shows the simulation results anticipating also an increased pressure loss due to increased heat exchanger performance.

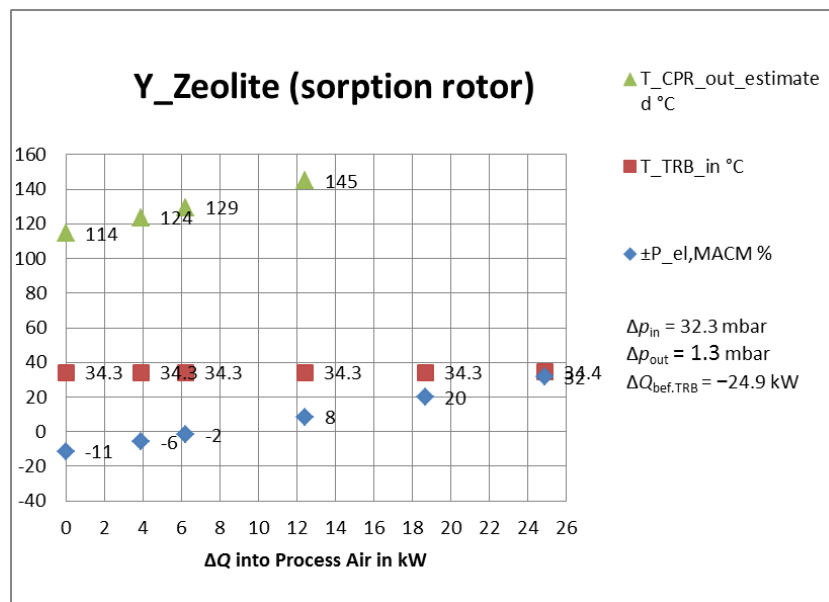


Figure 57: Simulation of power saving using sorption rotor dehumidification

Anticipating the same amount of heat transfer to the processed air flow as in chapter 5.5.5 leads to the heat exchanger setup according to Figure 58 and Table 18

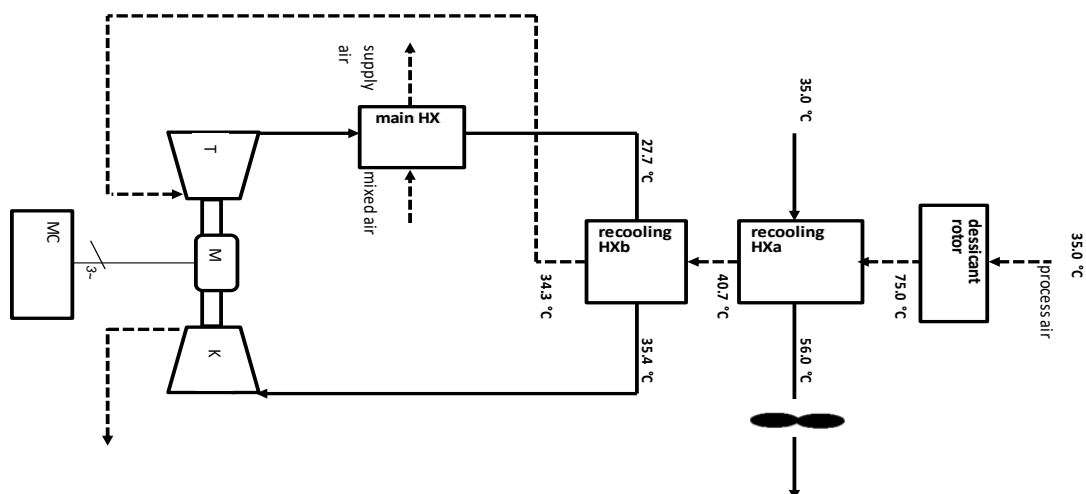


Figure 58: Re-cooling architecture using the sorption rotor for dehumidification

Table 18: Heat exchanger characterization for re-cooling using the sorption rotor for dehumidification

re-cooling HX ambient (HXa)			re-cooling HX process air (HXb)		
CFL	350	mm	CFL	150	mm
HFL	400	mm	HFL	200	mm
NFL	625	mm	NFL	2x310	mm
core weight	43	kg	core weight	8.7	kg
Q	21	kW	Q	4	kW

The total power saving balance is in this case negative. Due the re-cooling effort anticipating a necessary fan power, which is in range of the power saving on the MACM motor, there is no benefit from the dehumidification left.

Table 19: Resulting power saving respecting re-cooling equipment for sorption rotor

power MACM basis ICE3 [kW]	35.8
power MACM desiccant dehumid [kW]	33.8
power reduction MACM [kW]	2.0
power fans for re-cooling [kW]	2.4
net power reduction [kW]	-0.4
net power reduction [%]	-1.1

The full potential of the dehumidification is obviously not useable by this re-cooling concept. Using only ambient air for re-cooling according Figure 59 has an even worse impact on the power saving.

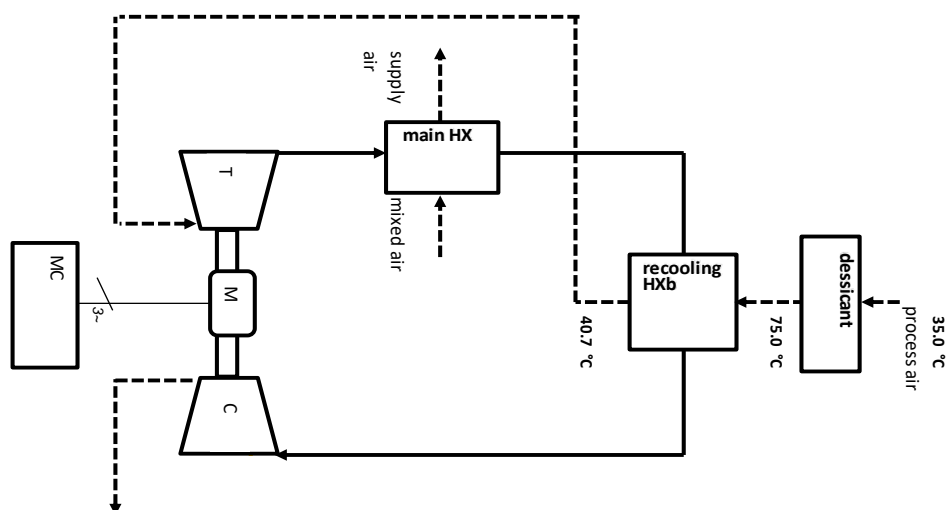


Figure 59: Re-cooling using only ambient air as heat sink

Table 20: Resulting power saving using only ambient air as heat sink

power MACM basis ICE3 [kW]	35.8
power MACM desiccant drying [kW]	35.1
power reduction MACM [kW]	0.7
power fans for re-cooling [kW]	2.4
net power reduction [kW]	-1.7
net power reduction [%]	-4.8

Alternate Measures for Power Saving on ACS HVAC

As shown in the previous chapter , there is a significant effort necessary to re-cool the air flow upstream the turbine stage to gain a benefit out of the dehumidification. This means extra installation space which is in general at all railways ACS HVAC units the limiting factor.

Table 21 shows the power saving potential considering improving the main heat exchanger instead of implementing a dehumidification/re-cooling installation. The target was to meet the same power saving on the MACM motor as in Table 19. Enlarging the main heat exchanger does not need any additional measures, therefore all the saving on the motor power can be utilized and the net power saving is higher than in Table 19.

Table 21: Resulting power saving using only ambient air as heat sink

power MACM basis [kW]	35.8
power MACM enlarged main HX [kW]	33.8
power reduction MACM [kW]	2.0
net power reduction [kW]	2.0
net power reduction [%]	5.7

Assessment of Measures for Power Saving on ACS HVAC

The installation of desiccant device and re-cooling equipment means increase of integration space, weight and cost on the HVAC system. Table 22 compares weight and cost of the different results found in the previous chapter.

Table 22: Weight and cost of power saving measures

	weight [kg]	cost [€]	Comment
batch test sorption, re-cooling partly with ambient, partly with process air			
desiccant	26	n.n.*)	2x8 kg desiccant, 10 kg containment & ductwork
HXa	42	950	cross flow plate HX
HXb (incl. header)	10	240	cross flow plate HX
fan assembly	15	1000	
ductwork	15	1000	
total	108	3190	
sorption rotor, re-cooling partly with ambient, partly with process air			

Energieforschungsprogramm – 4. Ausschreibung

Klima- und Energiefonds des Bundes – Abwicklung durch die Österreichische Forschungsförderungsgesellschaft FFG

desiccant	52	n.n.*)	2 rotor assemblies each 26 kg
HXa	43	980	cross flow plate HX
HXb (incl. header)	10	230	cross flow plate HX
fan assembly	15	1000	
ductwork	15	1000	
total	135	3210	
sorption rotor, re-cooling only with ambient air			
desiccant	52	n.n.*)	2 rotor assemblies each 26 kg
HXa	43	980	cross flow plate HX
fan assembly	15	1000	
ductwork	5	300	
total	115	2280	
improve main heat exchanger instead of process air drying			
main HX enlargement	45	1020	
main HX header enlargement	2	290	
total	47	1310	

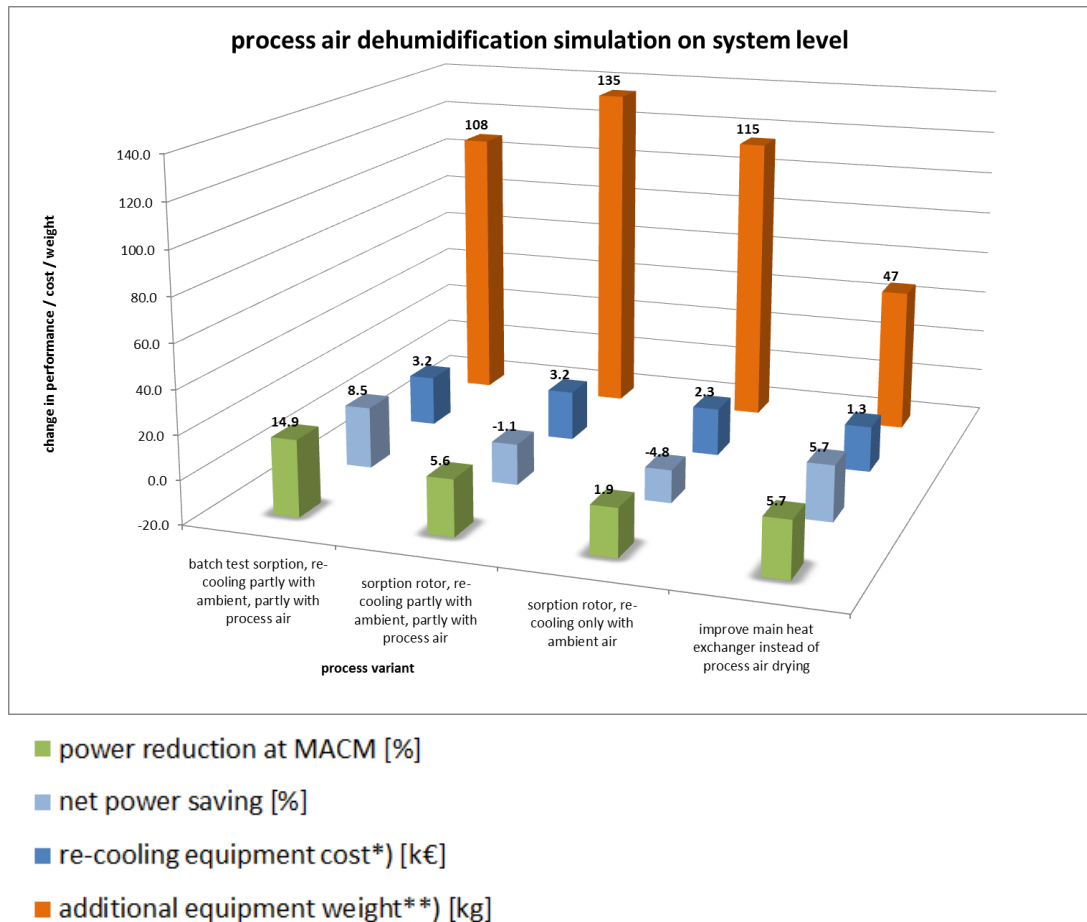
*) price of 2000€ per desiccant rotor, price for desiccant material and rotor for serial application unknown

Table 23: Comparison of power saving variants

variant	desiccant	dehumidification rate, [g/kg]	temperature increase in process air flow [K]	re-cooling power with ambient air [kW]	re-cooling power with process air [kW]	power reduction at MACM [kW]	power reduction at MACM [%]	fan power consumption for re-cooling [kW]	net power saving [kW]	net power saving [%]	additional equipment weight**) [kg]	re-cooling equipment cost*) [k€]
batch test sorption, re-cooling partly with ambient, partly with process air	Y-zeo	10.0	27	13.0	4.0	5.3	14.9	2.3	3.0	8.5	108	3.2
sorption rotor, re-cooling partly with ambient, partly with process air	Y-zeo	6.8	40	21.3	3.9	2.0	5.6	2.4	-0.4	-1.1	135	3.2
sorption rotor, re-cooling only with ambient air	Y-zeo	6.8	40	21.3	0.0	0.7	1.9	2.4	-1.7	-4.8	115	2.3
improve main heat exchanger instead of process air drying	none	0.0	0	0.0	0.0	2.0	5.7	0	2.0	5.7	47	1.3

*) heat exchanger and fan assembly

**) desiccant, heat exchanger and fan assembly



*) heat exchanger and fan assembly

**) desiccant, heat exchanger and fan assembly

Figure 60: Comparison of power saving variants

Conclusions and Outlook on HVAC System Level

Dehumidification of the ACS process air shows the potential for power saving, if the dehumidification rate is high and the heat impact on the process air flow is low.

The critical points are the additional need of installation space, weight and cost for the dehumidification equipment. These are in general the limiting elements on an ACS HVAC optimization. Comparing the effort for desiccant dehumidification and re-cooling with other ACS immanent optimization measures (enlarging the main heat exchanger) shows, that the performance of the desiccant materials must be significant better, than found in this study according the state of the art.

Future development should be focused on compact equipment with increased dehumidification rate and an integrated high efficient re-cooling system in the sorption device.

6 Line D: Industrial waste heat recovery with novel thermochemical heat storage

Goal:

Identification of industrial application fields for sorptive and thermochemical energy storage materials. Development of storage materials, reactors and application concepts (especially concerning process integration) at medium ($< 400^{\circ}\text{C}$) and low ($< 250^{\circ}\text{C}$) temperature levels.

6.1 Boundary conditions and system design:

For industrial applications the boundary conditions are defined by the type of the energy/heat source (gaseous or liquid). If a mass flow has to be cooled down for heat recovery its composition has to be taken into consideration. Mass flow and temperature of the certain mass flow are the major properties, which are characterizing the energy source.

Key parameters are energy density, power (represented by reaction kinetics for TCS) and process parameters which have to be taken under consideration, dependent on the field of industrial application. General methods within the project are modelling and simulation in combination with process integration, materials and reactor development as well as economic evaluation.

6.2 Materials selection and development

6.2.1 Sorptive Materials:

Introduction:

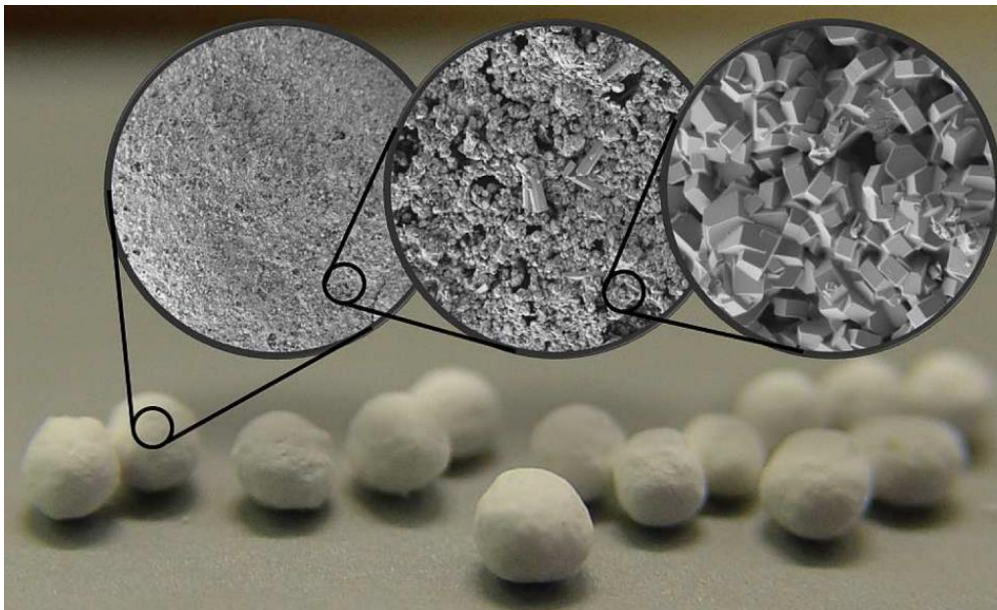


Figure 61: Zeolite beads and their structural surface

The fundamental research to store heat from solar systems with zeolite started in the late 1970s. These projects in the idea of a long-term storage of the solar gains in the summertime leads to a better understanding of the reaction kinetics and overall, how to use sorption material to store thermal energy.

Up to now, the research focuses in the increasing of the reaction kinetics, measuring of adsorption diagrams of inorganic and also organic sorbents, the hydrothermal and mechanical stability and hence, the cycling stability of sorption materials. In this project the aim was to enhance the natural zeolite Clinoptilolite with salt and agglomerate it to relevant particle size (about 2,5 mm spherical globes), to achieve low production costs of the material with the same energy density and behaviour of standard synthetic zeolite. While the impregnating with salt, the production process and different binder materials affects also the mechanical strength, our focus was beside the water sorption, which is a good indicator for the energy density, also research about the attrition and compression behaviour of the developed materials was carried out.

In more detail, the cycle stability depends on the material compound and which binder was used. In addition, the production process, a fluidized bed agglomeration or a disc agglomeration and secondary treatments (like calcination) affects the mechanical and thermal stability of the material. The present research focuses on the stability of such materials under typical application conditions. Therefore, there is already in the production of sorption material a wide range of possibilities to affect the material characteristics of the thermal sorption storage material. In Figure 62 an overview of the manufacturing methods of zeolites is given.

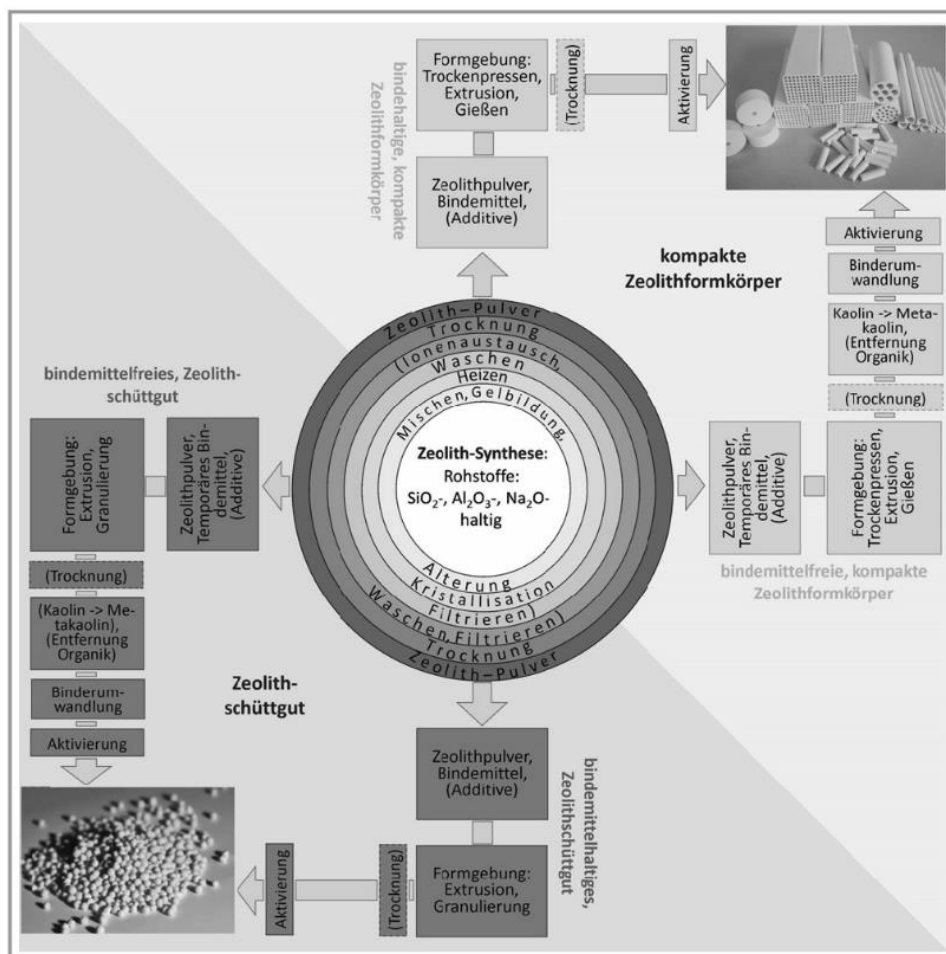


Figure 62: Overview of the different manufacturing methods of zeolites ⁹

The first part is the zeolite synthesis, the raw materials and the treatment define which zeolite powder is produced. The further processing is of more interest, it can be classified into binderless zeolite granulate and zeolite granulate with binder (attapulgit, bentonite,...). The choice of the binder material, which shaping process is used and in the last step, the calcination parameter, are highly influencing the thermal and mechanical stability of the material.

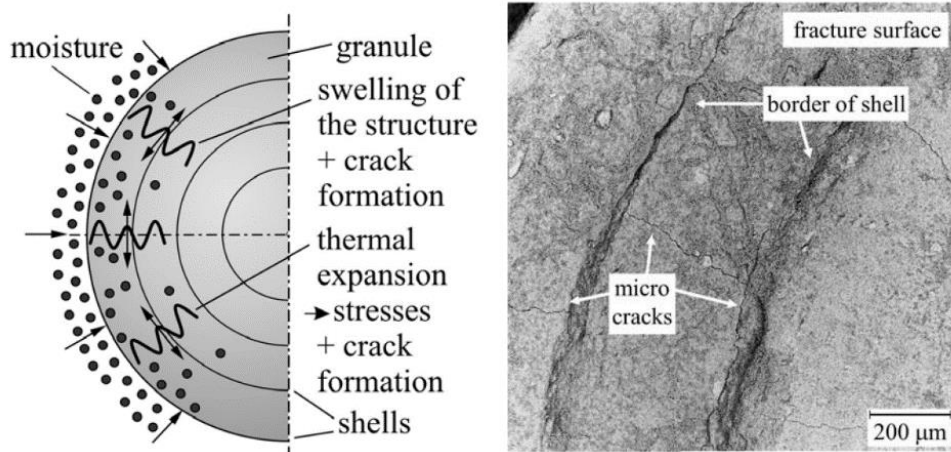


Figure 63: Scheme of the formation of stresses and cracks due to thermal expansion at moistening (left), SEM recording of the fracture surface of a Köstrolith 4A K granule composed of shells and exhibiting macro cracks after moistening ¹⁰

During the project duration the most promising production steps were used to produce new sorption materials. The focus was set to develop zeolite beads with binder in fluidized bed agglomeration or a disc agglomeration, the used test facility is shown in Figure 68. With this systems it was possible to modify the content of binder, changing the bead size or using different binder materials and compare the new developed zeolite beads. Afterwards the disc agglomeration method was used, because it consumes less energy in the agglomeration step and the zeolite beads seem to have a higher mechanical stability, due to a higher density.

Beside the production process, the cycling stability depends also on the application and which reactor is used. A fixed bed reactor has less requirements to the mechanical stability of the sorption materials than a drum reactor or fluidized bed reactor, which forces the sorption material with higher friction. So mechanical testing of sorption material for evaluation of the possible reactor types, like fixed bed, agitated bed or fluidized bed is necessary. And for this reason the types of load on the zeolite beads is essential to know.

Due to moistening of the zeolite and the binder (clay mineral attapulgit), a slight swelling of the structure occurs (Theng, 2012). Noack et al. (2009) have observed an irregular expansion and contraction of the unit cell dimension for different zeolite crystals as a function of temperature and moisture content. This

⁹ K. Gleichmann, et. Al.: Industrielle Herstellung von zeolithischen Molekularsieben, 2017

¹⁰ Peter Müller, et al.: Influence of binder and moisture content of the strength of zeolite 4A granules, Chemical Engineering Science, 2014

represents a considerable parameter that could influence development of stresses and macro-crack formation, in addition to existing stresses due to thermal expansion, see Figure 63.

So the thermal and mechanical stability depends on temperature, the water load and how often the material is cycled. A method to identify the damage of the sorption material on a detailed level is to use a scanning electron microscope (SEM), shown in Figure 64.

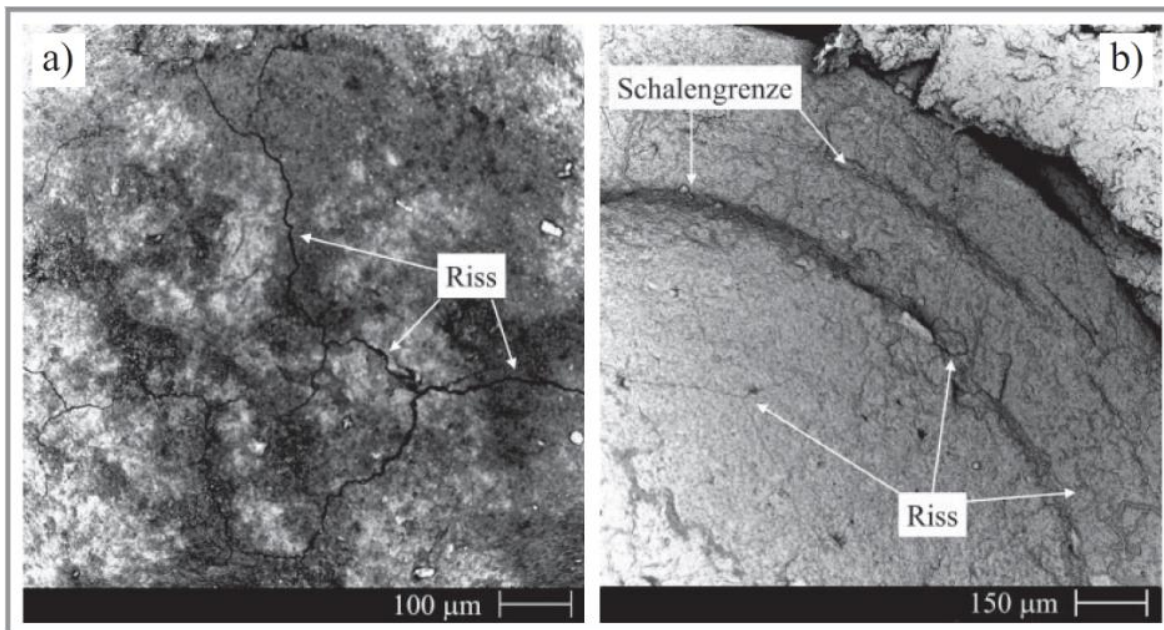


Figure 64: scanning electron microscope (SEM) of granulates (4A) after 20 cycles (225x magnification) of the surface (a) and the fracture plane ¹¹

On a macroscopic scale, a particle distribution before and after a test is a good indicator of the material change due to mechanical and hydro thermal stress. This can be done with a sieve analysis or a particle analyser device Figure 65.

A drawback of the sieving method is, that during this measurement also attrition occurs, changing the result depending on the sieving time and frequency. The method is also used for measuring the mechanical stability and attrition of wood pellets, so for our characterisation of zeolite beads the non-invasive optical measurement of the particle diameter is the better choice.

All in all, it is necessary to determine how long the lifetime of the products will be having passed several cycles of moisture-loading-unloading without remarkable reduction in strength.

So the first approach was to search for possible methods to characterize the mechanical stability for the material zeolite and Clinoptilolite. The two most relevant values, the break resistance and the attrition strength are used to describe the mechanical stability of the material.

Unfortunately there is no defined standard, how to measure these values. Some papers describe the break resistance referring to the standard ASTM D6175-03 (Standard Test Method for Radial Crush

¹¹ Peter Müller, et al.: Mechanische Eigenschaften zyklisch be- und entfeuchteter Zeolithgranulate, Chem. Ing. Tech., 2015

Strength of Extruded Catalyst and Catalyst Carrier Particles).¹² A similar principle using compression tests at a constant velocity (0.02 mm/s) shows Figure 66.



Figure 65: Sieve analyser device (left) and particle analyser device (right)

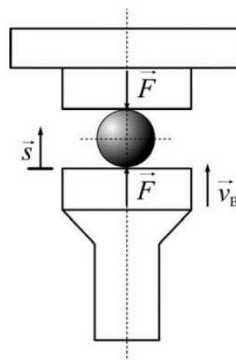


Figure 66: Scheme of single granular compression test

The granule to be examined is placed at the starting position of the lower piston. Subsequently, the piston moves upwards to the measurement position. As soon as the granule is in contact with the upper piston, the diameter of the granule is measured and the measurement of values (force progression, displacement, time) starts. The granules exhibit a large inhomogeneity concerning their microstructure, particularly in the distribution of bonds i.e. solid bridges. Further, they exhibit a high porosity, a high surface roughness and an almost non-spherical shape. Thus, the standard deviations are comparatively large. However, to obtain reproducible and representative statistically invariant results, the tests were repeated 100 times per series of samples. Another method is to test the mechanical stability with a colliding cannon, which is shown in Figure 67. With a pneumatic system individual particles are shot to a plate to measure the fraction amount over the fraction velocity.

¹² E. Goldnik, T. Turek: Herstellung und Charakterisierung von reaktiven Adsorbentien – Untersuchung zum Reaktionsablauf, Chem. Ing. Tech, 2016.

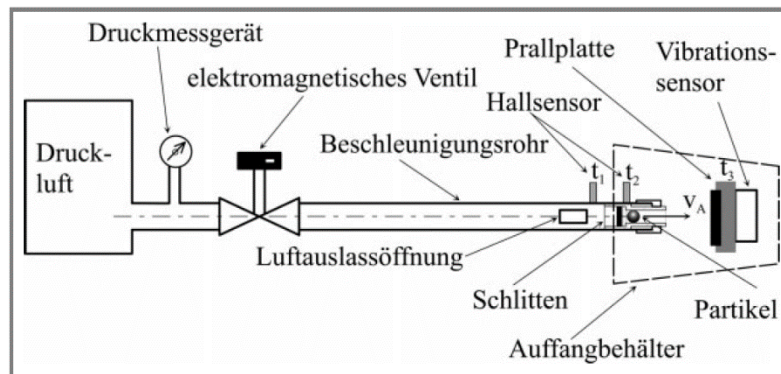


Figure 67: Schematic overview of the pneumatic colliding cannon

To describe the attrition from form bodies, granulates or tablets, normally an attrition drum, also called Friabilator is used.^{13,14} Some research groups tried the measurements out referring to the Ph. Eur. 2.9.7.¹⁵ In fact, that the mechanical stability depends on the temperature and the water load, an on-line sensor should be implemented in the attrition drum, to clearly document the determining factors during the measurement. An attrition test with a vibration sieve is also proposed in a paper.¹⁶ This procedure was referred to the experiment regulation from the quality management of a zeolite manufacturer.¹⁷

System requirements

For the temperature- level of waste heat recovery applications below 250°C, the sorption heat storage material zeolite and different salt hydrates were examined. In view of economic factors and theoretical boundaries of these sorption materials, it was decided to use inexpensive but less reactive natural zeolite instead of the common technical zeolite 4A or 13X. Prices of natural zeolites vary with zeolite content and processing. Unit values, obtained through the U.S. Geological Survey canvass of domestic zeolite producers, ranged from \$110 to \$440 per metric ton.¹⁸ Clinoptilolite shows in the preliminary test the best results and costs about 300 € per metric ton, when buying in big amounts >100 tons.¹⁹ So it is only about a third of technical zeolite 4A and a tenth of the costs of zeolite 13X. Another important boundary condition is to use materials with low primary energy consumption. Especially for long term heat storage the total amount of stored energy should exceed the resources used for production with a reasonable number of cycles. A life cycle analysis of technical zeolite 4A results that one ton zeolite needs 7.34 MWh.²⁰ Silkem, a Slovenian manufacturer of technical zeolite 4A, gives us the information that about 250 m³ of natural gas are needed for producing one ton. Natural zeolite like Clinoptilolite is the better option, if one assumes that the exploitation has the same primary energy consumption like sand, it need only 0.13 MWh.

¹³ R. Polke, W. Herrmann, K. Sommer, Chem. Ing. Tech. 1979, 51 (4), 283 – 288.

¹⁴ E. G. E. Shafer, E. G. Wollish, C. E. Engel, J. Am. Pharm. Assoc. 1956, 45 (2), 114 – 116.

¹⁵ Pharmacopoea Europaea, Europäisches Arzneibuch, 7. Ausgabe, Deutscher Apotheker Verlag, Stuttgart 2011.

¹⁶ J.G.C. Storch: Materialwissenschaftliche Untersuchung an zeolithischen Adsorbentien für den Einsatz in offenen Sorptionssystemen zur Wärmespeicherung, Dissertation, 2010.

¹⁷ B. Unger, CWK Chemiewerk Bad Köstritz, personal conversation.

¹⁸ S. Jawell: Mineral Commodity Summaries 2014, U.S. Department of the Interior, U.S. Geological Survey, Virginia 2014

¹⁹ Communication Dr. Somitsch Walter

²⁰ M. Fawer: Life Cycle Inventory for the Production of Zeolite A for Detergents, St. Gall, 1996

To overcome the energy density gap between technical and natural zeolite when using it in storage applications, post-manufacturing processes know-how (like pelletizing and calcination) of zeolite were adopted and used for the natural zeolite and composite material. In addition, binders and salts are necessary to produce a composite material out of it and to obtain comparable storage properties like the benchmark zeolite 4A. Another advantage of composite materials are the possibility to change the thermophysical properties by changing salt types and mixtures when using different fractions of mixing, so for a given application one can tune material properties.

Material treatment

To adapt the sorption material to the application and reactor design, several material treatments like agglomeration methods, thermal activation and salt impregnation were tried and results compared. In order to use natural zeolite as a heat storage material several modifications have to be done: With an appropriate agglomeration method, it is possible to change the rheological behaviour, mechanical strength, and the grain size of the particles as well as the material composition. With salt impregnation, it is possible to increase the energy density and thermal power of the material. Thermal activation provides also to increase the mechanical strength of the particles.



Figure 68: fluidised bed agglomeration facility AMMAG (left) and plate agglomeration facility ARP (right)

The first materials were produced by project partner AMMAG with a fluidised bed agglomeration facility. With these first experiments, it was possible to produce a material with ideal core diameter and different binders. Nevertheless, not all interesting types of binder were applied due to process limitations and the energy consumption of this method is quite high. Alternative methods, like plate pelletizing was used for further material experiments.

The microscopic structure, mechanical stability and thermophysical properties of the produced modified materials were determined.

Scanning Electron Microscopy of outer and fracture surfaces of the pellets showed mostly homogeneous distribution of clinoptilolite, binder and impregnated salts along with macropores, though few clusters of salt crystals within the zeolite-binder-matrix also could be observed. The outer surface was much more compact and exhibited less macropores than the fracture surface. For microscopic examination a Quanta SEM FEG 250 from Thermo Scientific, equipped with an EDAX EDS System Microprobe for

elemental analysis was used. The samples were prepared by sputter coating with gold using an EDWARDS Scancoat Six sputter coater.

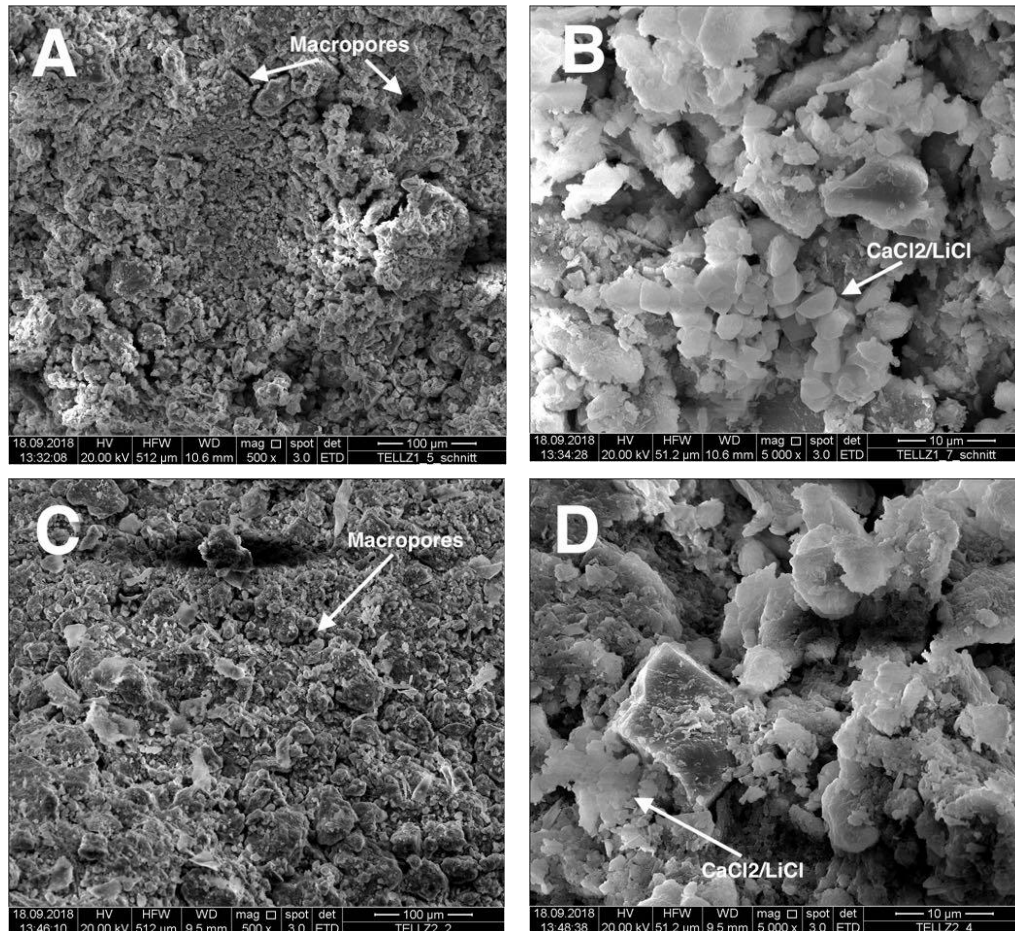


Figure 69: SEM images from $\text{CaCl}_2/\text{LiCl}$ impregnated clinoptilolite pellets. A, B: binder attapulgite, fracture surface. C, D: binder Li-silicate, outer surface.

Beside the binder PVP (Polyvinylpyrrolidon), other types like Attapulgite, Bentonite (clay minerals) and Waterglass (silicate based binder) were tested. With the different materials, it could be proved that neither the agglomeration method, the binder ratio nor the thermal activation has a big impact to the moisture absorption rate, which is the leading criterion for adsorption heat generation. The advantage of agglomeration and thermal activation, to obtain a higher mechanical strength, outweighs the small decrease of moisture absorption. The humidity absorption is a good indicator, how much energy can be stored in the material. Another good indicator is the dynamic of the reaction, because over a longer period it is difficult to get a useful temperature lift.

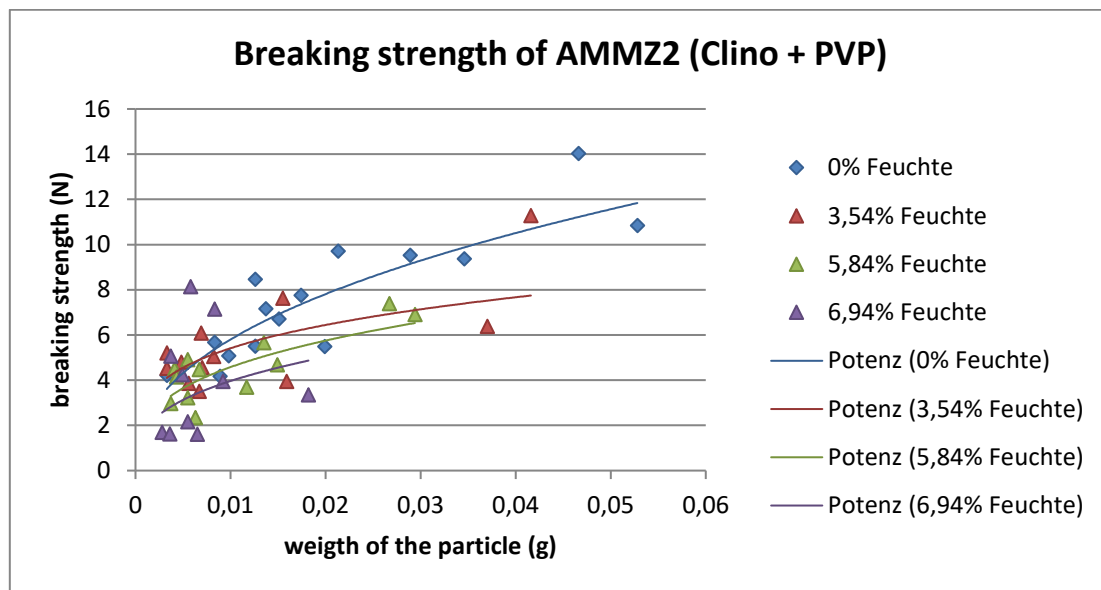


Figure 70: breaking strength of AMMZ2 with different water content and different particle weight

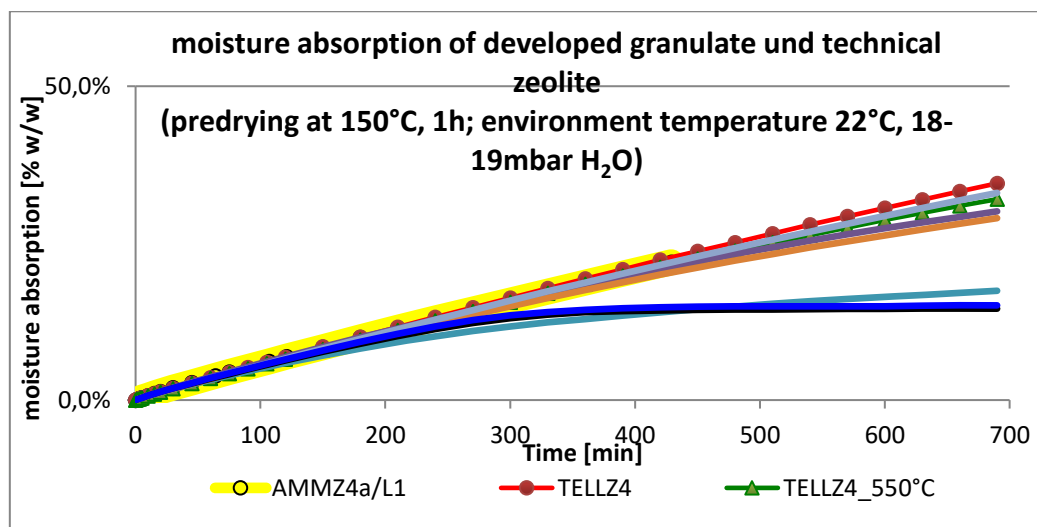


Figure 71: Comparison between the moisture absorption of the produced materials and technical zeolite

The reaction and the moisture absorption of the produced material shows in comparison to the technical zeolite good values. The salt content of the developed materials can absorb more water than zeolite. This behaviour is noticeable after 150 min, when the absorbing rate of zeolite 4A and 13X decrease, but the absorbing rate for the developed materials is nearly constant. It is necessary to control the water content of the materials with salt amount, because the mechanical strength of the particle decrease while absorbing water. Figure 72 displays the layer structure of a wet fluidised bed and a plate-agglomerated particle. The plate-agglomerated particle shows a more homogeneous structure and a higher moisture absorption to the core.

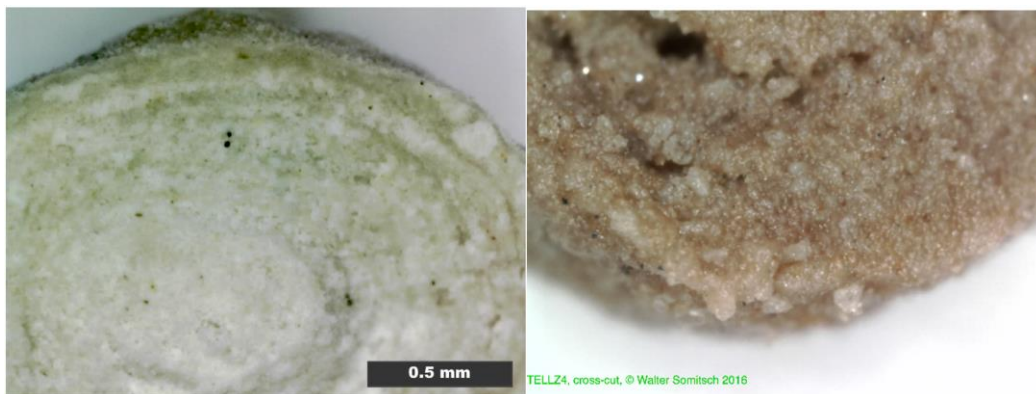


Figure 72: the layer structure of a wet fluidised bed (left) and a plate-agglomerated particle (right)

With low binder content and without thermal activation, the mechanical strength and the crack resistance of the developed material are very low and did not fulfil the requirements of a storage system. Further research focus to increase the mechanical strength and measure the materials with break resistance and attrition tests. The cyclic stability of the developed materials should be also taken into account, but due to limited resources, it is not possible to do this in this project.

Methodology and component for material testing

For a better comparison validation of our developed sorption material compounds, it was decided to set the priority to describe the break resistance and attrition behaviour of the materials. Both values are necessary for using it either in a fixed bed or moving bed reactor, whereas the material losses during a time period is an important value.

The method to describe the break resistance and also the protocol of the execution can be found in the attachment (20160128_Messprotokoll_Bruchfestigkeit_Granulate_IBSW.pdf) and was realised from our project partner Dr. Walter Somitsch. Beside this measurements, also attrition tests were carried out. Because there is no standard of measuring the attrition from zeolite agglomerates, an own attrition test set up was constructed, which design was based on a friability tester, used in pharmacy. To increase the number of degrees of freedom, the angular of the drum, the speed and also the drum diameter was variable (see Figure 73).



Figure 73: Friability tester used in the pharmacy (left) and experimental device (right).

With this set-up, the first attrition tests and comparison with a fluidized bed agglomeration material (AMMZ3a), a salt impregnated clinoptilolite (CompS3), disc agglomerated material with two different

diameters (TELLZ a or b), calcinated disc agglomerated material (TELLZ_550°C) and the commercial available 4A Zeolite from the company CWK and Silkem were investigated. The results of the first attrition test can be seen in Figure 74.

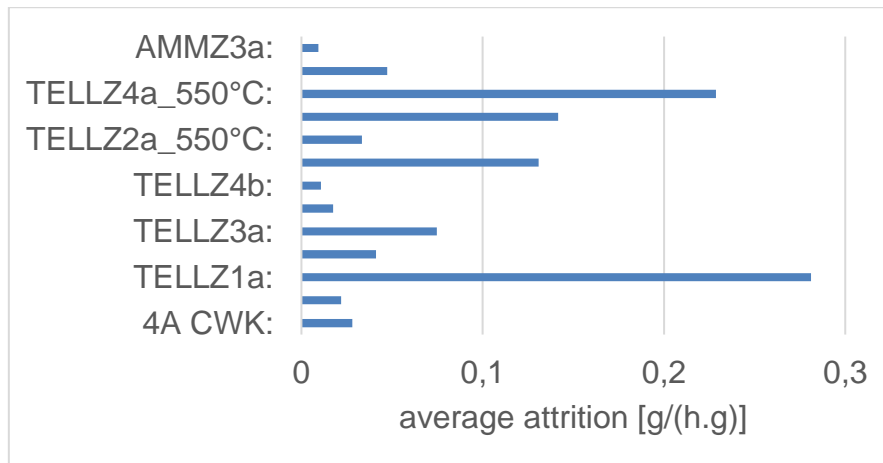


Figure 74: Attrition test derived from experimental device

Because of some irregularities at these attrition results, which were not reasonable (e. g. TELLZ4b had a better attrition behaviour than commercial available 4A zeolite or the calcinated material sample), more time was invested to find out, which factors can influence and sophisticate the results.

Attrition test component design

All the material samples should have the same initial state (e. g. geometry, size, humidity,...) and material stress during the attrition test. To avoid the influence of the air humidity to the material samples during the test, the drum can be sealed with a lid. Also the initial state of the material sample was not defined very well, so the samples should be sieved all, to get a uniform particle spectrum. In order to get reliable results, the material samples should be also separated from their initial dust which adheres on their surface after the sieving, which can be done with oil-free compressed air.

The failure impact during the handling of the material samples (take the material from the drum to the precision balance, etcetera) could be reduced with using a higher amount of about 1 kg. Also the not perfectly round drum and small dc-motor which had no constant velocity should be improved to get more reliable results. In a second step a lab scale agglomeration and attrition unit was designed by AMMAG to create better attrition results and be more flexible and independent in producing improved material samples. As reference points and for dimensioning calculations, a literature research was investigated.

21,22

²¹ M. Stieß: Mechanische Verfahrenstechnik 2, Springer-Verlag Berlin Heidelberg GmbH, 1997.

²² K. Sommer, W. Herrmann: Auslegung von Granulierteller und Granuliertrommel, Verlag Chemie GmbH, 1978.

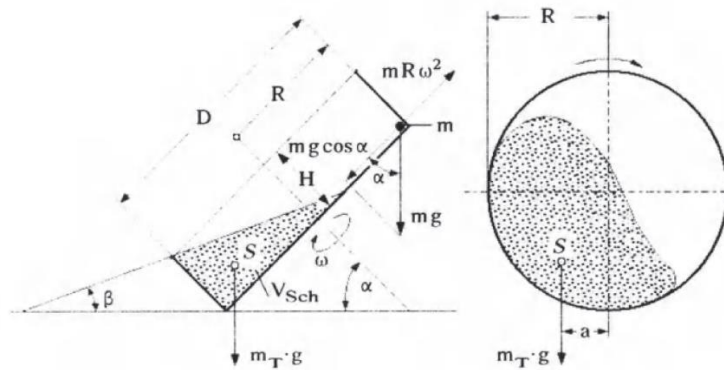


Figure 75: Values for calculation of an agglomeration and attrition unit ¹³

To get a deeper insight of the material behaviour in the initial state and after the attrition test, also two special sensors were purchased. The first sensor measures the temperature and the humidity on-line during the measurement. The second important sensor is a particle analyser, which can give a good statement of the particle distribution and dust amount before and after the attrition test. With the bigger drum a more round and stable attrition test with a sample amount of 1 kg could be achieved. In addition a holder for installing the humidity and temperature in-line sensor was realized.

Concept of the attrition plate:

The design of the rotating plate (see Figure 76 and Figure 77), used within this project for examination of granular attrition of zeolite-based products was driven by several demands and needs:

- 1.) Functions
 - a. Attrition/stability testing of solid/granular storage media
 - b. Formation and shaping of granules, mainly on zeolite basis
- 2.) Highly adjustable in order to simulate the conditions of different reactors (fluid bed, drum, screw conveyor), i.e.:
 - a. Variable rotation speed
 - b. Variable slope of the plate
 - c. Usage of different amounts of product
- 3.) Integration of online moisture sensor for solids
- 4.) Integration of sensor for online particle size
- 5.) Long term stability of speed
- 6.) Avoidance of change in particle moisture during attrition measurement
- 7.) Mobile, to be used at the labs of various project partners
- 8.) Calculation of speed according to Literature²³

²³ K. Sommer, W. Herrmann: „Auslegung von Granulierteller und Granuliertrommel“, Chem.-Ing.-Tech 50 (1978) 7, p. 518-524

Energieforschungsprogramm – 4. Ausschreibung

Klima- und Energiefonds des Bundes – Abwicklung durch die Österreichische Forschungsförderungsgesellschaft FFG

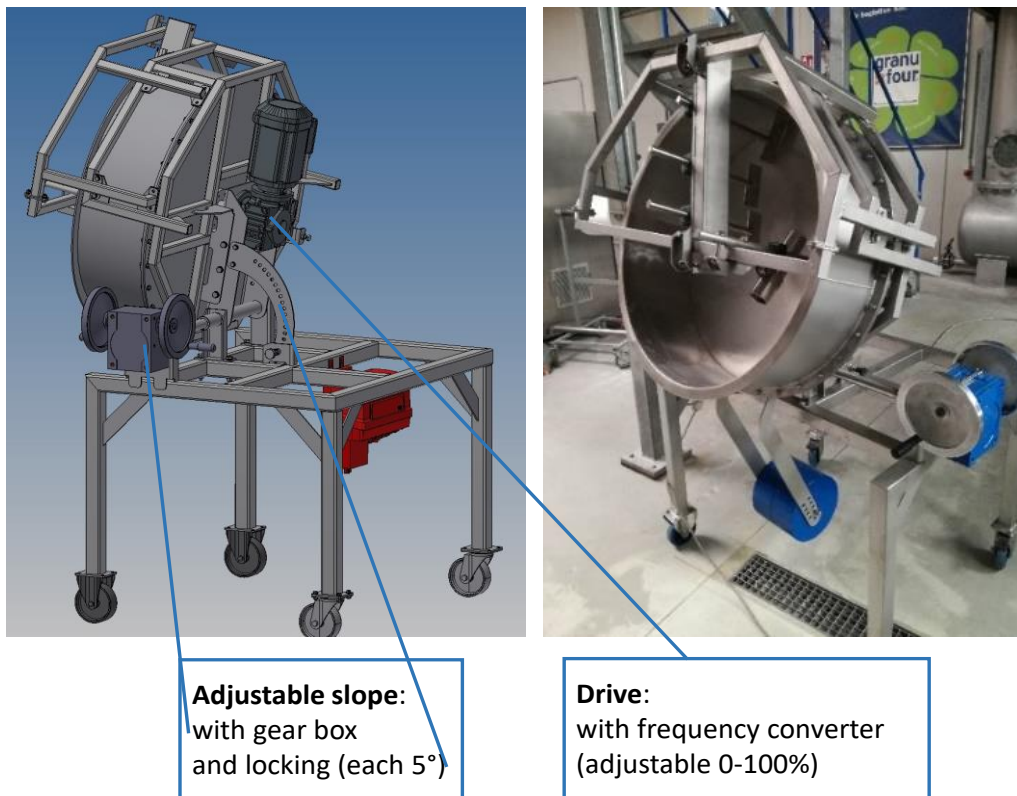


Figure 76: 3D-view and photo of rotating plate

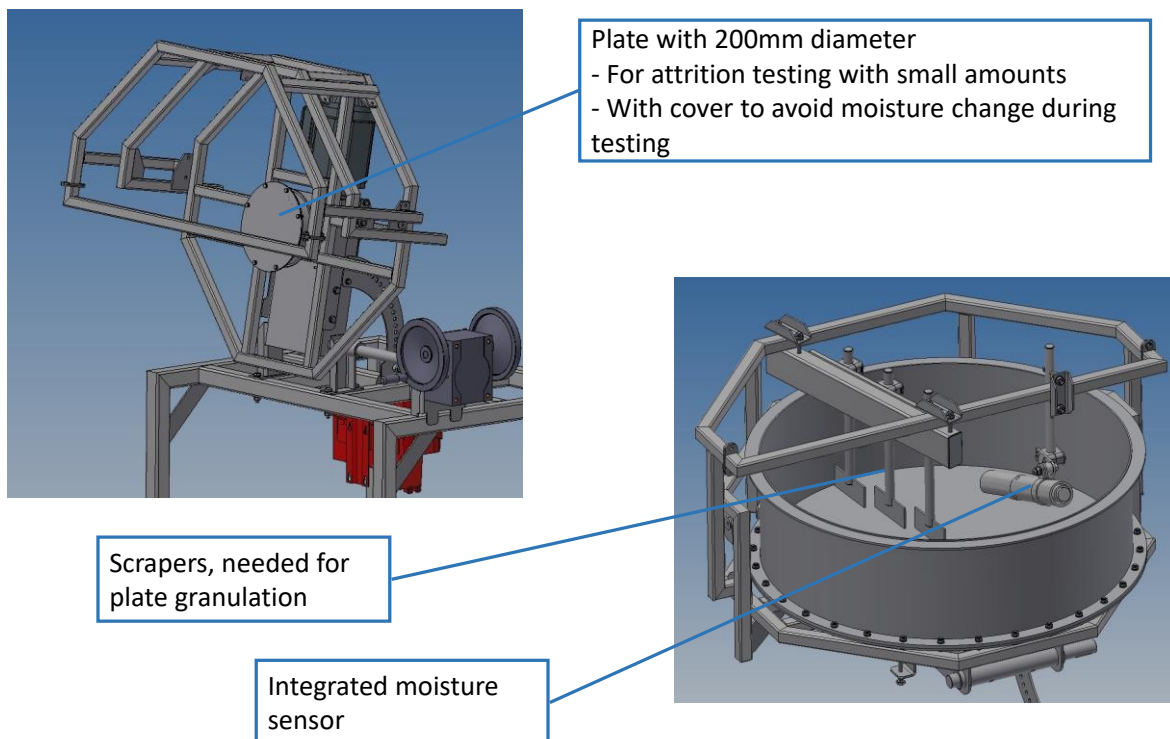


Figure 77: additional 3D-views of rotating plate

Humidity measurement



Figure 78: disc agglomeration and attrition unit with sensor (left) and detailed picture of installation in contact with the sorption material (right)

The data of the sensor **Sono-Silo** was implemented in the existing measurement system ALMEMO and logged during the whole measurement to enhance the repeatability and reproducibility. This sensor uses a radar-based dielectric measuring procedure (TDR – Time-Domain-Reflectometry) with a frequency pulse of 1 GHz. It was installed in an angle of 45°, so that the measuring surface is fully dipped into the streaming bulk material (see Figure 78, right side).

Particle analysis

The particle analyser **Parsum IPP 70-S** (shown in Figure 79) was used to define the initial and final status of the sorption material during the attrition test. This sensor is able to detect particle size between 50....6000 µm at a very high rate (theoretical data rate up to 20000 particles per second).

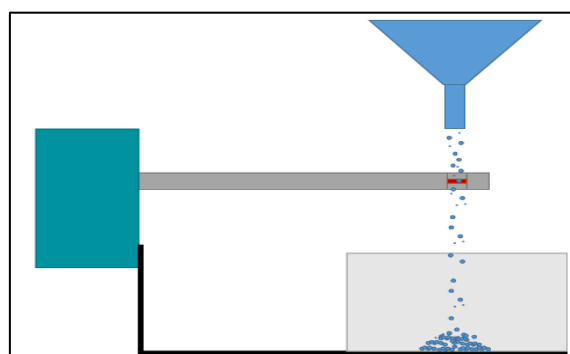


Figure 79: Schematic test set-up

The Parsum Probes use the technique of Spatial Filter Velocimetry to measure particles. The sensor works by using a fiber optic patented measurement principle and simultaneously measures the size and velocity of individual particles. Statistical techniques associated with the technique allow calculation of chord length distributions.

The software **Inline Particle Probe 8.01** from the manufacturer was used to evaluate and compare the results. With this program different possibilities to depict the size distribution, or creating a sieve fraction with defined sieve diameters.

The set-up for measuring the particle diameter was used for all the material samples, to have always the same measuring conditions. Minimum 0.5 kg mass was extracted from the attrition drum and the zeolites in the drums were mixed so that no segregation, which happens during the attrition test in the drum, falsify the results.

6.2.2 Attritions tests

Material 1: Zeolite 4A, Manufacturer CWK,

This type of material contains approx. 30 % bentonite binder, is quite stable when used in thermochemical heat storage reactors with moving bed (slowly moving – rotating cylinder- 60 cm diameter). Therefore, materials like this (bentonite bound, commercially available) act as kind of benchmark to evaluate the usability of other types of granulates.

The CWK 4A zeolite was delivered as granulate with sphere diameter ranging from 1.6 to 2.5 mm. prior and after the abrasion testing particle size analyzation, photo-documentation and mass determination (with humidity correction) was used.

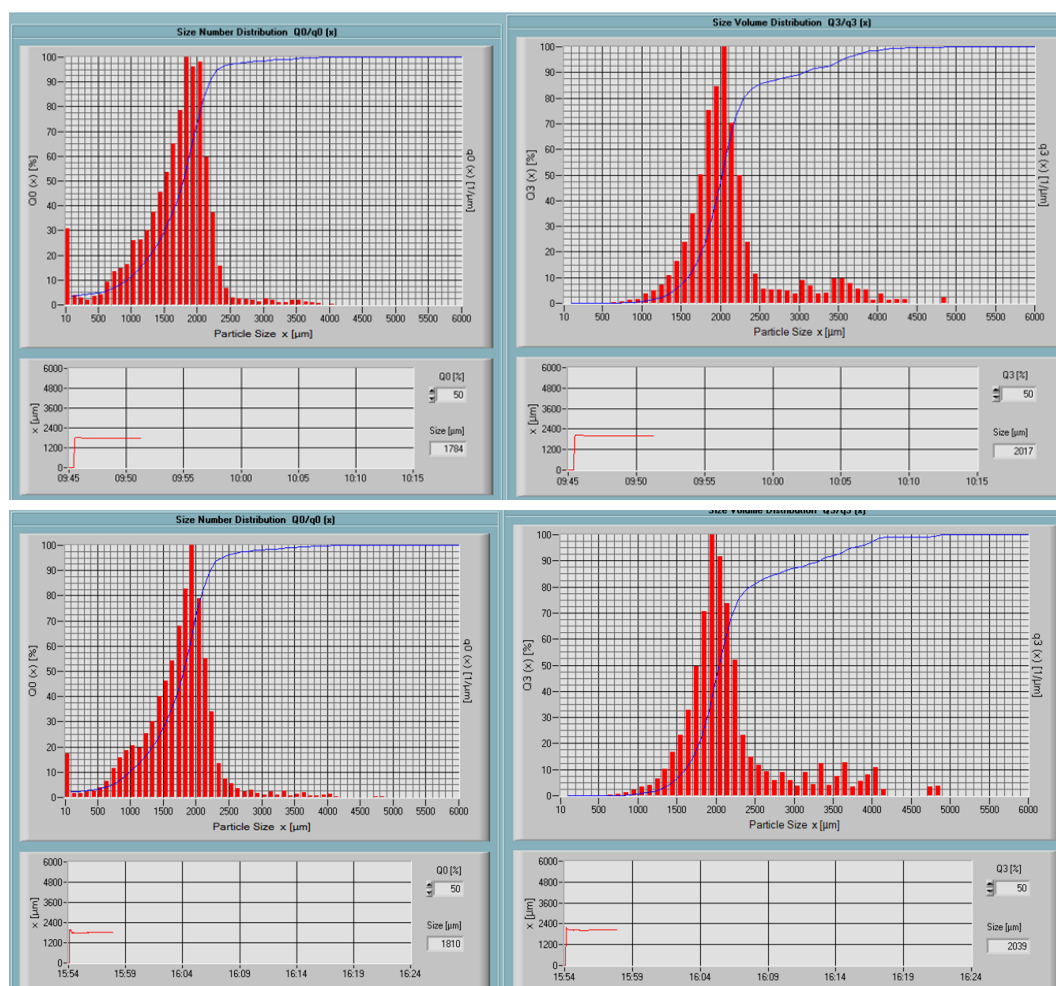


Figure 80: CWK 4A zeolite particle size analysis prior (above) and after 24h of abrasion testing (below)

Table 24: CWK 4A (>10 μ) zeolite particle size distribution in terms of number and volume

All values in μm	Prior	After 24 hours
Small particles (0.1 quantile)	1000	900
Median (0.5 quantile)	1800	1800
Large particles (0.9 quantile)	2200	2200
Volume 0.1 quantile	1600	1600
Volume 0.5 quantile	2000	2000
Volume 0.9 quantile	3300	3300

The numbers in Table 24 indicate that 10 % of all particles are smaller than 900 μ m (0.1 quantile), 50 % of the particles are smaller than 1800 μ m (median or 0.5 quantile), and 90 % are smaller than 2200 μ m (0.9 quantile).

The total volume of the storage material is covered to 10 % of particles smaller than 1600 μ m (vol. 0.1 quantile), half the volume is covered by particles smaller than 2000 μ m (vol. 0.5 quantile), and 90 % of the volume is covered by particles smaller than 3300 μ m (vol. 0.9 quantile). While the particle size distribution is more illustrative, these values can greatly be influenced by the dust fraction if very small particles are present in large numbers. Dust is hardly influencing the volumetric distribution, which is most depending on very large particles. Table 24 indicates that there is no measurable influence on the particle size distribution after 24 h of abrasion treatment. Nevertheless, the influence on particle mass was measurable.

Table 25: CWK 4A zeolite particle mass

Mass values in g	Sample mass	Mat. water content	Dry mass	Abrasion
Prior	1026.52	11,98 %	903.40	
After 24 h@ 3.8 J	966.98	14,10%	830.64	72.76 (8.1%)

The numbers in Table 25 indicate that there is a loss of 73 g of dust material (removed by ventilation and sieving) after 24 h of abrasion testing - that corresponds to 8.1 % of the original dry mass. The impact of the abrasion treatment (indicated as 3.8 J in Table 25) refers to the next paragraph below.

In order to characterize the load applied to the material (intensity of friction and collisions) by the rotation of the plate the mechanical energy of the lifting movement of the rotation plate was calculated.

In case of free falling of a mass from a height of 0.4 m a velocity of $v=(2gh)^{0.5}=2.8$ m/s would be reached in the end. Average velocity is 1.4 m/s and the time to fall down is 0.286 s. It was assumed that the material needs twice the time to roll down the plate compared to a free fall (0.57 s). The time of lifting depends on the rotation speed of the plate. In case of an 80 % setting of the frequency transducer of the motor controller a rotational speed of 39 revolutions per minute was measured. The circumference velocity $v=\omega r=2\pi r f=1.6$ m/s the circumference section of lift is 30 % and lifting time 0.47 s. Altogether, for one abrasion cycle movement, a grain needs 1.04 seconds. For several settings of the motor controller cycle times are listed in Table 26.

As a measure for abrasive loading, the mechanical energy of lift is used. This amount of energy is the reason for material abrasion, the higher and more frequent the material is lifted the more energy for

deformation (abrasion) is available. As a simple measure, the integral lifting energy per unit mass (1 kg) and unit time is used.

Table 26: Abrasion test conditions

Motor setting	Cycle time in s	Abrasion energy measure in Joule /kg /s
80%	1.03 s	3.8 J /kg/s
70%	1.10 s	3.6 J /kg/s
60%	1.18 s	3.3 J /kg/s
50%	1.31 s	3.0 J /kg/s
40%	1.49 s	2.6 J /kg/s
30%	1.79 s	2.2 J /kg/s

6.3 Line D, WP3: Component Development

Component design in pilot- or demo scale wasn't done in development line D. The main components developed where test rigs for testing thermochemical materials. As described before an attrition test apparatus was built, see Figure 76 and Figure 77. For the tests under fluidized bed conditions AMMAG and TU Wien designed and had built a stationary fluidized bed reactor, which was used to perform dehydration and hydration experiments.

Figure 81 shows a picture of the test rig; the module of the test rig containing the TCS-material is retractable. So it is possible to charge and discharge the material quickly.

Instead of a metal reactor-module even a quartz glass-module is available to be able to observe particle's movement.

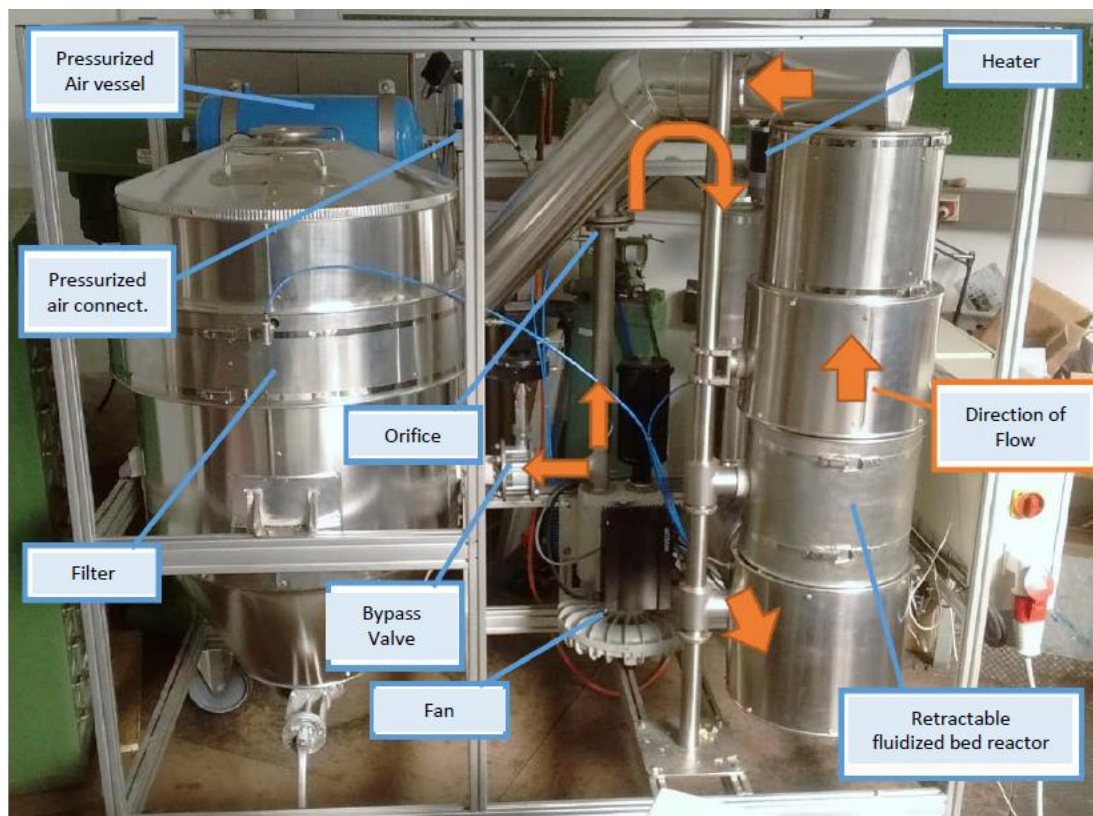


Figure 81: Fluidized bed reactor for dehydration- and hydration tests

Functional description:

The scheme in Figure 82 shows the GUI of the test rig. The air enters the system via a frequency-controlled fan, being pumped to an air heater, where it can be heated up to temperatures of about 400 °C. Before entering the air heater, an orifice-based mass flow measuring system is installed. Different orifices for different mass flows are available. Behind the air heater, steam can be mixed to the preheated air for hydration experiments.

Temperature and water loading of the air are measured at the reactor's inlet and compared to a nominal value.

Inside the reactor several temperature measuring points exist to observe heat consumption during dehydration and heat release during hydration experiments. Additionally differential pressure along the air distributor as well as the bed's height are measured.

At the exit of the reactor the temperature of the off-gas and moisture content are monitored. Even these measuring values are needed to evaluate the dehydration and hydration process.

The last part of the test rig is a baghouse filter, which can be cleaned by pressurized air.

Pressure difference along the filter and temperature are measured to observe loading and to prevent overheating.

To inhibit high temperatures in the baghouse-filter a bypass line connects the outlet of the fan with the off gas line, to reduce temperature by mixing.

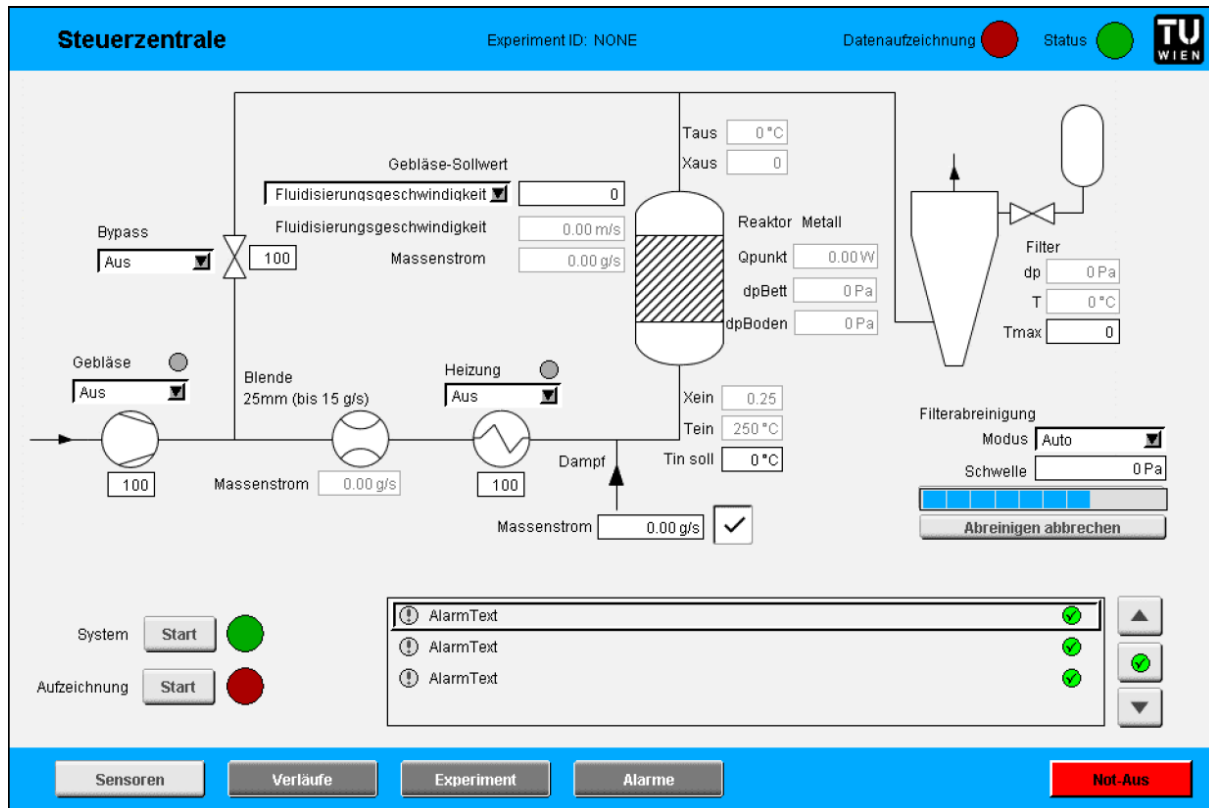


Figure 82: Control screen for fluidized bed reactor

Measuring concept:

The reactor can be used for experiments of dehydration- and hydration.

Cold experiments:

The very first of investigations to be done are fluidization experiments at ambient temperature. These experiments return information about fluidization behaviour (channelling, adhesive behaviour of powders) and size reduction mechanisms caused by pure mechanical effects. The concept of the experiment is, to fluidise a sample of TCM for a certain time span and to evaluate size reduction mechanisms by PSD-comparison before and after the experiment.

Dehydraton:

At dehydration a certain amount of thermochemical material (about 200 g) e. g. $\text{Mg}(\text{OH})_2$ is put into the reactor. The material is fluidized by preheated air ($\vartheta_{(\text{Alr}, \text{in})} \approx 370^\circ\text{C}$) and the decomposition reaction takes place. After a certain time span (for instance 2 hours) the material is put out of the reactor and mass difference is detected by weighing. From the mass difference as well as from chemical analysis the degree of conversion to MgO can be determined.

Furthermore the size distribution of the material is analysed before and after the experiment by sieving or using an optical PSD-analysis method. From the difference of PSD, size reduction mechanisms like fragmentation and attrition can be evaluated. Thermochemical materials are estimated to suffer from extensive size reduction phenomena during heating but especially during hydration.

Hydration:

Here a sample of decomposed material (approx. 200 g MgO) is put to the reactor. Steam is added to the preheated air and hydration of the material takes place. So the original $\text{Mg}(\text{OH})_2$ is formed again. Temperature rise at the thermocouples inside the reactor and at the reactor's outlet indicate the progress of the reaction. Even the time dependent moisture content in the off gas of the reactor will help to describe the progress of reaction. Special procedures are required to start the experiments at well-defined initial conditions (e. g. preheated reactor and material). Comparison of size distribution of TCM before and after the experiment is necessary because size reduction is expected to be dominant, especially at hydration experiments.

The fines captured in the filters can be analysed optically and physically. Together with the material remaining in the reactor (measuring its mass and size distribution before and after the experiment) size reduction mechanisms (fragmentation and attrition) during hydration and dehydration can be observed.

6.4 Line D, WP4: Storage system development

Thermochemical storage materials like MgO or CaO for application in fluidized beds typically belong to group B of the Geldart classification. If materials from group B are fluidized, they exhibit bubbling behavior once the fluidization velocity exceeds the minimal fluidization velocity. Bubbles may impact the reaction conditions in the reactor adversely, since a share of the gas traversed the bed in the bubbles without getting in contact with the particles.

During their ascent through the fluidized beds bubbles coalescent and grow in size. The bigger the bubbles, the larger the share of gas that passes through the bed without getting in contact with the particles. Designing the reactor in a way that prevents bubbles from growing indefinitely by braking them up might improve the reaction conditions. The simplest method for breaking up bubbles is to mount the heat exchanger in a manner that prevents bubbles from growing. To get an insight into how different tube arrangements in the fluidized bed influence bubble growth and the conversion rate, Baracuda-Simulations were performed.

Figure 83 shows that the mean bubble size increases with larger spacing parameters. Figure 84 illustrates the bubbling in the fluidized bed with internals (left) and without internals (right).

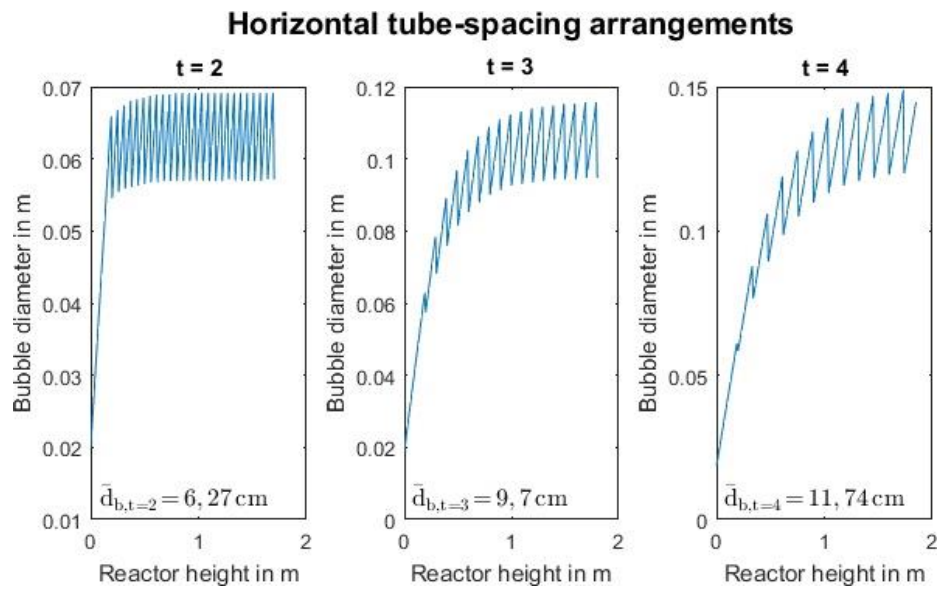


Figure 83 Effect of tube spacing arrangements on bubble growth.

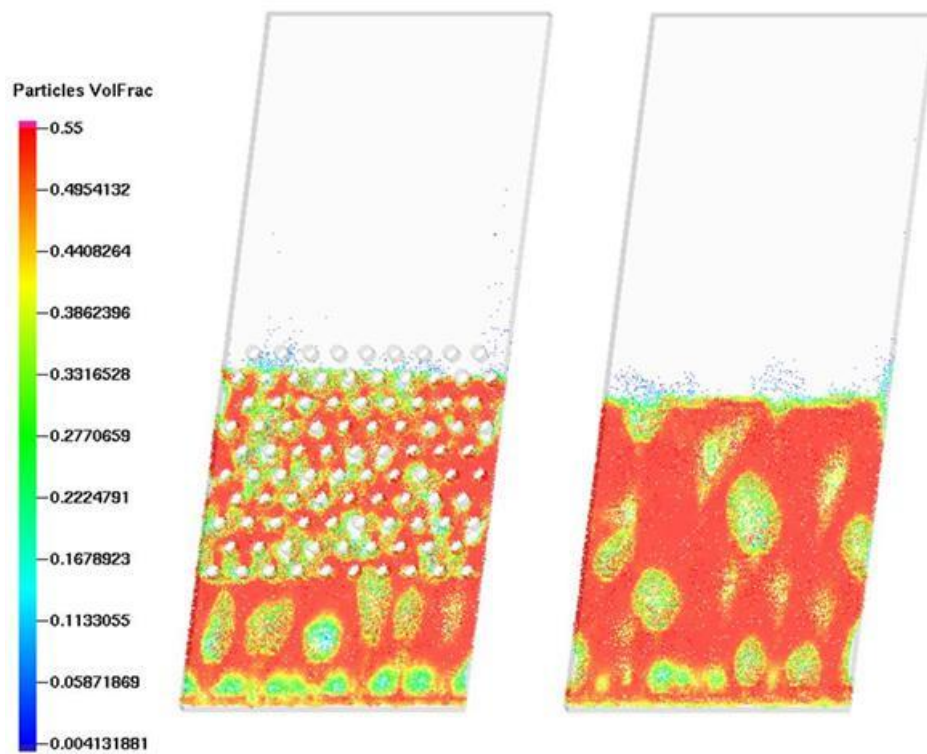


Figure 84 Bubbling in fluidized bed reactor with and without internals.

7 Line E: Novel medium temperature PCMs for industrial applications

Our overall goal was to demonstrate a novel organic PCM in a lab-scale PCM storage, which was successfully achieved within the last project phase. In addition we designed, synthesized and characterized a wide variety of organic PCMs with some completely new ones.

7.1 Boundary conditions and system design

Because erythritol turned out to be the only long-term stable sugar alcohol (see below), the results of the application survey carried out within the first two project years have been revisited. For erythritol as a PCM, applications with (pressurized) hot water or low temperature steam are now in the focus.

We could identify two promising applications where the PCMs developed in the Tes4seT project could be employed. A separate European project was set up (HYCOOL project (European Union's H2020 program under Grant Agreement No. 792073)).

The first case is from food industry and targets specialized small food industries in high solar irradiation areas with cooling needs in their processes. Here narrow configurations are aimed to optimize efficiency, so a simple system will be selected to obtain maximum outputs based on the conditions of use. BO DE DEBÒ will be the pilot site for the food industry case. This company exerts in its current facilities the activity of preparing precooked fresh dishes based on meat, fish and vegetable products. The scope of action regarding both the acquisition of raw materials and the commercialization of products is basically the Spanish territory.

The industrial cold installation is necessary for the good preservation of the product, it serves different rooms to achieve them the following final temperatures in the chamber:

- Production area: 6-8 °C
- Delivery area: 10-12 °C

The second case is a chemical use case within HYCOOL and targets industries with several processes in high solar irradiation areas with steam and cooling needs. Here a more complex configuration is aimed to optimize operational flexibility, so a more complex system will be implemented, able to be switched among different options based on weather, season and production schedule. Givaudan will be the pilot site for the chemical industry case. Givaudan is the global leader in the creation of flavours and fragrances. In close collaboration with food, beverage, consumer product and fragrance partners, Givaudan develops tastes and scents that delight consumers over the world. Givaudan, has established an ambitious set of eco-efficiency targets, as part of their agenda to achieve excellence in climate action, which takes action for the environment across their operations and beyond. Their cold installation makes use of a glycolic water chiller to keep the water entering the liquid ring of the vacuum pumps at 7 °C. The thermal demand for the installation was calculated at 125.5 kW. Interchangeability between glycolic water and liquid ring water 74 kW.



Figure 85: Bo de Debò Plant investigated within the side-project HYCOOL (<http://hycool-project.eu/pilot-sites/>)



Figure 86: Givaudan Plant within the side-project HYCOOL (<http://hycool-project.eu/pilot-sites/>)

7.2 Materials selection and development

Organic Compounds as PCMs

The main task at TU Wien, IAS, was to select suitable organic PCMs for medium temperature application. The prerequisites for our selection can be summarized as follows: On the basis that several industrial processes are carried out in boiling water as solvent (or heated by water steam) at ambient or elevated pressure, a target temperature range for our organic PCMs was defined, starting a bit below 100 °C. Thermal stability is paramount too since PCMs must be used in thermal energy storages (TES) devices and hence up-scaled at some point to industrial scale, where a typical volume is $\geq 10 \text{ m}^3$.

Therefore, the material has to be cheap and stable upon repeated melting and crystallization. A facile

synthesis with minimal work-up has to be used instead of synthetic modifications via multi-step routes in order to favour a low-cost product. Moreover, an intended lifetime of 10 year with a daily phase transition would end up in 3650 melting/crystallization cycles. This fact highlighted a need for developing more stable compounds since a material decomposition would affect significantly to the storage capacity in a negative way. Due to all these project requirements, this study is oriented to temperatures between 80 to 300 °C where a wide range of organic compounds have their melting points. Hence, several families of compounds were analyzed and chemical modifications within each family were undertaken in order to influence the melting points and ideally get to higher latent energies and favorable cycle stability. With this approach, new application temperatures within a given compound class became available and the following pages summarize the results.

Compound class identification

Before starting to synthesize a wide range of compounds, it was checked which organic materials with a suitable melting point are commercially available at a reasonable price. Next, they were tested for their capacity to store waste energy. This led to abandoning several compound classes and to modifications of some promising candidates. Initially, a short summary of the abandoned compound classes is reported, before describing the suitable ones in more detail.

Aromatic compounds

Catechol and resorcinol are the most relevant compounds of this group. Both generate well defined DSC graphs with a phase change in our required temperature range. The main disadvantage is the melting energy which is lower compared to sugar alcohols and dicarboxylic acid derivatives. In terms of stability, only melamine and anthraquinone decompose when they melt but others start to decompose shortly after the melting point and are hence unsuitable as PCM.

Amino acids

At first sight, amino acids might seem an interesting group because of their functional groups which can take part in hydrogen bonding. Alanine was reported as the organic compound with the highest melting energy (387 J/g) in this class. Unfortunately, all the amino acids with no exceptions decompose when they melt. Hence, this group had to be discarded as well.

Purines and pyrimidines

Most of the Purines and pyrimidines analyzed in this project, just as amino acids, used to decompose when they change the phase. Only caffeine is stable and even in this case, the melting energy is far from our energy requirements. For all these reasons, the group was discarded.

Fatty acids

Fatty acids are one of the most commonly used phase change materials for technical applications. However, they were initially ruled out due to their low melting points. If it is the case of interest in PCMs with a melting point slightly below of our target melting point, then we might consider both, palmitic and stearic acid which melt at 62.9 °C and 69.3 °C respectively. Another interesting option would be the amides of this fatty acids. They show higher melting points than their respective acids and they can be

prepared easily or obtained at low cost. However, the melting energies were too low for all tested compounds, and hence also the fatty acid amides had to be abandoned.

Organic dyes (diazo-dyes and indigo dyes)

Due to the fact that one important requirement which must be considered beyond the melting point and melting energy is the cost of the material, different organic compounds from industrial applications were analyzed. Dyes are widely employed in the textile industry and will offer bulk discounts when a set amount is purchased.

Nevertheless, none of these dyes have shown appropriate properties. Generally, the materials decompose at the melting point. In case a decomposition was not observed, the energy released is lower than our minimum melting energy target, $>150\text{ }^{\circ}\text{C}$. In all cases, dyes are not an interesting group for PCMs applications.

Sugars and derivatives

Amongst other organic compounds, sugars are nowadays one of the most interesting and studied candidates for PCMs. They can reach high melting energies for organic materials up to 300 kJ/kg and melting temperatures in our operational range. They usually show fitting phase change temperatures for medium temperature storage and offer high melting energy capacity, favorable safety and economic conditions. For all these reasons, they immediately become a main target group and its screening study was divided in sugar alcohols, sugar acids, other sugars and different simple modifications of the aforementioned.

Sugar alcohols

Considering all the sugars, sugar alcohols represent the most interesting group in terms of phase change material behavior. They are able to absorb and release a big amount of energy due to their hydroxy groups which allow efficient hydrogen bonding. In a first series of experiments we conducted simultaneous thermal analysis (STA) measurements of commercially available sugar alcohols.

It was found that most of the tested compounds have suitable melting points and they offer well-defined peaks in their DSC with a big gap between melting and degradation, as can be seen from Table 27 and Figure 87. At this stage, we observed outstanding phase energies for aliphatic sugar alcohols, such as mannitol, sorbitol and dulcitol, because of their structural symmetry. That distribution of the hydroxy groups favored effective hydrogen bonding which results in higher latent energies. Only the complex sugar alcohols are not appropriate for the PCMs applications. Lactitol, maltitol and isomalt show a low melting energy. Moreover, isomalt could only recrystallize in the presence of water which limits its applicability in industrial settings.

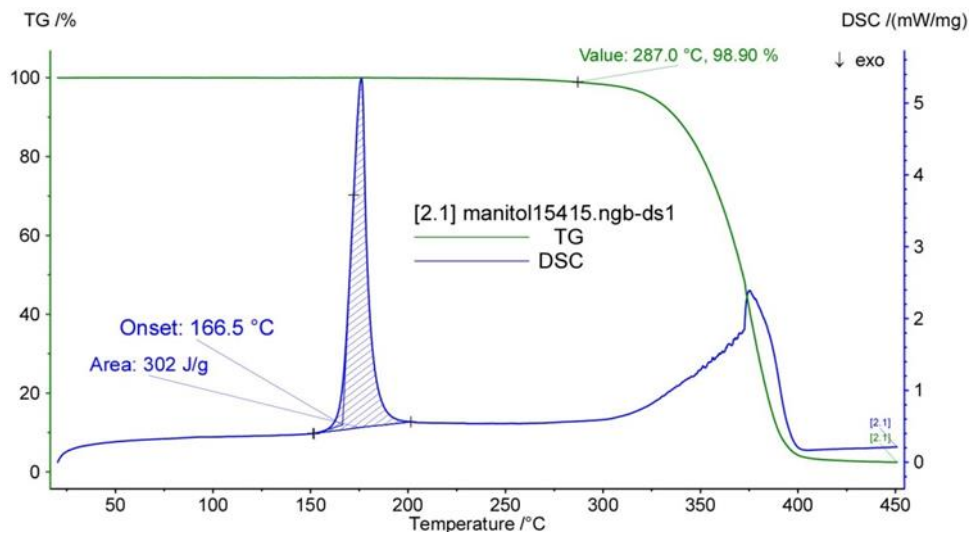


Figure 87: Mannitol STA graph

Since most of these sugar alcohols fit well to the project requirements, thermal stability tests were done. Accordingly, mannitol experienced supercooling and degradation after several cycles because of the oxidation of the material in oxygen atmosphere. A simple and effective solution to this problem might be using an inert atmosphere. However, cycle tests carried out at our project partner Südzucker reveal that even under argon atmosphere mannitol loses energy storage capacity after 100 cycles. In this case, the material underwent not only decomposition but also formation of dimers. Something similar occurs with pentaerythritol which present decomposition and formation of by-products. For others, such as dulcitol, cycle stability was even less reliable.



Figure 88: Erythritol sample after (left) and before (right) 100 cycles under argon atmosphere

Only regular erythritol has shown a remarkable thermal behaviour and after 100 cycles it presented significant stability and no significant degradation as long as the maximum temperature reached did not exceed 150 °C (Figure 88). If the temperature rises to 180 °C, some little decomposition was observed. Moreover, some thickening agents such as carboxymethyl cellulose were investigated but finally did not result in higher thermal stable. Regarding the issue of supercooling in sugar alcohols, it has been

observed that the addition of some nucleation agents can overcome this problem. The complete dataset for tested sugar alcohols is displayed in Table 27.

Table 27: Sugar Alcohols STA measurements data

Compound	MP exp. (°C)	ΔH Exp (KJ/kg)	Degradation T(TGA)
Pentaglycerine	200	249	-
Tris(hydroxymethyl)aminomethane	136	352.8	-
Aminoglycol	78	-	-
Erythritol	119	444.2	244.6
Pentaerythritol	187	321.3	238.5
Dipentaerythritol	218	349.3	244.5
Arabitol	102	365.8	239
Xylitol	93	330.4	278.5
Ribitol	102	356.4	255.5
Mannitol	166	307	287.0
Sorbitol	99	265.7	293.3
Dulcitol	187	409.2	318.5
Perseitol	184	260.8	-
D-erythro-L-manno-octitol	261	352.2	-
D-erythro-L-gluco-octitol	164	163.8	-
Myo-Inositol	224.5	270.7	341.3
Isomalt	147.6	113.7	285.1
Lactitol	-	142(lit)	-
Maltitol	150	200.3	274
Dianhydro mannitol	84	175.5	-

Acetylated sugars

In order to improve cycle stability, chemical modifications could also be beneficial in order to get to less reactive and hence more stable compounds. In this regard, acetylation reactions on sugar alcohols are the natural first choice since these reactions are typically high yielding and only use inexpensive starting materials, which is important for the large quantity application we have in mind. Additionally, these reactions are often used to block reactive hydroxy groups in sugar chemistry and are well-established. Acetylation leads of course to the loss of hydrogen bonding, which would lead to a (desired) decrease in melting point but also in melting energy. On the other hand, the molecular weight is significantly increased, which typically has the exact opposite effect, an increase in melting point and eventually also in melting energy. So, it had to be seen, which of the two parameters is of greater importance, possibility for hydrogen bonding or molecular weight. In our hands, all investigated acetylations have shown quantitative yields for all the sugars that were modified. With the acetylated sugars in hand again STA analyses were performed. The acetylation of sugars provides a product with lower melting point and lower melting energy than the starting material due to the absence of hydrogen bonding possibilities, showing that this is the dominant effect. Our goal of obtaining a lower melting point was achieved but, unfortunately, once the hydroxy groups are substituted by acetyl groups the properties of the material decline regarding latent energy. Considering all these points, acetylation does not improve the overall properties of sugar alcohols as PCMs.

Sugar acids and derivatives

Regarding hydrogen bonding, sugar acids seemed to be an excellent option but decomposition was observed when they melt. Carboxylic acid functional groups can undergo decarboxylation reactions upon heating, which might explain their behavior during the phase change. In order to confer more stability some modifications such as esterification or amidation were considered. Esterification of tartaric acid generates derivatives with melting points lower as required, with diethyl tartrate being a liquid at room temperature. Meanwhile, esterification of mucic acid with methanol or ethanol gave compounds with a suitable melting point but too low melting energy.

Towards carboxylic acids and derivatives

The group of carboxylic acids and derivatives is probably the most promising one together with the well-known group of sugars. At first sight, it might seem that they are not as stable as other groups because of the reactive carboxylic group but some dicarboxylic acids do not show decomposition when they melt and an energy capacity close or even bigger than sugar alcohols. As in the sugars, some modifications such as esterification or amidation were done in an attempt to overcome the problem of stability that some acids showed. In general terms, esterification has not been successful because of the hydrogen bonding loss but amidation gave some interesting products with outstanding properties for medium temperature storage.

Dicarboxylic acids

From all the carboxylic acids, the dicarboxylic acids are both more stable and able to store more energy than the rest. Considering this fact, the aim was to increase the length of the alkyl chain between the two terminal carboxylic acid groups in order to find a trend that could deliver an outstanding material and to help to improve other different compounds in a future. Simple dicarboxylic acids show a particular behavior. Depending on his carboxylic group disposition they are going to be named “odd” when the functional group are oriented in the same direction due to the carbon chain length or “even” when carboxylic groups are oriented in different direction (Figure 89).

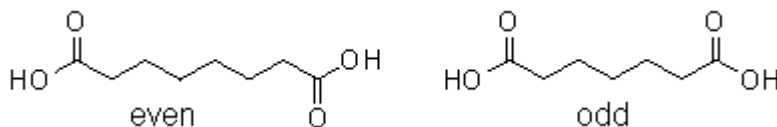


Figure 89: Dicarboxylic acid structures

These two different geometries are going to determine the properties of the material. It was observed that because of the functional group orientation, odd or even, the acids offer different values of temperatures and enthalpy.

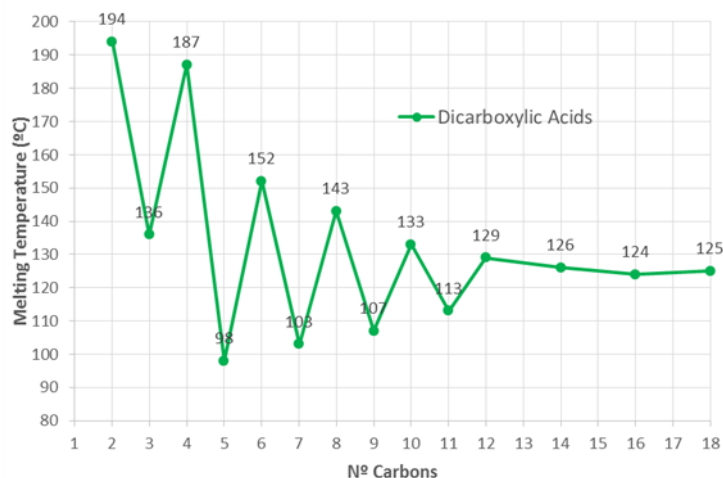


Figure 90: Melting points of dicarboxylic acids as a function of number of C-atoms

A glance at Figure 90 gives a better understanding of the differences between odd and even compounds. Even compounds show always higher melting points than odd ones but as long as the alkene chain in between the terminal carboxylic acid groups increases, this difference becomes smaller and smaller until it levels out. This levelling can be observed in the even compounds (acids with 14, 16 and 18 carbons) and between odd and even acids. The odd-even effect is observed in the melting energy as well to some extent (Table 28 and Figure 91). For this reason, It makes no sense in going further on the synthesis of higher dicarboxylic acids than octadecanedioic acid.

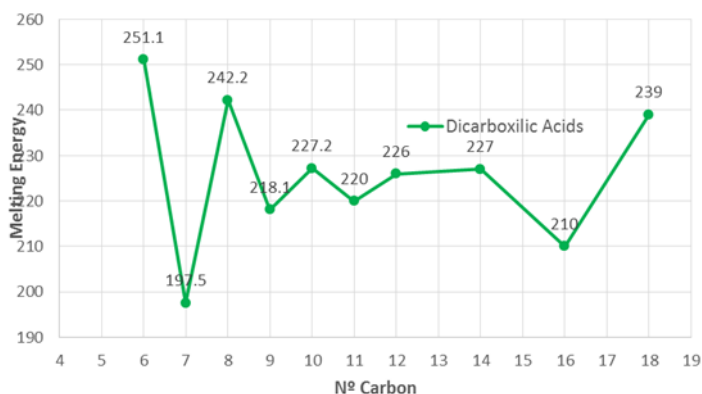


Figure 91: Dicarboxylic acid melting energies

According to this effect we considered adipic- (C6), suberic- (C8), sebacic- (C10) and dodecanedioic acid (C12) among the most interesting materials. It can be expected that sebacic- and dodecanedioic acid are the more stable ones in long term cycle tests since adipic acid may undergo intramolecular reactions to form a favorable 6-membered ring. In contrast, 10 and 12-membered rings are not so easily formed. Anyhow, most of the dicarboxylic acids seem to fit excellent to our requirements. Only oxalic and succinic acids decompose when they melt.

Table 28: STA measurement data of dicarboxylic acids

Compound	MP lit. T (°C)	MP exp. T (°C)	ΔH Exp (KJ/kg)	Degradation T(TGA)
Oxalylic acid dihydrate	101.5	194.3	Decomposition	-
Malonic acid	135	136.3	295	153.8
Succinic acid	187	187.7	Decomposition	197.8
2,2 – dimethyl succinic acid	139	142.9	Decomposition	159.9
Glutaric acid	95	98.7	237.3	190.2
Adipic acid	151	152.4	312.6	312.6
Pimelic acid	105	106.5	322.3	144.2
Diaminopimelic acid	316	267.3	Decomposition	122.1
Suberic acid	143	143.2	239.5	218.5

Aliphatic- α,ω -diamides

When modifications of dicarboxylic acids were planned, the first idea that came to mind were amides since they still preserve hydrogen bonding and hence looked like a very promising group. Oxalamide, malonamide, succinamide and adipamide are commercially available diamides.

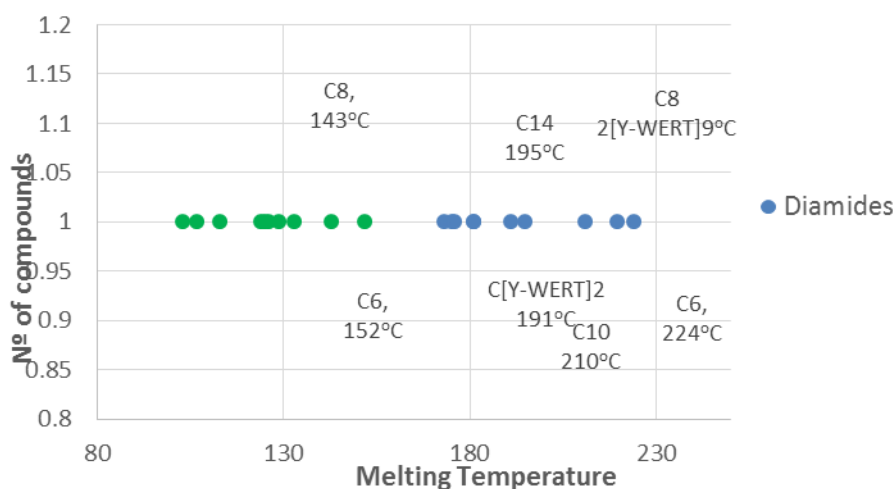


Figure 92: Melting point comparison of diamides and diacids

The rest of the tested α,ω -diamides has been synthesized. Regarding physical behaviour of this new class of compounds, higher melting points for the respective diamides were observed (Figure 92). After measurements, aliphatic- α,ω -diamides presented better properties than the corresponding α,ω -dicarboxylic acids since they could release and absorb a bigger amount of energy (Figure 93). A more accentuated “odd-even” effect was observed.

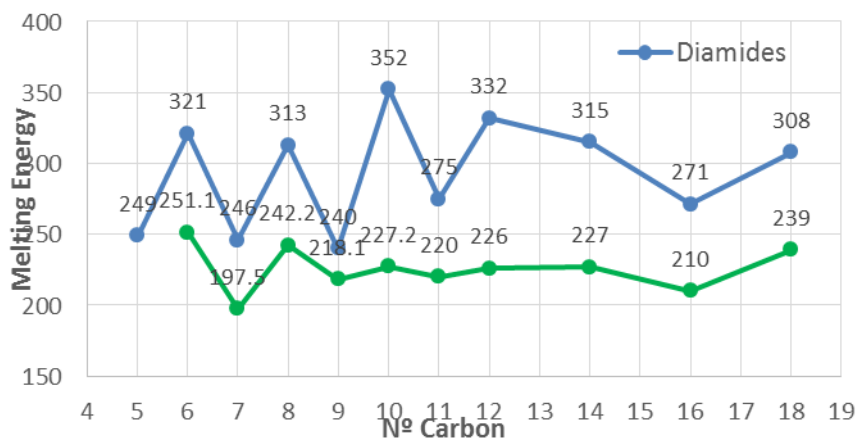


Figure 93: Dicarboxylic acid and diamide melting energy comparison

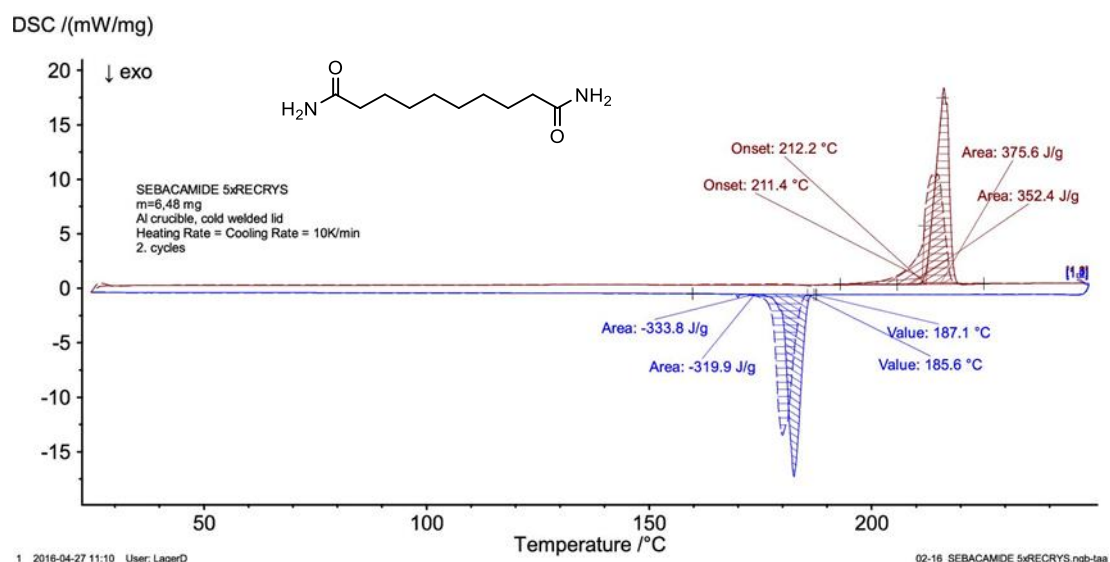


Figure 94: Sebacamide DSC cycle test

The most favourable in terms of energy were sebacamide and dodecanediamide. For these two, DSC cycling tests were performed at the Austrian Institute of Technology. Figure 94 and Figure 95 to confirm the two diamides as very promising materials. Sebacamide has the highest melting energy obtained in this study, 375 J/g, and the gap between melting and recrystallization is acceptable. Even though dodecanediamide does not have a melting energy as high as sebacamide, it was considered as the better candidate because of a smaller melting-recrystallization gap and still a high phase energy of 338 J/g.

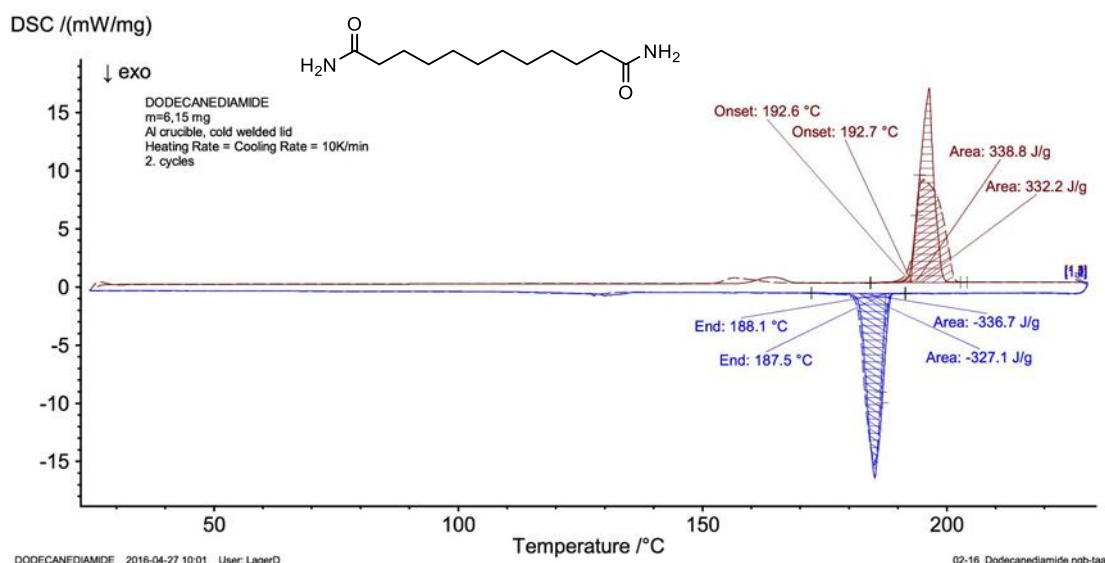


Figure 95: Dodecanediamide DSC cycle test

One of the important achievements of the diamides and dicarboxylic acids families is the big range of temperatures covered. Meaning that one or another compound would be more suitable for a particular production process and giving more options for industrial applications.

Table 29: Diamides STA measurements data

Compound	MP lit. (°C)	MP exp. (°C)	ΔH Exp (KJ/kg)	Degradation T(TGA)
Oxalamide	299	290.2	decomposition	229.5
Malonamide	171	172.1	304.5	217.1
Succinamide	263	-	decomposition	-
Glutaramide	181	180.3	260.3	165.7
Adipamide	226	224.7	371.0	268.1
Pimelamide	173	173.3	277.2	238.8
Suberamide	220	219.5	335.1	265.6
Azelamide	177	175.3	247.8	-
Sebacamide	210	210.9	375.6	260.5
Undecane diamide	178	179.1	271.0	244.0
Dodecanediamide	193	191.0	338.8	246.9
Tetradecanediamide	196	194.6	319.9	-
Hexadecanediamide	179	181.4	282.9	-
Octadecanediamide	179	181.7	264.7	-

Towards 3,6-diazaoctane-1,8-diol and derivatives

Another compound with interesting properties was identified as N,N'-bis(2-hydroxyethyl)ethylenediamine (NN-Bis), which has a significantly high melting energy with a low melting point (Figure 96). This melting temperature of 100.05 °C could allow us to employ a PCM in a range of industrial processes related to steam and its residual heat. The melting point of the best diamides candidates (C10 and C12) is

approximately twice as high. Bearing in mind all these features, NN-bis was purchased in order to measure its physical properties in DSC.

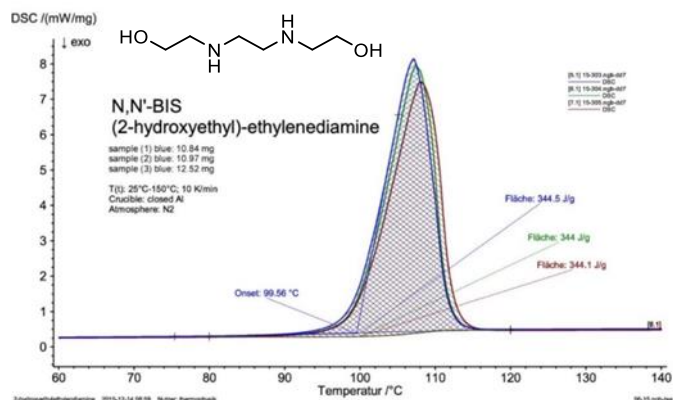


Figure 96: NN'-Bis (2-hydroxyethyl)ethylenediamine DSC measurement

Subsequent STA measurements showed no degradation and the expected melting properties. Accordingly, cycle tests were carried out in the DSC machine from the Austrian institute of technology in order to have better accuracy. However, the cycle analysis reveals one possible drawback (Figure 97). The presence of a huge gap between melting and recrystallization meaning that the temperature has to drop from 98.5 oC to 38.85 oC if there is an intention to recover that energy. A loss of energy is expected once we tried to reach again the melting point. Thus, further modifications for reducing this gap had to be undertaken.

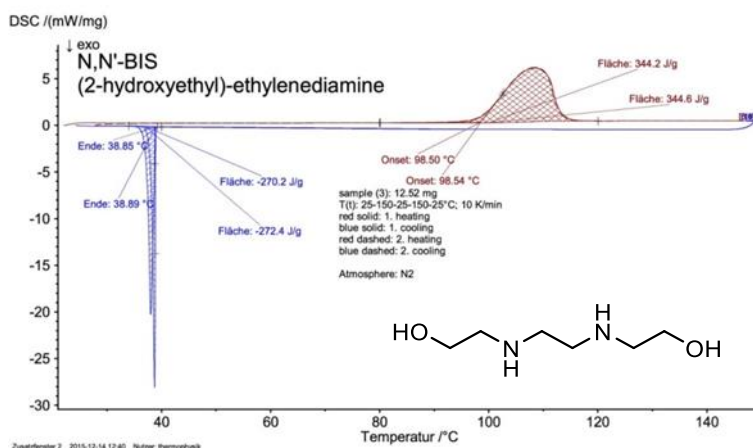


Figure 97: NN'-Bis (2-hydroxyethyl)ethylenediamine cycle DSC measurement

A modification that came to mind was changing the terminal hydroxyl group for an amide group. The terminal amide group has been tested with good results in diamides giving high melting energies. On the other hand, the pattern of the modified NN-bis would correspond to Sebacamide in terms of chain length among amide groups, therefore we might expect improvements in the area of stability and a lower gap between the melting and recrystallization.

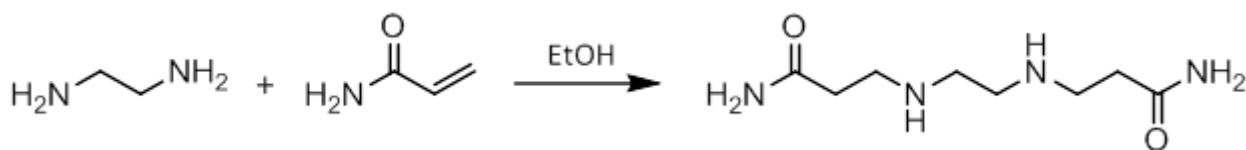


Figure 98: 4,7-diazadecanediamide (Azamide) synthetic scheme

In view of all these facts, a new derivative of NN-bis, 4,7-diazadecanediamide (azamide), was synthesized following the reaction in Figure 98. An advantage of this resulting product is its low cost. Both starting materials are bulk chemicals which can be obtained at a reasonable price.

Figure 99 shows the cycle test for the azamide. Once the two hydroxy groups from the NN-bis are replaced by amides, an interesting new material is obtained. The melting point is half way between NN-bis and sebacamide, and it still has a phase transition enthalpy as high as sebacamide. On this occasion, however, recrystallization was not observed. Looking at the present situation, another experiment was carried out in order to try the capability of the NN-bis derivative to recrystallize in larger scale. 1,5 g of our product was placed in a closed vial and it was heated to a temperature of 200 °C for 30 min until complete melting. Afterwards the vial was cooled to room temperature and recrystallization was observed. In any case, physical issues such as recrystallization can be always improved by adding different nucleating agents.

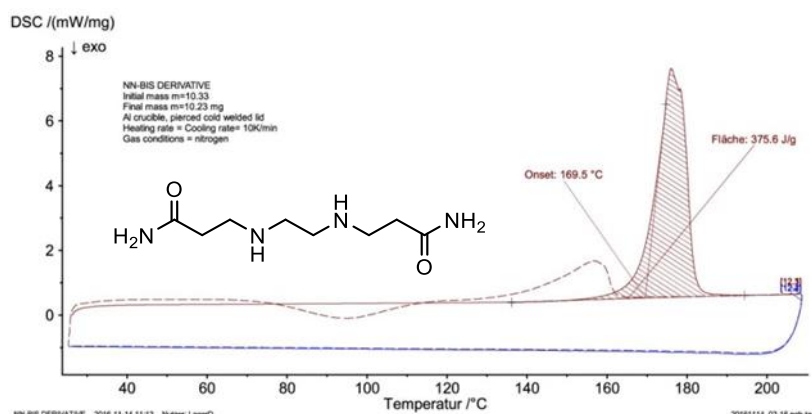


Figure 99: 4,7-diazadecanediamide cycle DSC measurement

Unfortunately, long-term stability tests showed that after some cycles the material is degraded during heating to end up in an orange glass-like shape which is going to lose the ability for storing energy. It is at this point when modifications of azamide took place to improve the thermal stability. These derivatives were planned in two different ways. On one hand, an elongation of the chain pattern between its two terminal diamides was intended, as we did for the NN-bis. On the other hand, a substitution of the heteroatom located in the main chain was aimed for. Taking into account the good nucleophilicity of other atoms, our targets were oxygen and sulphur instead of nitrogen. For this reason, we tried to synthesize both, 4,7-dioxadecanediamide (oxiamide) and 4,7-dithiodecanediamide (sulfuramide). Additionally, for the oxygen derivatives an elongation of the chain was considered.

After the target compounds were synthesized, we carried out the new corresponding DSC measurements. As can be seen in Figure 100, they offer a good stability after melting and a well-defined peak. Only in the case of the short derivative, oxiamide, we have a solid-solid transition immediately

before the melting point. All of them present melting temperatures between 85 and 117 oC but, unfortunately, only one showed a melting energy above 250 J/g (Table 30). Taking all the above into account, it can be found no need to continue further with the elongation and synthesis of new compounds, so it was decided to move on to the next material.

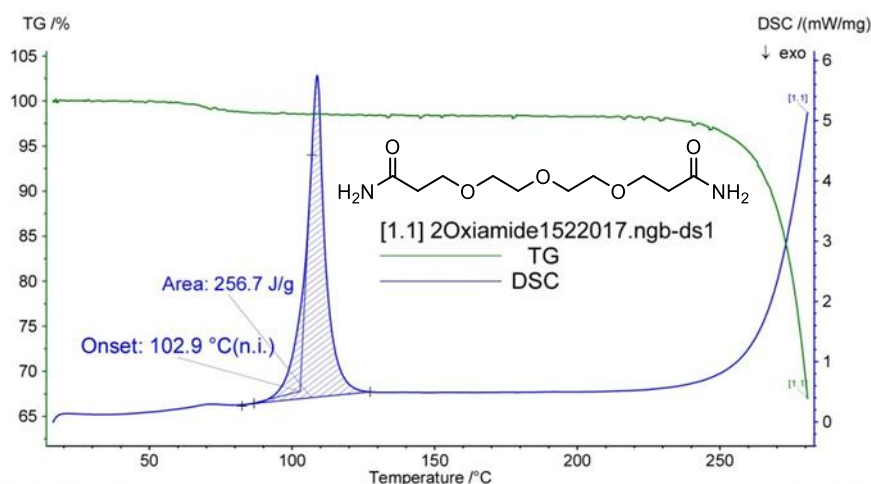


Figure 100: 4,7,10-trioxatridecanediamide STA measurement

Table 30: Comparison of the thermal properties for oxygen NN-bis derivatives

	Oxiamide	4,7,10-trioxatridecanediamide	4,7,10,13-tetraoxahexadecanediamide
Structure	<chem>NC(=O)CCOCCOCCOCCOCC(=O)N</chem>	<chem>NC(=O)CCOCCOCCOCCOCCOCC(=O)N</chem>	<chem>NC(=O)CCOCCOCCOCCOCCOCCOCCOCC(=O)N</chem>
MP T (°C)	116.9	102.9	189.6
ΔH Exp (KJ/kg)	206.2	256.7	177.4

Ending the series of modification for the NN-bis, the corresponding sulfuramide was synthesized and measured via STA (Figure 101). As already indicated, sulphur compounds are better nucleophiles than nitrogen or oxygen ones, meaning that the reaction would take place easily and with good yields. Due to this reactivity, however, this sulphur compounds are of high toxicity with direct negative consequences for human health and the environment.

Even when the toxicity is usually high, the starting material (1,2-Ethanedithiol) employed in the sulfuramide synthesis present a low level of toxicity, slightly higher than ethylene glycol. Finally, the yield was 89% in a small scale of 0.2 mmol, which is the best in the class of NN-bis derived compounds. The thermal data could be considered good since we have a melting energy around 280 J/g and a melting point of 183.5 °C

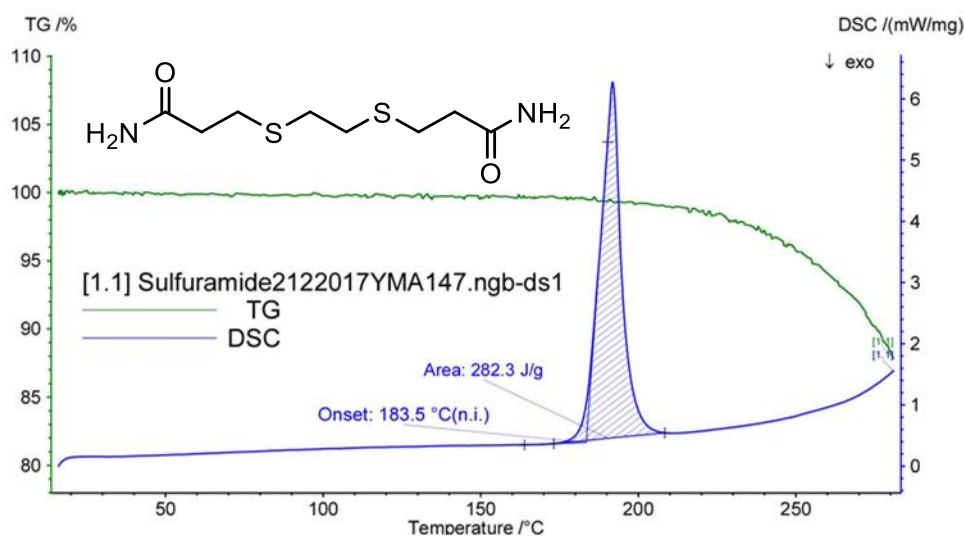


Figure 101: Sulfuramide STA measurement

An overview of all obtained data on NN-bis and its derivatives can be found in Table 31.

Table 31: NN-bis derivatives DSC/STA measurements data

Compound	Structure	MP exp. T (°C)	ΔH Exp (KJ/kg)	Degradation T(TGA)
N,N'-Bis(2-hydroxyethyl)-ethylenediamine	<chem>OCCNCCNCCO</chem>	99.6	344.5	-
4,7 –diazadecanediamide	<chem>NC(=O)CCNCCNCC(=O)N</chem>	169.5	375.6	206.3
4,7-dithio decanediamide (Sulfuramide)	<chem>NC(=O)CCSCCSCC(=O)N</chem>	183.5	282.3	-
4,7 – dioxadecanediamide (Oxamide)	<chem>NC(=O)CCOCCOCC(=O)N</chem>	117	206.2	-
4,7,10 – trioxatridecanediamide	<chem>NC(=O)CCOCCOCCOCC(=O)N</chem>	102	257	-
4,7,10, 13 – tetraoxahexadecanediamide	<chem>NC(=O)CCOCCOCCOCCOCC(=O)N</chem>	99.6	177.4	-

7.2.1 Conclusions

The main objective from this study at TU Wien was to identify organic compounds with suitable properties for PCM application. It can be concluded that this goal was achieved considering the set of attractive PCMs which have been developed above. It has been seen progress in three of the several groups researched: sugar alcohols, carboxylic acids and “NN-bis” and its derivatives.

Regarding sugars, sugar alcohols were the most remarkable compounds. Natural-occurring sugar alcohols were widely investigated for PCM applications before, so the scope of this thesis was on modifications of this compound type and the synthesis of longer sugar alcohols hitherto not investigated. Both, modifications and synthesis were planned to avoid the initial drawbacks of these materials. Regarding stability, erythritol shows an excellent condition after 100 cycles but there is room for improvement for the rest of the sugars tested. Acetylations were tried as an affordable chemical modification for sugars but they cut half the melting point and melting energy due to a loss of hydrogen bonding, so they were discarded.

Dicarboxylic acids and their diamides are the most outstanding materials from the group of carboxylic acid derivatives. They show better thermophysical properties than sugar alcohols and they are able to cover a wide range of temperatures for medium temperature applications, starting from 103 °C and reaching 225 °C. Even though dicarboxylic acids show a great performance as PCMs, diamides tend to present higher storage capacity. From all of these diamides, two are specifically interesting: sebacamide and dodecamide. Sebacamide has offered a melting energy of 375.6 kJ/kg, the highest melting energy registered in this study. On the other hand, dodecamide has presented 338.8 kJ/kg as melting energy. Nevertheless, dodecamide showed a better performance as PCM than sebacamide because the gap between melting and recrystallization is almost non-existent, allowing an ideal adaptation to the system. This is the reason why dodecamide was chosen as one of the promising materials to upscale. However, custom synthesis of this compound at the kg scale could not be carried out successfully by the contractor.

Three more interesting organic materials are located in the NN-Bis group. NN-bis itself has an outstanding energy of 344.6 kJ/kg and a very convenient melting point which fits with the boiling point of water. This fact makes it an interesting candidate for industrial applications related to steam. The synthetic route is possibly affordable in bulk amount since it is already a cheap commercially available product. This material only displays a disadvantage regarding recrystallization and the gap between different phase transition temperatures. More research has to be done to improve physical properties. Furthermore, sulfuramide had an easy synthesis with an excellent yield and a phase energy of almost 300 kJ/kg. Finally, azamide is one of the most promising materials which was already upscaled. This material had the highest melting energy together with sebacamide, 375.6 kJ/kg and an easy synthetic route with common chemicals as acrylamide, ethanol and ethylenediamine to finally get the product after a minimal workup. Long-term stability tests unfortunately showed degradation, however azamide should still be kept in mind since there are precedents for the improvement of physical properties once organic compounds are combined with other materials in composites.

7.3 Component Development

For the final tests of large quantities of the developed storage materials in a real storage tank a test storage has been designed (see Figure 102).

A tube bundle heat exchanger made of parallel steel tubes was selected to minimize costs. A collecting manifold at the inlet and outlet distributes the heat transfer medium equally through all parallel tubes. As a container material, we selected carbon steel which was mechanically enhanced at the top cover to

even allow for evacuation of the PCM containment, which is beneficial for certain organic phase change materials to reduce thermo-oxidative degradation and thus ensure long-term storage durability.

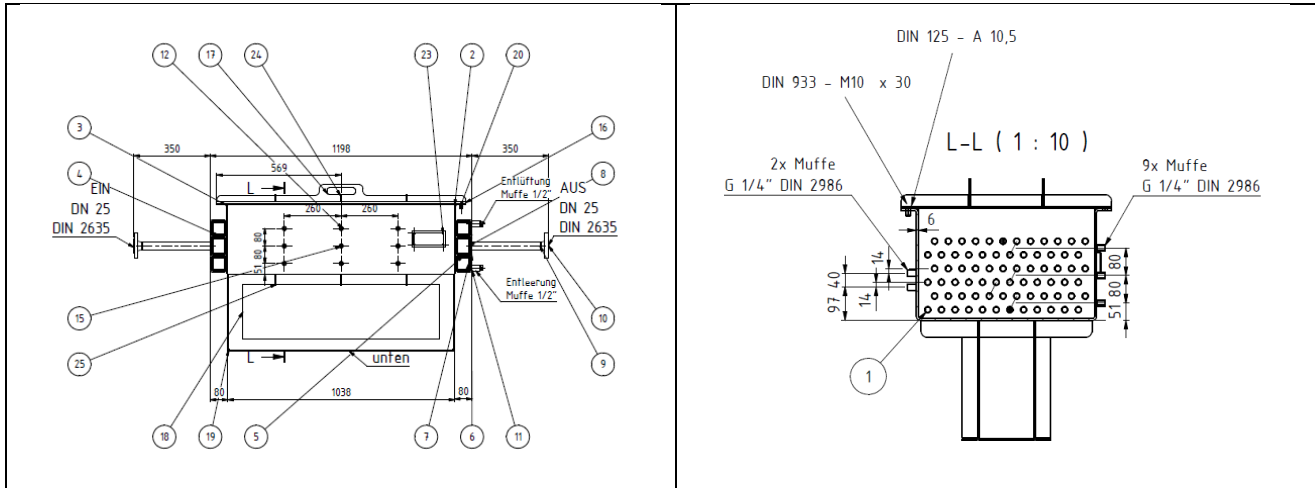


Figure 102 Test storage for sugar alcohols.

Furthermore, we developed a flexible and cost-effective insulation solution: a special steel construction is used in combination with CPL boards to serve as a container for different kinds of insulation. Based upon the experiences of a related FFG-project (ISOLar, <https://www.energieforschung.at/projekte/252/isolar-screening-und-langzeit-eigenschaftsprognose-von-isolierwerkstoffen-fuer-solarthermische-kollektoren-und-waermespeicher>), we selected foam glass aggregate from the Austrian company Geocell, which serves perfectly as insulation material due to its low thermal conductivity and high temperature resistances. Also, it can be easily poured into the containment, which further saves manufacturing costs. The storage was manufactured by the German Company Kühner according to the design specifications of the AIT. In total, we ordered two storages to test two different organic PCMs as described below (Figure 103).



Figure 103: PCM storages designed by AIT. A bundle of parallel steel tubes was used as heat exchanger. The collecting manifolds at the inlet and outlet ensure uniform parallel flow of the heat transfer medium through the storage.

In order to experimentally characterize the thermal performance of the developed storages, we built a dedicated test rig at the Thermal Storage Lab at the AIT. Pt100 sensors were mounted at the inlet and outlet of the storage and an ultrasonic flow measurement device by FLEXIM (Fluxus) was employed to measure the volume flow through the storage. In addition, several thermocouples were placed directly into the PCM containment (i.e. between the steel tubes) to measure the temperature profile of the storage materials locally (Figure 104, Figure 105).

As heat transfer medium, we selected the thermal oil Marlotherm SH due to its well-known thermal properties and widely proven application in many industrial use cases as well as its thermal stability up to some 300 °C.

As a result of the thermal stability tests performed at Südzucker and previously at AIT and TU Wien (DSC, Hot Plate) we chose Erythritol as the most promising organic sugar alcohol because of its high phase change enthalpy as well as best thermal stability even at atmospheric ambient conditions.

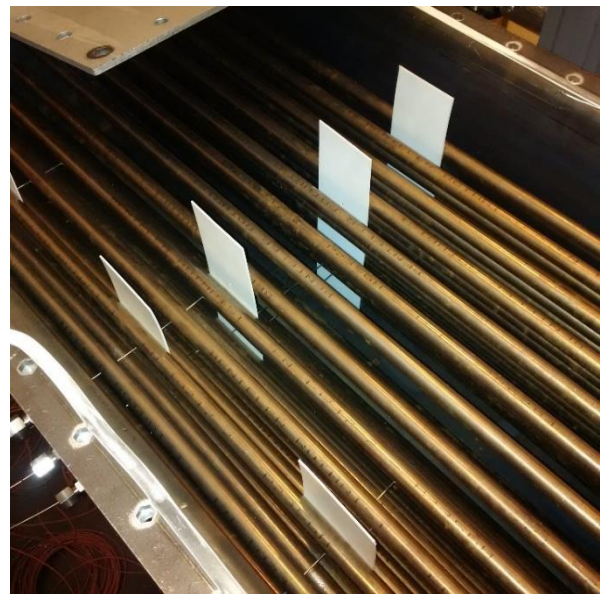


Figure 104: A dedicated test rig was designed and set up at the Thermal Storage Lab at the AIT capable of providing up to 100 kW of heating and cooling power. Various sensors were mounted around and inside the storage to characterize the PCM storages in detail.

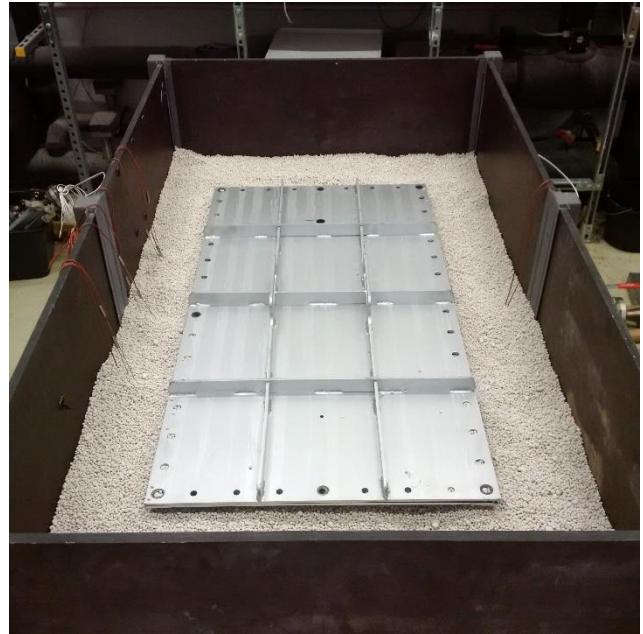


Figure 105: A special steel construction in combination with CPL boards was developed to serve as the insulation container. Foam glass aggregate from the Austrian company Geocell was used as an insulation material and was poured into the insulation containment.

Erythritol, similar to most other organic PCM, however has a rather low thermal conductivity in the range of 1 W/mK. Thus, various efforts were undertaken to add different kinds of additives to improve the thermal conductivity of such a compound. It turned out that certain graphite types (ideally in the geometric form of platelets and as expanded graphite) perform best in terms of price-performance ratio. In hot plate experiments, we investigated various graphite-Erythritol mixtures and especially analysed their long-term stability. We found that under the special circumstances in a PCM storage with cyclic melting and solidification it might happen that the compound de-mixes to some extent. Thus, in order to avoid such de-mixing (sedimentation), we furthermore investigated another class of thickening additives which should finally stabilize the compound. After some unsuccessful experiments with organic fillers, it turned out that fumed silica serves best to stabilize the graphite-silica-Erythritol compound (Figure 106). The compound was first tested on a gram-scale on hot plates at AIT and subsequently produced at a 100 kg scale at the company Südzucker (Figure 108).



Figure 106: Fumed silica was used as a thickening additive (thixotropic agent) to prevent the de-mixing (sedimentation) of thermally conductive graphite-alditol compounds.

Finally, we chose two different PCMs, pure Erythritol and a thermally conductive graphite-silica-Erythritol compound to test them within the lab-scale storage described above. The materials were filled into the storage and molten using the test rig. This process had to be repeated a few times to achieve proper storage filling (Figure 107, Figure 108, Figure 109).



Figure 107: Left: Pure Erythritol was filled into the Kühner tube bundle storage. Right: Upon melting the material appears translucent and possesses a viscosity similar to liquid water (cf. small molecules).

Energieforschungsprogramm – 4. Ausschreibung

Klima- und Energiefonds des Bundes – Abwicklung durch die Österreichische Forschungsförderungsgesellschaft FFG



Figure 108: Left: As-delivered graphite-silica-Erythritol compound produced by Südzucker. Right: The compound was molten within the storage and possesses a very high viscosity as can be seen from the darker region where the PCM compound is already molten but still does not flow easily to the bottom of the storage. The light gray part is a PCM that is not molten yet.

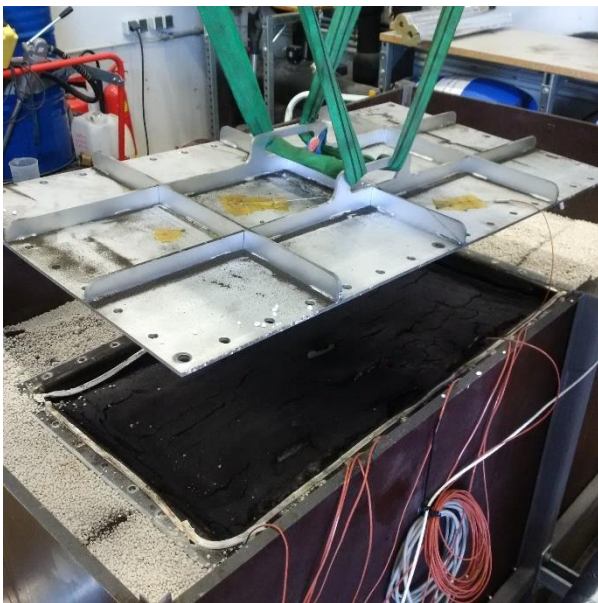


Figure 109: Left: After several filling/melting cycles the PCM compound was successfully filling the storage. The picture shows the material after re-crystallization as a black, rather solid block. Right: As top insulation we tested glass foam bricks from the company Foamglass that are thermally stable and can be easily cut to size.

In order to characterize the thermal performance of the storages, we used the heating and cooling test rig at the Thermal Storage Lab at AIT. Contrary to an electrical storage where usually the lowest and highest voltage are fixed due to battery chemistry, in thermal storages their thermal analogues, the charging and discharging temperatures, depend on the application the storage is finally used. Also, the driving temperature, i.e. temperature between current PCM temperature level and heat transfer fluid, may change during the process. E.g. when one wants to preheat certain goods from ambient temperature to some final value, initially the storage is fully charged and rather hot (large driving

temperature difference), while the storage gets cooler and the to-be-preheated-good may get warmer during preheating which reduces the driving temperature range. When the PCM crystallizes, the temperature of the storage remains rather constant for a certain time, which is one of the key features of such latent heat storage.

In total, this means that the storage charging/discharging power profile are not constant in general (except one employs a mass flow control). However, it is a good means to characterize a storage by investigating the thermal step response. If this is done for different initial and final temperature and mass flows, one may map out the behaviour of the storage thoroughly. We performed such a characterization campaign with both storages and report some of the complex results found in the as follows.

Figure 110 shows the step response of the storage filled with pure Erythritol for a discharging step from 150 °C down to a final temperature of 60 °C with a constant mass flow of 2.8 kg/s.

From the temperatures of the PCM (cyan, green, black) at the top figure one can observe a pretty complex melting behaviour of the storage material, which however proceeds roughly from the front of the storage to the back. Also, one can clearly observe a subcooling of roughly 20 °C, which is in line with our previous investigations and shows the very important result that the subcooling within a real-scale storage is much, much smaller than in a DSC or T-History. Thus, DSC measurements are not a reliable means to investigate the subcooling of a phase change material (even when performed at low cooling rates).

The lower part of the figure shows the storage discharging power (brown) and the integrated discharged energy (green). Using a constant storage mass flow one achieves a discharging peak in the beginning which then turns into the PCM-typical plateau and finally diminishes as the storage gets fully discharged. In total we could retrieve roughly 25 kWh from the storage for this initial and final temperature level.

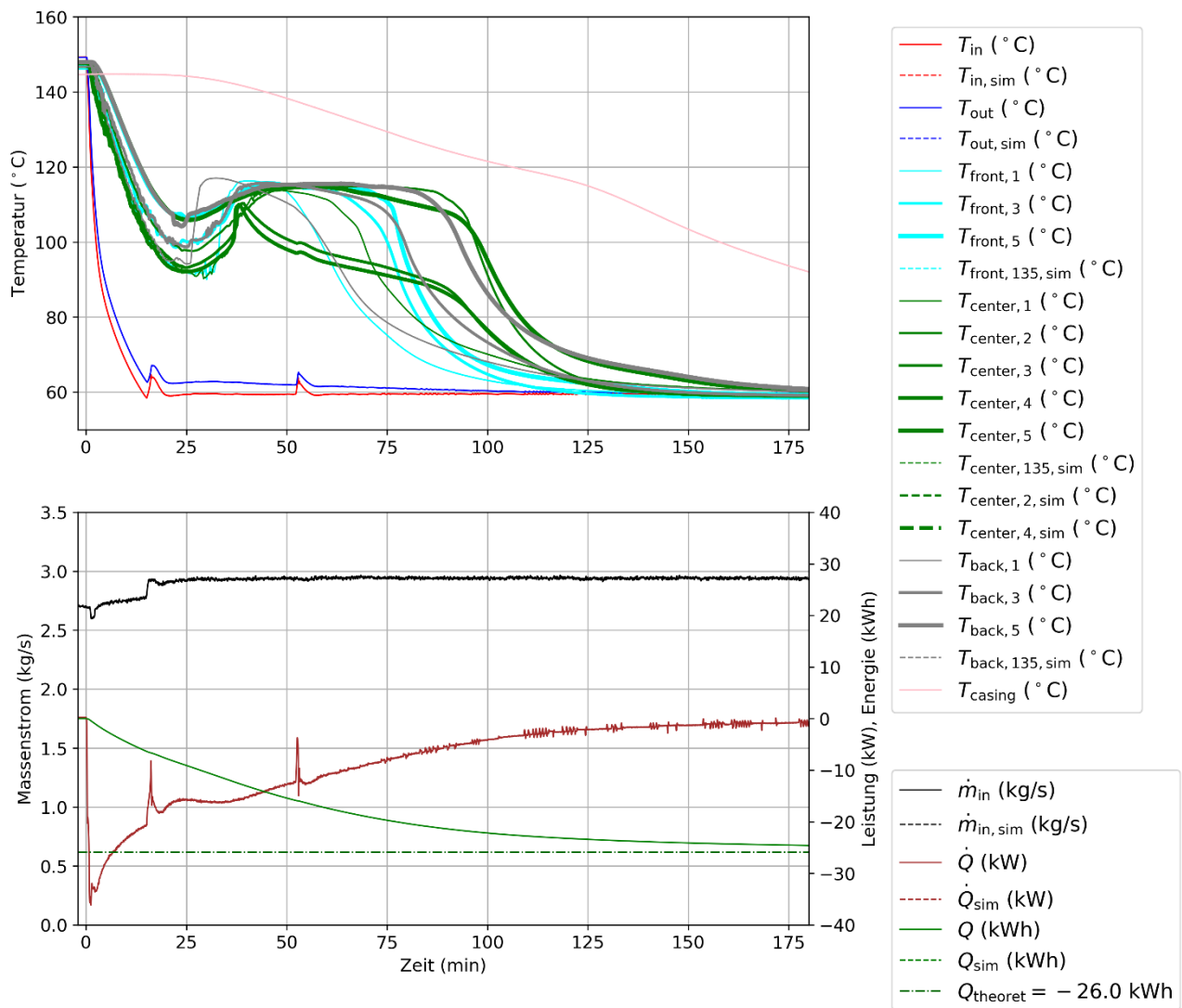


Figure 110: Step response of the Erythritol storage. Top: PCM temperatures show a subcooling of roughly 20 °C. This is much lower than for DSC measurements, which are not a reliable means to characterize the subcooling of a PCM within a real-scale storage. Bottom: discharge power profile for constant mass flow discharging revealing a peak at the beginning followed by the PCM-typical plateau. In total we could discharge 25 kWh from the storage for these initial and final PCM temperature levels.

In Figure 111 we summarize the results from different step response experiments for discharging the storage filled with the graphite-silica-Erythritol compound.

Subcooling is slightly depending on the final discharge temperatures too and is again much less than for DSC. Also, as expected, the discharge power profile and especially the PCM-typical plateau depend very much on the driving temperature difference (PCM-temperature minus mean heat transfer fluid temperature). This is also reflected in the integral values (retrieved energy), which provides information on the sensible part of energy stored within the device.

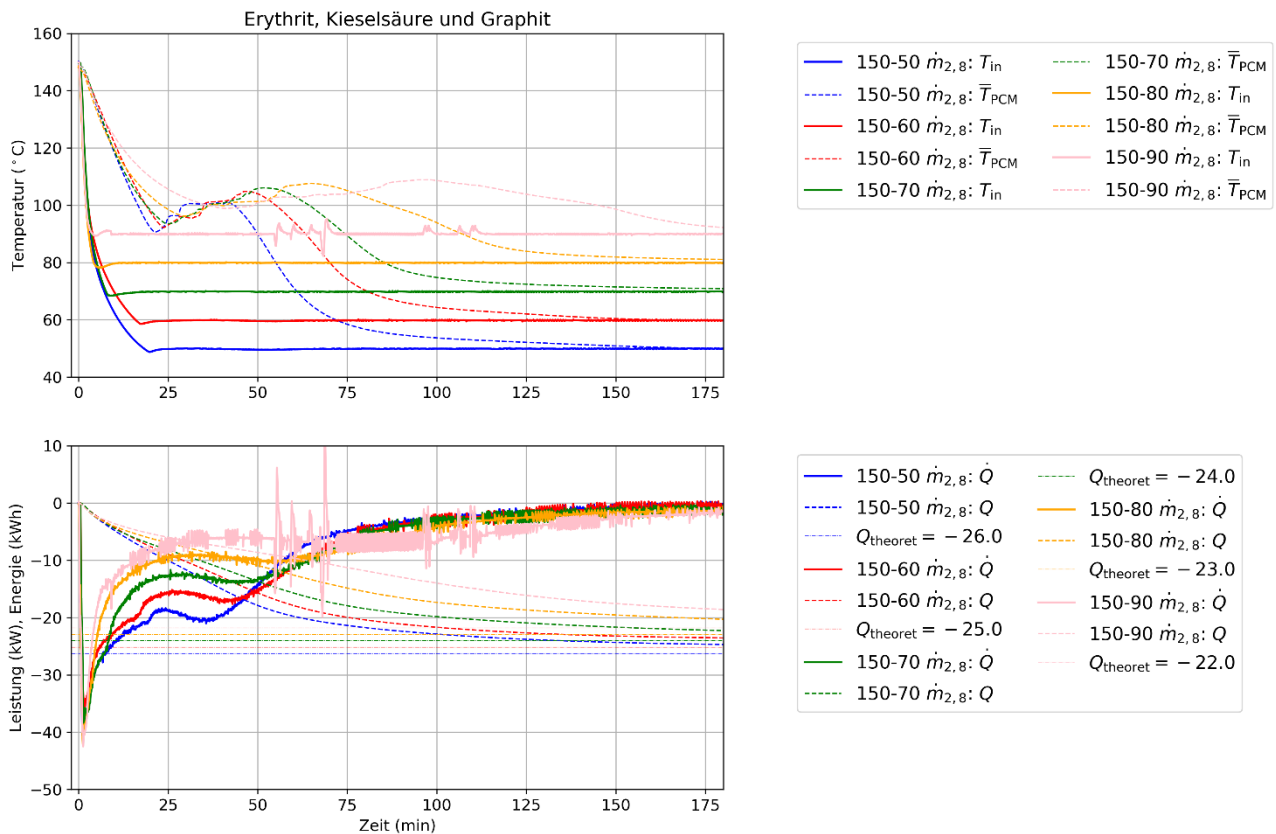


Figure 111: Discharging the graphite-silica-Erythritol storage to different discharging temperature levels. Subcooling and power profiles depend, of course, on the driving temperature.

Finally, we show in Figure 112 a comparison between the pure Erythritol and the compound Erythritol storages for a charging step response from 60 to 150 °C with a constant mass flow of 2.8 kg/s.

Especially by directly comparing the power and energy profiles (top right figure), one can nicely observe that the storage filled with the thermally conductive PCM is being charged more quickly. However, due to the additional filler materials which, of course, do not contribute to the latent heat, the total energy is higher for the storage filled with the pure PCM.

As an important concluding remark, we want to state that neither one of the storages is “better” *per se*, but it crucially depends on the application which storage is better suited. E.g. for some lower power applications there might be no need for a quick storage charging, while for other applications one even has to increase the graphite-filler content and/or employ additional fins to the tubes to be able to achieve sufficiently high storage power.

Also, it is important to notice that the actual storage power can be widely controlled by varying the mass flow and integrating the storage within a proper hydraulic scheme as is currently being investigated within another FFG project StoreITup-IF (FFG 848914).

Energieforschungsprogramm – 4. Ausschreibung

Klima- und Energiefonds des Bundes – Abwicklung durch die Österreichische Forschungsförderungsgesellschaft FFG

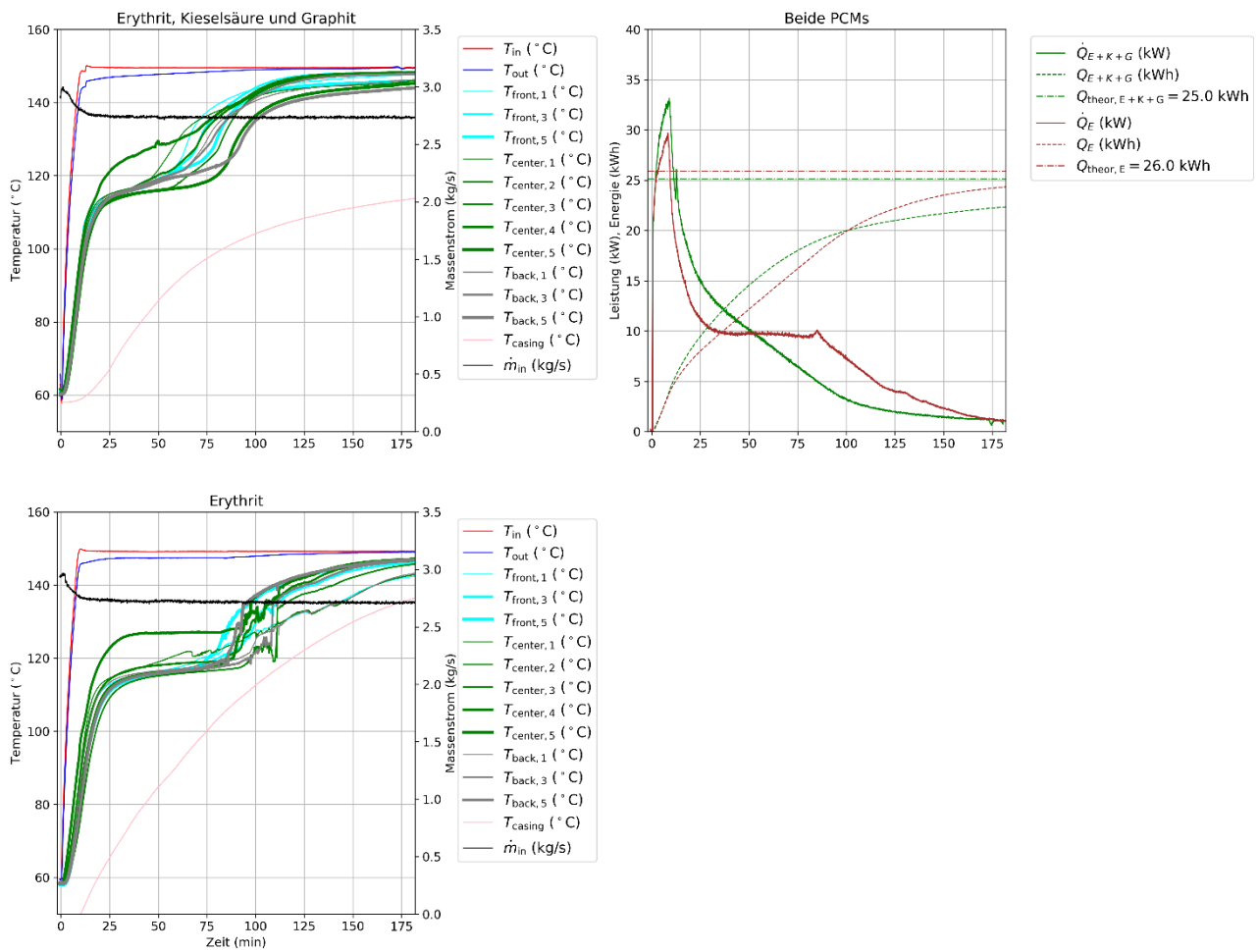


Figure 112: Comparison of both storages (pure Erythritol and graphite-silica-Erythritol). Employing a thermally conductive PCM enables higher storage power but with slightly lower total storage capacity. Ultimately one has to exactly design the appropriate storage and PCM compound depending on the application needs (power, capacity, charging/discharging temperature) in addition to a proper hydraulic integration scheme and mass flow control strategy (cf. FFG project StoreITup-IF).

8 Results and conclusions

8.1.1 Development Line A

The goal of Line A is to develop and demonstrate a seasonal closed sorption storage system to cover the domestic hot water and space heating demand of a single family house. The aim is to use the surplus of heat produced by solar thermal collectors in summer to store it for covering the heat demand in winter. Since the storing period is over several months a technology with low losses is required. In addition, the system should have a high compactness because of limited available space in a residential building. A technology, which can meet these requirements, is the sorption technology. The aim of Line A is to improve the performance of a sorption storage system by optimizing the so-called charge boost process and evaluate to which extent the performance can be improved.

For the investigations, a realistic scale storage system was designed and built up in the laboratory of AEE INTEC, which comprises several sorption storage vessels (two main storages and a room storage) and a new solar collector with integrated sorption material. The system was equipped with extensive measurement equipment in order to enable a detailed analysis of all components and of different operational modes. A system simulation model was set up, in order to represent the storage system with all its main components. The model was built in TRNSYS using about 60 single component models. Measurements from the laboratory test rig were used to parameterize and validate the model. Annual simulations were performed in order to test the developed control strategy and to assess the system efficiency for different configurations of the system.

8.1.2 Development Line B

The general goal of Line B is to develop a thermal management for batteries in electric or hybrid vehicles based on sorption thermal energy storage technology. The range of possible scenarios in this respect is too broad for a single project, thus we focused on hybrid vehicles only. In that case there is the additional benefit that waste heat of the combustion engine can be re-used to charge the thermal storage, which can then later be discharged to supply either heat or cold. The thermochemical material (TCM) (Sapo34 and water vapour) was chosen according to the prevailing temperature levels. A numerical tool was developed and a dedicated test rig assembled for the material selection. Critical components have been discussed extensively. A custom adsorber design has been developed, including adsorbents as coating and as granules. The performance of this design was compared experimentally to two other adsorber designs, based on coating and direct crystallization, and found to be superior. The evaporator/condenser was dimensioned accordingly in a compact way, and examined experimentally in a dedicated test rig. Various designs have been discussed for the vacuum vessel using finite element calculations, and a rectangular shaped was suggested with vacuum forces carried by the heat exchangers. A functional module of the storage system was assembled and assessed in experiment, where a cooling power peak of 2 kW and an average power of 1 kW for a total energy of 0.55 kWh was measured. Assuming an optimized system design including compact vessels, this translates into key performance indicators (KPIs) of about 27 Wh/l resp. 27 Wh/kg and 55 W/l resp. 55 W/kg for cooling. For heating, we propose a novel operation mode, where no external heat source is coupled to the evaporator during evaporation. Instead, we allow part of the water to freeze, such that the crystallization enthalpy serves as evaporation enthalpy. The concept hence combines TCM with phase change material as latent heat storage, where

the latter is used as a buffer to provide the evaporation enthalpy. This process was demonstrated in experiment, yielding heating KPIs of 34 Wh/l resp. 34 Wh/kg and 68 W/l resp. 68 W/kg for heating. Simultaneously to the experiments, a simulation model was developed. The thermal storage was modelled in Trnsys and the vehicle with all other components in Simulink. A co-simulation interface has been constructed to couple these models. Detailed system simulations have been performed for five distinct realistic scenarios. These have shown energy savings of 60% for cooling the battery during fast charging, 11% for cooling the combustion engine while regenerating the thermal storage compared, saving 80 seconds for heating a chilled battery up to 20°C and saving 26 seconds for preheating the combustion engine up to 80°C.

8.1.3 Development Line C

The aim of this development line is to develop an improved and experimentally verified thermal storage concept for the conditioning of the railway passenger compartments by adding functionality of thermal storage devices to the system. Three applications are studied in this development line: Optimized underground heat rejection of subway trains and enhanced part-load behaviour of conventional conditioning systems by the use of PCM storages. The third application deals with the improvement of Air-Cycle-Cooling (ACS) systems by the use of adsorption materials. In order to simplify readability, and to establish cross-connections, the three applications were subdivided into two parts concerning the different storage concepts:

- Improvement of underground heat rejection of subway trains, improvement of part-load behaviour of conventional conditioning systems by the use of PCM storages
- Improvement of Air-Cycle-Cooling (ACS) systems by the use of adsorption materials

8.1.3.1 Part-load behaviour of conventional conditioning systems (Objective Ca) and Underground heat rejection of subway trains (Objective Cb)

Concerning the improvement of underground heat rejection of subway trains, improvement of part-load behaviour of conventional conditioning systems by the use of PCM storages were done. These improvements of the part-load behaviour can be accomplished by using a storage evaporator assembled to the air condition system. The usage of an evaporator with integrated PCM is one possibility to reduce or even avoid the part-load operation of the refrigerant compressor resp. the whole air conditioning system. As the part load operation is inefficient using a fixed speed compressor, this leads to a higher system efficiency. The storage evaporator is being discharged during the operation of the air conditioning system and being charged during the standstill of the compressor by the cabin air. For the later on simulation model adjustment and validation, an off-the-shelf storage evaporator for automotive applications was evaluated resp. measured. The measured data lays the foundation for a scalable simulation model in the future. The automotive storage evaporator grants an air outlet temperature lower than 15 °C for $t = 109$ s with a previous PCM discharge time of 4 minutes (@200 kg/min air mass flow and ambient air temperature of 30 °C). This means an average cooling capacity of 1055 W is available during this 109 s.

Additionally, different PCM/Aluminium modules were tested to determine thermal power and storage density. For this RT5HC was used as storage material. It is a PCM with a melting area from 5 to 6 °C and a heat storage capacity of 250 kJ/kg (in a temperature range from -2 to 13 °C). The heat conductivity of both phases is 0.2 W/(m K). Several charging and discharging cycles with different mass flow rate,

different geometry of the modules and different hydraulic concepts were performed. From these experiments measured data were used to parametrize a TRNSYS storage model for further system simulations. For these investigations Dymola was used for the HVAC system and the TRNSYS storage model was integrated using the co-simulation tool BCVTB.

8.1.3.2 Improvement of Air-Cycle-Cooling (ACS)((Objective Cc)

Regarding the improvement of Air-Cycle-Cooling (ACS) systems by the use of adsorption materials the aim of this report is to describe the consequences derived from material characterization on the concept and dimensioning of the components needed to integrate storage functionality into the Air-cycle-cooling system (ACS). To reach a most realistic data base, a second step of air conditioning was built to test some selected materials in the adsorption and desorption simultaneously. Therewith more reliable data were found. Additionally some components already existing were tested. These components show somehow similar functionality compared to the required desiccant unit for the ACS application.

In particular, a finned air heat exchanger, coated with a kind of adsorbent material (SAPO34, produced by MITSUBISHI PLASTICS/JP) and a desiccant wheel with incorporated silica gel (produced by SCHEUCHL/D) were tested. The development of the air dehumidification unit was made by further experimental studies of selected sorption materials as packed bed specimen as well as component tests of existing devices. Simulation studies were performed by LIEBHERR internal Software.

In the ideal case a dehumidifying capacity of 10 g/kg can be reached with the Material Y zeolite, which results in a power saving of 22 % of the unit with constant cooling capacity. The technique results in an additional process air cooling capacity of up to 17 kW. The additional cooling process parameter is an essential feature that must be considered in the detailed design and construction phase.

8.1.4 Development Line D

The goal of Development Line D is to develop a thermochemical energy storage system (TCES). The aim is to work on different aspects of the technology simultaneously, namely on the construction and initial operation of a fluidised bed reactor for hydration and dehydration reactions, the development of a method for modelling TCES, the process design and integration of TCES in waste heat recovery applications. In addition, the evaluation of the economic feasibility of such systems was investigated and the base materials are optimized in order to improve material properties that are of high importance for the process like reactivity and thermal conductivity.

A fluidised bed reactor for testing MgO/Mg(O)_2 was set into operation and extensive material testing has been performed. The results were summarised in the diploma thesis of A. Bartik, 2018.

A model of the reactor including all peripheral systems was implemented in the software gPROMS. The work is presented in an article published in *Energy (Int. J.)*, which uses methods from chemical engineering and reaction kinetics and applies it to thermochemical energy storage. Also it extensively discusses the limitations of a TCES process and the issue of the supply of the reactant gas on the overall process. Furthermore a process utilizing 3 different reaction pairs arranged in a cascade of reactors was investigated.

A study based on the overall factor method of Lang was done in order to evaluate the economic viability of TCES. The resulting values of the mass and energy balances from the simulation are used in order to yield the size of the utilized equipment. Via this method it is possible to obtain the total capital investment of a TCES system.

In order to enhance the reactivity of the $\text{MgO}/\text{Mg}(\text{OH})_2$ system calcium doping of magnesium oxide was performed. This procedure results in insignificantly increased water dissociation rates, thus enhancing the hydration rate and the completeness of hydration compared to pure MgO .

8.1.5 Development Line E

The goal of this development line is to develop novel medium-temperature PCMs based on sugar alcohols. Within the project, we completed the organic PCMs synthesis efforts. Within the class of sugar alcohols new chemical modifications (acetylations) and chain elongations have been investigated revealing not-yet-known candidate organic PCMs. In addition, thermal stability investigations were performed in DSC and larger volume samples ($\sim 1 \text{ dm}^3$) clarifying the situation for different atmospheric conditions. Erythritol was found to be the most stable compound with a high melting enthalpy. The systematics of melting range and enthalpy with regard to carbon backbone chain length was investigated in great detail for dicarboxylic acids and diamids. We found that there is an appropriate compound for every few degrees Celsius over a phase change range of $100 - 230^\circ\text{C}$. Among the newer investigated substances, we found three interesting organic PCMs in the NN-bis group with enthalpies up to 375 kJ/kg . Finally, we investigated the ease of production which, of course, directly relates to PCM costs and identified sulfuramide, azamide and sebacamide as interesting candidates in addition to sugar alcohols.

On the application side, we found two new industrial use cases for our organic PCMs storages related to solar cooling in food and chemical industries. They will be investigated up to demonstration level within the EU project HYCOOL (Grant Agreement 792073) which was successfully submitted and started in mid-2018.

In a final step we developed two lab-scale storages to demonstrate the feasibility of our organic PCMs on a 100 kg scale. Fast and versatile Dymola/Modelica models were implemented which allow a proper storage design. The models can be combined with different HVAC system libraries in order to simulate the behaviour of our PCM storages on a system level.

Different heat exchanger concepts were evaluated with regard to their economic and technical performance. Fin-tube and tube bundle heat exchangers were finally selected to serve within the lab-scale demonstrators. Erythritol was chosen as the most promising PCM which was compounded with graphite to increase its thermal conductivity and fumed silica to stabilize the mixture against sedimentation.

A dedicated storage test rig was developed at AIT and the storages were characterized in great detail demonstrating a total storage capacity in the range of 50 kWh . Various charging and discharging experiments revealed storage powers in the range of 30 kW . In addition to even allow for constant-power-(dis)charging a dedicated mass flow control strategy was developed and proven.

9 Literature

Asenbeck S., Engel G., Moser C., Weber R., Fumey B. (2015): COMTES – Combined development of compact thermal energy storage technologies, Deliverable 6.1 – Report on system simulation; EU grant nr. 295568

C. Bales, A. Heinz, und M. Haller (2012): „Deliverable 7.1 - Definition of Boundary Conditions, FP7 project MacSheep (grant agreement 282825)“, 2012.

Bertsch F., Fumey B., Heimrath R., Dröschner A., Schranzhofer H. (2013): Deliverable 1.2 – Description of the boundary conditions for each storage technology and of the models for the reference systems; European project COMTES, January 2013

U. Jordan und K. Vajen (2012): „DHWcalc - Tool for the Generation of Domestic Hot Water (DHW) Profiles on a Statistical Basis“. Universität Kassel, Institut für Thermische Energietechnik, 2012.

Meteotest. Meteonorm 6.1.0.9. (2009) Global Meteorological Database for Engineers, Planner and Educations, Software and Data on CD-Rom, Meteotest, Bern, Switzerland, 2009

SPF (2007): Solar Collector Factsheet Spring Solar SK-8 CPC (C815); SPF Testing, Institut für Solartechnik SPF, Hochschule für Technik Rapperswil HSR, CH-8640 Rapperswil, 16.02.2007

10 Contact information

ProjektnehmerIn (Institution)	AEE INTEC
AnsprechpartnerIn	Dr. Wim van Helden
Postadresse	Feldgasse 19, A-8200 Gleisdorf
Telefon	0043-3112-5886-228
Fax	0043-3112-5886-18
E-mail	w.vanhelden@aee.at
Website	www.aee-intec.at ;
Project website	Tes4set.at

Project partner(s):	partner	Country
	A AEE INTEC	AT
	P1 TU Graz	AT
	P2 ASiC	AT
	P3 AIT	AT
	P4 TU Wien, Energy Systems	AT
	P5 TU Wien, Synthesechemie	AT
	P6 Suedzucker AG	DE
	P7 AMMAG	AT
	P8 GREENoneTEC	AT
	P9 Solid	AT
	P10 Liebherr	AT
	P11 V2C2	AT
	P12 STM Meitz	AT
	P13 i2m	AT
	P14 SOMITSCH	AT
	P15 Fahrenheit	DE
	P16 Qpunkt	AT
	P18 RHI	AT